

THE UNIVERSITY OF ALBERTA

THE REACTIONS OF EXCITED METAL ATOMS

by



PETER JOHN YOUNG

A THESIS

SUBMITTED TO THE FACULTY OF GRADUATE STUDIES AND RESEARCH

IN PARTIAL FULFILMENT OF THE REQUIREMENTS FOR THE DEGREE

OF

DOCTOR OF PHILOSOPHY

DEPARTMENT OF CHEMISTRY

EDMONTON, ALBERTA

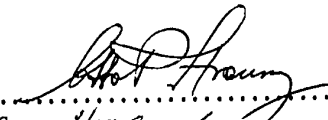
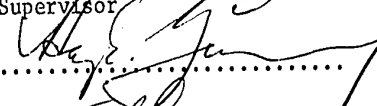

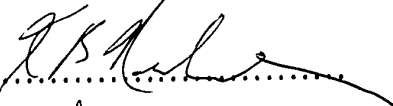
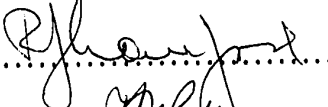

(Spring 1973)

THE UNIVERSITY OF ALBERTA
FACULTY OF GRADUATE STUDIES AND RESEARCH

The undersigned certify that they have read, and recommend
to the Faculty of Graduate Studies and Research for accept-
ance, a thesis entitled

"THE REACTIONS OF EXCITED METAL ATOMS"

submitted by PETER JOHN YOUNG in partial fulfilment of the
requirements for the degree of Doctor of Philosophy.


.....
Supervisor

.....

.....

.....

.....

.....
External Examiner

Date *February 23, 1973*

ABSTRACT

The flash photolysis of volatile alkyl-metals has been used as a source of metal atoms for kinetic studies in the gas phase at room temperature. The reactions of several different ground and excited state metal atoms have been studied with a variety of substrates.

Ground state cadmium atoms, from the photolysis of dimethyl-cadmium, react with halogen atoms from the co-photolysis of CF_3X to form the CdX ($X = Br$ or I) radicals. Similar reactions were also observed for zinc atoms.

When the flash photolysis of $Cd(CH_3)_2$ is carried out in the presence of methane, $Cd(^3P_{2,1,0})$ can be detected by absorption spectroscopy. Using kinetic absorption spectroscopy absolute rate constants and Arrhenius parameters have been measured for the first time for the quenching of the $^3P_{0,1}$ state of the cadmium atom with various types of quencher molecules. The 3P_0 and 3P_1 atoms appear under all experimental conditions near chemical equilibrium manifesting the role of 3P_0 atoms in 3P_1 photosensitization reactions.

An activation energy of 2.3 kcal/mole has been measured for the quenching of $Cd(^3P)$ by ethylene, the first activation energy detected for a quenching process. Data from this study has been combined with that of other workers and rate parameters for a series of quenching reactions have been calculated.

Quenching by hydrogen donor molecules results in the formation of the CdH radical and the appearance of its known band system in the absorption spectrum.

The flash photolysis of trimethylbismuth and trimethylantimony has been used to produce bismuth and antimony atoms in their ground and excited states. Relative rates of quenching of several antimony and bismuth states have been measured, and compared where possible to other quenching studies.

When two transitions from an excited state of antimony could be monitored, it was found that in some cases the apparent quenching rate varied, depending on the particular transition that was monitored. This phenomenon is due to the change in the relative transition probabilities of the two transitions caused by collisionally induced emission. The effect of pressure broadening and the appearance of satellite bands in the fluorescence spectrum of the Bi atom have been noted and reported.

General features of excited atom quenching are discussed.

ACKNOWLEDGEMENTS

The author wishes to express his gratitude to Dr. O. P. Strausz for his advice and guidance throughout the course of this investigation.

A very special thank you goes to Dr. John Connor for helping the author through his first few attempts at scientific research.

Thanks go to all members of the photochemistry research group for their advice, criticism and helpful discussion. The efforts of Dr. E. M. Lown and Mrs. R. Tarnowski who corrected and typed this thesis, respectively, are greatly appreciated.

The author would like to express his deepest gratitude to his wife, Sharon, who managed to run a household, look after her husband, and write an M.Sc. thesis at the same time.

The financial assistance provided by the University of Alberta and the National Research Council of Canada during the course of this work is gratefully acknowledged.

TABLE OF CONTENTS

	Page
ABSTRACT.....	i
ACKNOWLEDGEMENTS.....	iii
LIST OF TABLES.....	vii
LIST OF FIGURES.....	x
CHAPTER I. INTRODUCTION.....	1
1. Energy Transfer.....	1
2. Methods of Measuring Quenching Rates.....	6
a. Physical Method.....	6
b. Chemical Method.....	9
3. The Quenching of Excited Mercury.....	13
4. The Quenching of Cadmium (³ P) Atoms.....	18
5. Other Metal Atoms Studied.....	26
6. Flash Photolysis.....	29
7. Objectives of the Present Study.....	32
CHAPTER II. EXPERIMENTAL.....	34
1. Materials.....	34
2. Apparatus.....	37
a. Vacuum System.....	37
b. Flash Apparatus.....	37
3. Experimental Procedure.....	41

TABLE OF CONTENTS (cont'd)

	Page
CHAPTER III. THE PHOTOLYSIS OF DIMETHYLCADMIUM.....	42
1. Reaction Products and Primary Process.....	42
2. Electronic States of Cadmium Atoms.....	59
CHAPTER IV. THE UV SPECTRA OF CdBr, CdI, ZnBr AND ZnI.....	63
1. The UV Spectra of Cadmium and Zinc Halides	65
a. The Absorption Spectrum of CdBr.....	65
b. The Absorption Spectrum of CdI.....	65
c. The Absorption Spectrum of ZnBr.....	75
d. The Absorption Spectrum of ZnI.....	79
2. The Doublet Pi Splittings.....	89
CHAPTER V. THE QUENCHING OF CADMIUM (³ P) ATOMS.....	91
1. Rate Constants for the Deactivation of Cd(³ P).....	94
2. Activation Energy of the Cd* + Ethylene Reaction.....	119
3. Discussion.....	125
CHAPTER VI. QUENCHING OF EXCITED ANTIMONY AND BISMUTH ATOMS	130
1. The Quenching of Excited Bismuth Atoms....	130
2. The Quenching of Excited Antimony Atoms...	155
3. Discussion.....	171

TABLE OF CONTENTS (cont'd)

	Page
CHAPTER VII. SUMMARY AND CONCLUSIONS.....	173
BIBLIOGRAPHY.....	179
APPENDIX.....	185

LIST OF TABLES

Table	Page
I-I	Some Metal Atoms Used as Sensitizers..... 3
I-II	Some Quenching Cross Sections for Cd, Hg and Na..... 21
I-III	Some Relative Quenching Efficiencies..... 23
I-IV	Quenching Cross Sections from Jenkins..... 27
II-I	Source and Purity of Materials Used..... 35
II-II	Source and Purity of Materials..... 36
III-I	The CdCH ₃ (A ← X) Spectrum..... 45
III-II	The CdCH ₃ (B ← X) Spectrum..... 46
III-III	The ZnCH ₃ (A ← X) Spectrum..... 52
III-IV	The ZnCH ₃ (B ← X) Spectrum..... 53
III-V	Species Observed in Flashed DMCD-CH ₄ Mixtures..... 61
IV-I	The $^2\Pi_{3/2}^-$ - $^2\Sigma$ System of CdBr..... 66
IV-II	The $^2\Pi_{1/2}^-$ - $^2\Sigma$ System of CdBr..... 68
IV-III	The $^2\Pi_{3/2}^-$ - $^2\Sigma$ System of CdI..... 69
IV-IV	The $^2\Pi_{1/2}^-$ - $^2\Sigma$ System of CdI..... 73
IV-V	The $^2\Pi_{3/2}^-$ - $^2\Sigma$ System of ZnBr..... 76
IV-VI	The $^2\Pi_{1/2}^-$ - $^2\Sigma$ System of ZnBr..... 78
IV-VII	The $^2\Pi_{3/2}^-$ - $^2\Sigma$ System of ZnI..... 80
IV-VIII	The $^2\Pi_{1/2}^-$ - $^2\Sigma$ System of ZnI..... 83
IV-IX	$^2\Pi$ Splittings of Zn, Cd and Hg Halides..... 90

LIST OF TABLES (cont'd)

Table	Page
V-I	Data for Cd(³ P) Decay in 300 torr CH ₄ at Room Temperature..... 95
V-II	Data for Decay of Cd(³ P) in 300 torr CH ₄ at 110°C... 96
V-III	Data for Decay of Cd(³ P) in 650 torr CH ₄ at Room Temperature..... 97
V-IV	Data for the Fluorescent Decay of Cd(³ P ₁) at Room Temperature..... 98
V-V	Data for Cd ³ Decay in C ₂ H ₄ At Room Temperature..... 100
V-VI	Data for Cd ³ Decay in C ₃ H ₆ at Room Temperature..... 101
V-VII	Data for Cd ³ Decay in <i>c</i> -C ₄ H ₈ at Room Temperature.... 102
V-VIII	Data for Cd ³ Decay in <i>t</i> -C ₄ H ₈ at Room Temperature.... 103
V-IX	Data for Cd ³ Decay in C ₂ H ₂ at Room Temperature..... 104
V-X	Data for Cd ³ Decay in H ₂ at Room Temperature..... 105
V-XI	Data for Cd ³ Decay in D ₂ at Room Temperature..... 106
V-XII	Data for Cd ³ Decay in C ₂ H ₃ F at Room Temperature..... 107
V-XIII	Data for Cd ³ Decay in <i>t</i> -C ₂ H ₂ F ₂ at Room Temperature.. 108
V-XIV	Data for Cd ³ Decay in <i>c</i> -C ₂ H ₂ F ₂ at Room Temperature.. 109
V-XV	Data for Cd ³ Decay in 1,1-C ₂ H ₂ F ₂ at Room Temperature 110
V-XVI	Data for Cd ³ Decay in C ₂ HF ₃ at Room Temperature..... 111
V-XVII	Data for Cd ³ Decay in C ₂ F ₄ at Room Temperature..... 112
V-XVIII	Data for Cd ³ Decay in SiH ₃ CH ₃ at Room Temperature... 113
V-XIX	Data for Cd* Decay in C ₂ H ₄ and H ₂ at Room Temperature..... 114
V-XX	Quenching Rate Constants for Cd(³ P)..... 116

LIST OF TABLES (cont'd)

Table	Page
V-XXI	Relative Rates of Cadmium and Mercury Quenching..... 117
V-XXII	Data for Cd ³ Decay in C ₂ H ₄ at 50°C..... 120
V-XXIII	Data for Cd ³ Decay in C ₂ H ₄ at 80°C..... 121
V-XXIV	Data for Cd ³ Decay in C ₂ H ₄ at 110°C..... 122
V-XXV	Rate Constants at 275°C, and Estimated Activation Energies and A-factors..... 124
VI-I	Species Observed in Absorption in Flashed TMBI..... 132
VI-II	The 2900-3100Å System Observed in Flashed TMBi..... 135
VI-III	Stern-Volmer Data for Excited Bi..... 139
VI-IV	Quenching Half Pressures for Excited Bi..... 150
VI-V	Quenching Cross Sections..... 154
VI-VI	Species Observed in Absorption in Flashed TMSb..... 156
VI-VII	Stern-Volmer Data for Excited Sb..... 161
VI-VIII	Quenching Half Pressures for Excited Sb..... 168

LIST OF FIGURES

Figure		Page
2-1	The Optical System.....	38
2-2	Schematic of the Electronic Components of the Flash Photolysis Apparatus.....	40
3-1	A Plot of $Cd(^1S_0)$ vs Flash Energy.....	44
3-2	The $CdCH_3$ (A \leftarrow X) Spectrum.....	47
3-3	The $CdCH_3$ (B \leftarrow X) Spectrum.....	48
3-4	A Plot of $[CdCH_3]$ vs Flash Energy.....	49
3-5	A Plot of $[CdCH_3]$ vs Pressure.....	50
3-6	The $ZnCH_3$ (A \leftarrow X) Spectrum.....	54
3-7	The $ZnCH_3$ (B \leftarrow X) Spectrum.....	55
3-8	A Partial Grotrian Diagram for Cadmium.....	58
4-1	The UV Absorption Spectrum of $CdBr$	85
4-2	The UV Absorption Spectrum of CdI	86
4-3	The UV Absorption Spectrum of $ZnBr$	87
4-4	The UV Absorption Spectrum of ZnI	88
5-1	A Plot of OD vs $OD_{1/2}$	93
5-2	First Order Plots for Fluorescent Decay of Cd^3	99
5-3	Typical First Order Plots for the Decay of Cd^3	115
5-4	Arrhenius Plot.....	123

LIST OF FIGURES (cont'd)

Figure		Page
6-1	Absorption Spectra of TMBi and TMSb.....	131
6-2	Energy Level Diagram for Bi.....	133
6-3	Emission from Bi($^4P_{1/2}$) at $3068\overset{\circ}{\text{A}}$	137
6-4	Stern-Volmer Plot for Excited Bi.....	145
6-5	Stern-Volmer Plot for Excited Bi.....	146
6-6	Stern-Volmer Plot for Excited Bi.....	147
6-7	Energy Level Diagram for Sb.....	157
6-8	Stern-Volmer Plot for Excited Sb.....	158
6-9	Stern-Volmer Plot for Excited Sb.....	159
6-10	Stern-Volmer Plot for Excited Sb.....	160
6-11	Effect of Added H ₂ on Emission from Sb($^2P_{1/2}$) at 3268 and $2598\overset{\circ}{\text{A}}$	169

CHAPTER I

INTRODUCTION

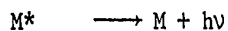
1. Energy Transfer

Since Cario and Franck (1) demonstrated the occurrence of electronic energy transfer from an excited metal atom to another atom or molecule, there has been an enormous volume of research expended on the phenomenon of photosensitization. Since the energies of electronically excited metal atoms are often of the order of those of chemical bonds, energy transfer can, in addition to physical changes, cause chemical changes as well in the energy acceptor molecule. The chemical changes brought about by photosensitization can provide valuable information pertaining to the mechanism of energy transfer (2-4) and since most metal atoms absorb in the UV region of the electromagnetic spectrum (2000 - 5000Å), the reactive intermediates are produced in the quenching reaction in well defined energy levels, usually the ground or first excited states.

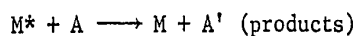
The first step in an atom sensitized reaction is the absorption of a photon to create an electronically excited atom:



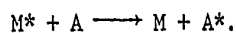
Metal atoms often exhibit an intense transition in a suitable region of the spectrum and the radiation corresponding to this transition, the resonance line, is then used to excite the metal atom. The excited atom may then fluoresce:



or interact with substrate in an energy transfer process. Energy transfer to a substrate A can lead to decomposition:



or to translational, rotation, vibrational, and/or electronic excitation:



The atomic photosensitization process can thus be divided into three consecutive steps:

- i. absorption of light by the atom (and fluorescence in the absence of a quencher),
- ii. transfer of energy to the substrate, and
- iii. physical and chemical changes in the substrate.

Step i. can be established from the absorption and emission spectra of the atom. Steps ii. and iii., however, must be inferred from both the physical and chemical properties of the donor and acceptor as well as effects produced through this interaction.

The requirements of a good sensitizing agent are: a) a chemically inert ground state, b) adequate vapour pressure, c) absorption of light of discrete wavelengths, and d) a long excited state lifetime. Mercury and many other metal atoms at elevated temperatures satisfy all these requirements. Table I-I lists some metal atoms which have been used as photosensitizers, the states, their energies and the wavelength of the resonance transitions involved.

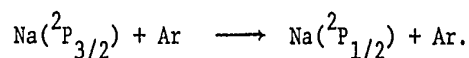
TABLE I-I

Some Metal Atoms Used as Sensitizers

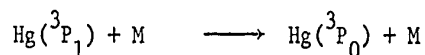
Metal	Energy kcal/mole	State	Transition	Wavelength Å
Hg	154.6	$1P_1$	$1P_1 - 1S_0$	1849
Hg	112.7	$3P_1$	$3P_1 - 1S_0$	2537
Cd	125.0	$1P_1$	$1P_1 - 1S_0$	2288
Cd	87.7	$3P_1$	$3P_1 - 1S_0$	3261
Na	48.5	$2P_{1/2, 3/2}$	$2P - 2S_{1/2}$	5890, 5896
Tl	75.6	$2S_{1/2}$	$2S_{1/2} - 2P_{1/2}^{\circ}$	3776
Pb	100.8	$3P_1^{\circ}$	$3P_1^{\circ} - 3P_0$	2833

Energy transfer processes have been reviewed recently by Callear (5) and can be divided into several categories such as vibration-translation and vibration-vibration; only those involving the transfer of electronic energies will be discussed here.

Electronic-vibration and electronic-translation energy transfer processes involving less than one electron-volt (eV) of energy most often involve spin-orbit relaxation of the excited atom. For example, spin-orbit relaxation of $\text{Na}(^2\text{P})$ occurs at every collision with inert gases (6):



Spin-orbit relaxation of mercury:

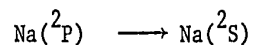


is the major process occurring in the presence of N_2 and its importance in the $\text{Hg}(^3\text{P}_1)$ -paraffin system has only recently been recognized (7); with noble gases it is too slow to measure at ambient temperatures (8). Spin-orbit relaxation of $\text{Se}(4^3\text{P}_0)$ (9), $\text{Fe}(a^5\text{D}_3)$ (10), $\text{As}(4^2\text{D}_{5/2})$ (11), and some non-metal atoms (5) has also been studied.

Attempts to correlate the reciprocal of the spin-orbit quenching efficiency to the amount of energy which must go into translational modes of the acceptor (taking into account possible vibrational activation but ignoring rotational activation) have not met with great success, although in general spin-orbit relaxation is more efficient the smaller the energy difference between spin states. The discrepancies between experiment and theory are explained in terms of

attractive interactions in the transition complex, chemical affinities, and tunnelling between potential surfaces (10).

Electronic energy transfer processes involving energies greater than one eV display different characteristics than those involving less than one eV. Most of the experimental work on quenching and photosensitization reactions of this type has been done with $\text{Na}(^2\text{P})$, $\text{Hg}(^3\text{P}_1)$, and $\text{Cd}(^3\text{P}_1)$ atoms. The quenching of excited sodium is almost always of a physical nature since the energy of the transition:



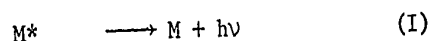
is only 48.3 kcal/mole, which in general is not sufficient to bring about dissociation of chemical bonds. With mercury and cadmium in their first triplet excited states, having 112 and 87 kcal/mole excitation energy respectively, both physical and chemical quenching are possible.

2. Methods of Measuring Quenching Rates

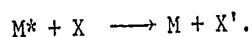
The two most common methods of measuring quenching rate constants are a) measurements of the intensity of fluorescence and application of the Stern-Volmer formula (12) (often called the physical method); and b) a chemical method based on relative rate measurements. For mercury these methods have been discussed in detail (2,3).

a) Physical Method

If a cell containing metal atom vapour is irradiated with resonance radiation fluorescence will occur:



where M and M* represent a metal atom in its ground and excited state respectively and Ia and I are the intensities of the exciting and fluorescence radiation respectively. If a non-absorbing gas is added a quenching process also takes place in competition with fluorescence:



If we assume that bimolecular quenching and fluorescence are the only processes occurring, steady-state treatment leads to the following equations:

- i. in the absence of quencher

$$I_a[M] = k_f[M^*]$$

- ii. in the presence of quencher

$$I_a[M] = k_f[M_q^*] + k_q[M_q^*][X]$$

(in the presence of quencher the steady-state concentration of excited sensitizer will not in general be the same.) Combining and rearranging these equations leads to:

$$\frac{I_0}{I} = 1 + \frac{k_q}{k_f} [X]$$

where I_0 and I indicate the intensity of emitted resonance radiation in the absence and presence of quencher respectively. Thus a plot of I_0/I vs. $[X]$, the concentration of quencher, is a straight line having a slope of k_q/k_f . If the lifetime, τ , of M^* is known ($\tau = 1/k_f$) the quenching rate constant can be obtained directly.

In flash photolysis experiments where steady-state treatments are not applicable, the intensity of fluorescence is considered to vary as the fraction of processes leading to emission compared to all processes taking place.

i. in the absence of quencher

$$I_0 \propto \frac{k_f[M^*]}{k_f[M^*]} = 1$$

ii. in the presence of quencher

$$I \propto \frac{k_f[M_q^*]}{k_f[M_q^*] + k_q[M_q^*][X]}$$

Since the proportionality constant is the same in both cases the Stern-Volmer relationship is valid.

The results of fluorescence quenching experiments are often

quoted in terms of classical collision theory, as quenching cross sections, σ^2 :

$$Z = k_q [X] = \sigma^2 \left(\frac{8\pi RT}{\mu} \right)^{1/2} [X]$$

where Z is the classical collision frequency and μ is the reduced mass of the colliding pair. This leads to:

$$\sigma^2 = k_q \left(\frac{8\pi RT}{\mu} \right)^{-1/2}$$

and the quenching cross sections, σ^2 , are often discussed in terms of the "superefficiency" or inefficiency of the reaction compared to classical collision theory.

The major disadvantage in applying the Stern-Volmer relation is the problem of applying the imprisonment correction to the natural lifetime of the excited atom, from which k_f is derived. The problem of imprisonment of radiation arises from experimental limitations in that only the macroscopic properties of the system are being observed. The true lifetime of any individual excited atom is constant in all systems (except when collisional phenomena are important; this will be discussed later). However, if the concentration of metal atoms is moderately high, as is the case of most sensitization experiments, the emitted radiation from an excited atom can be absorbed by a ground state atom, be re-emitted, and so on. The depopulation of the excited state is therefore slower, or expressed in another way, the observed fluorescence intensity is less than that expected from the natural rate of decay of the excited atom.

There have been several theoretical treatments of imprisonment

reviewed and examined in detail for the case of mercury by Michael and Yeh (13); however the input parameters for the various theoretical calculations are not well known, especially for atoms other than mercury.

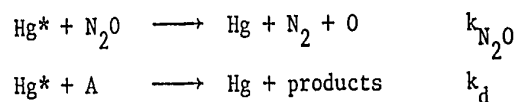
Regardless of the absolute value of the quenching cross sections, the ratio of any two values determined by a particular experimental method is independent of the imprisonment correction used. Thus the ratio of two slopes from Stern-Volmer plots becomes:

$$\frac{S_1}{S_2} = \frac{k_{q1}/k_f}{k_{q2}/k_f} = \frac{k_{q1}}{k_{q2}}$$

which is independent of k_f . An accurate comparison of quenching cross sections can therefore be made without knowing their absolute values accurately.

b) Chemical Method

This technique, developed by Cvetanovic (3) for mercury and by Sato and co-workers (14) for cadmium, is based on competitive quenching between a standard and another compound A. For mercury the reference quencher is N_2O :



where Hg^* represents $\text{Hg}(^3P_1)$. The quantum yield of nitrogen in the complete quenching region is given by:

$$\Phi_{N_2}^{-1} = \alpha + \beta \frac{[A]}{[N_2O]}$$

where α and β are related to the relative quenching cross sections:

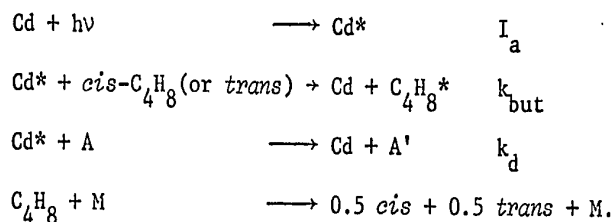
$$\frac{\sigma_A^2}{\sigma_{N_2O}^2} = \frac{\beta}{\alpha} \left(\frac{1 + M_{Hg}/M_{N_2O}}{1 + M_{Hg}/M_A} \right)^{1/2}$$

and $\beta/\alpha = k_d/k_{N_2O}$, assuming that the products of the reactions do not affect the production of nitrogen. These relationships were derived from a simplified treatment which does not take into account the formation of $Hg(^3P_0)(Hg^{\circ})$ atoms. Bellas, Rousseau, Strausz and Gunning (15) and others (16) have criticized this method since there are significant discrepancies between physical and chemical measurements. It was suggested (15) that Hg° atoms could be formed by quenching with some substrates and could also participate in the chemical quenching of N_2O ,



thus leading to low values of σ_A^2 . Also, the quenching cross sections of some compounds determined by the chemical method appear to be dependent on the light intensity (17).

In 1960 Cundall and Palmer (18) suggested that the *cis-trans* isomerization of butene-2 could be used as a standard for competitive determinations of relative quenching rates. Sato and co-workers (19) used this method in the study of relative rates of quenching of $Cd(^3P_1)$ atoms (Cd^*):



Steady-state treatment gives:

$$\frac{R_0}{R} = 1 + \frac{k_d[A]}{k_{\text{but}}[\textit{cis-C}_4\text{H}_8]}$$

where R_0 and R are the rates of isomerization of butene-2 in the absence and presence of A, respectively. This treatment assumes that only $\text{Cd}(^3\text{P}_1)$ atoms are present and does not take into account the possible formation or reactions of $\text{Cd}(^3\text{P}_0)$ (Cd°).

Recently, flash photolysis has been used to study the quenching efficiencies of excited mercury, cadmium, thallium and sodium. Callear and co-workers have used mercury (20-25) and cadmium (26,27) resonance flash lamps to create large concentrations of the respective excited metal atoms. These resonance flash lamps have a short duration, high intensity output consisting primarily of the metal atom resonance lines. Kinetic absorption spectroscopy was used to monitor atomic concentrations; a relatively simple procedure and no gross errors of interpretation should occur. This method also allows a baseline for atomic decay to be measured and therefore imprisonment effects can be directly determined. With cadmium the work was carried out at elevated temperatures.

Brus (28) and independently Bellisio and Davidovits (29) have flash photolysed thallium and sodium halides to produce the metal

vapour, and studied the quenching of $\text{Tl}(7^2\text{S}_{1/2})$, $\text{Tl}(6^2\text{P}_{3/2})$, and $\text{Na}(2\text{P})$ atoms by monitoring the emission lifetimes. Here again high temperatures were necessary to create sufficient vapour pressure of the parent compounds, although the temperatures used were not as extreme as those necessary to produce the same vapour pressure of the metal.

3. The Quenching of Excited Mercury

The macroscopic characteristics of the quenching of mercury by a wide variety of compounds have been established. The electrophilic character of Hg^* has been established from trends observed between σ_q^2 and certain structural parameters of the quencher, such as the number and size of the electron-donating groups, degree of unsaturation, etc. (4,30).

Where unshared electrons are present, it is believed that these orbitals represent the initial interaction site with Hg^* . For example, oxygen, nitrogen, and halogen containing compounds (except fluorine) interact with Hg^* through their lone electron pairs and silicon compounds possibly via the unfilled d orbitals of the silicon atoms.

With paraffins and hydrogen the primary photochemical step is the formation of HgH and a radical (31,32). The large kinetic isotope effect, k_H/k_D , observed in the quenching of Hg^* by paraffins or H_2 is probably due to a primary isotope effect (30), that is, Hg^* interacts directly with the H atom of the C-H or H-H bond. The much lower k_H/k_D effect for H_2O , NH_3 and C_3H_6 was attributed to a secondary isotope effect.

Olefins and carbonyls interact through their double bond systems exclusively (33) in an extremely efficient energy transfer reaction which forms a triplet state olefin or carbonyl and ground state mercury. The triplet state olefin or carbonyl may then undergo isomerization, fragmentation, or deactivation.

Interactions of excited mercury atoms with rare gases are of

interest because the quenching reaction is restricted to photophysical processes. The quenching rates are slow, but not negligible ($0.1\text{\AA} < \sigma^2 < 0.9\text{\AA}^2$) (8). Oldenberg (34) observed fluorescence bands on both sides of the mercury resonance line in the presence of rare gases. In the presence of helium and neon one band on the short-wavelength side of the 2537\AA line was observed, while in Ar, Kr and Xe two diffuse bands appeared in the same region. In addition to these band systems, discrete bands on the long-wavelength side of the resonance line were also observed in the presence of argon and krypton. Preston (35) also found emission bands associated with 13 lines of the mercury discharge spectra, with 12 lines of cadmium, and with 6 lines of tellurium in the presence of He and Ar.

Various proposals have been put forward to explain the origin of this band fluorescence. Kuhn (36) suggested that the bands originated from transitions between repulsive branches of the ground and excited state potential surfaces. Jefimenko (37) showed that the presence of auxiliary minima and maxima in the excited potential energy curve could adequately explain these satellite bands. On the other hand Leycuras (38) suggested that local perturbations of the optical electron oscillations during collision were responsible for emission of light other than the resonance line. Fiutak and Frackoweak (39) pointed out that the electronic correlation and potential energy relations of the Hg-Ar van der Waals molecule would lead to slightly bonding states for the ground state of mercury as well as the Hg*-Ar state.

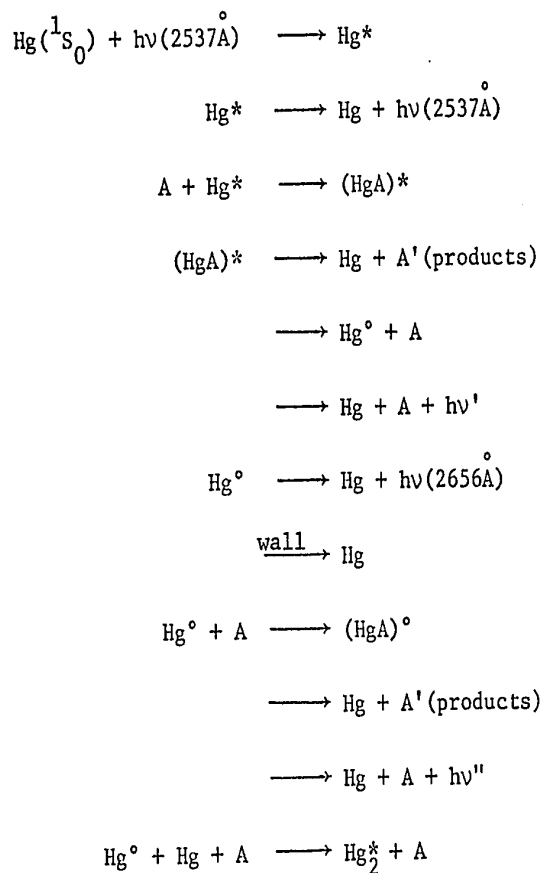
Jablonski (40) proposed that quenching of Hg* by the rare gases was due to crossings of the repulsive potential curves representing

the $\text{Hg}^* - \text{M}$ and $\text{Hg} - \text{M}$ surfaces. Laidler (41) proposed that the quenching reaction also involves a strongly attractive $\text{Hg}^+ - \text{M}^-$ polar or ionic curve, which then intersects with the $\text{Hg}-\text{M}$ surface. Neither of these theories explain the band fluorescence observed. Gunning, Penzes, Sandhu and Strausz have shown (8) however that quenching of Hg^* by noble gases occurs exclusively by radiative dissipation of the energy of the $\text{Hg}^* - \text{M}$ complex. Simple Lennard-Jones potential curves for the $\text{Hg}^* - \text{M}$ and $\text{Hg} - \text{M}$ systems indicated that within reasonable limits, crossing to the ground state as proposed by Jablonski is of little importance. All the band systems observed could be assigned to transitions between quantized levels of the van der Waals molecules, $\text{Hg}^* - \text{M}$ and $\text{Hg} - \text{M}$ (42).

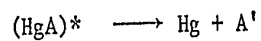
The intervention of complex formation between an excited species and a ground state molecule has been proposed in several other systems. Structureless emission and absorption bands associated with particular spectral lines of the alkali metals observed in the $\text{Na}(^2\text{P})$ -noble gas and $\text{Na}(^2\text{P})$ -paraffin systems have been attributed to excited complexes (43,44). Mercury also forms a variety of complexes with paraffins, alcohols, and ammonia (7,45,46,47) and band emission from a $\text{Cd}^* - \text{NH}_3$ complex has been detected (48). These band emissions are usually on the long-wavelength side of the particular atomic resonance line, often separated from the resonance line by many tens of angstrom units, indicating a significant binding energy. It is thus essential to include the formation of intermediate complexes in the mechanism of deactivation of Hg^* and of other excited species.

A general mechanism for the quenching of Hg^* , taken from

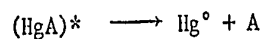
reference (7) can be described as follows:



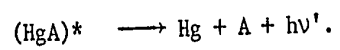
In general the formation of the van der Waals complex $(\text{HgA})^*$ is the initial step. This complex may then decompose via quenching to ground state Hg



(where A' may be products or excited substrate), spin-orbit relaxation:



or emission:



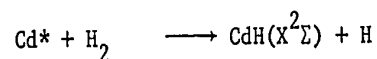
Analogous reaction may occur for Hg^0 . The relative importance of each mode of reaction will depend not only on the accessibility of a particular reaction surface, but also on the competitive rates of processes into different channels.

4. The Quenching of Cadmium (3P) Atoms

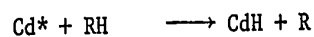
In order to better understand mercury photosensitization early workers (49-53) also studied the analogous cadmium (3P_1) reactions. Since the electronic properties of Hg^* and Cd^* were believed to be identical it was felt that the role of energy, being the only variable, could be discerned. In fact the temperatures necessary to produce sufficient cadmium vapour pressure for cadmium sensitization resulted in experimental difficulties, restricted the choice of substrates, and complicated the evaluation of experimental data. Thus cadmium sensitization reactions have not been as well documented as those of mercury.

Bates and Taylor (49,50) and Steacie and LeRoy (51-53) carried out some early qualitative work and found that the reactions of Cd^* paralleled those of Hg^* but that Cd^* caused much less decomposition.

Bender (54) and independently Olsen (55) had shown that the reaction

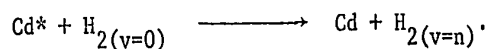


occurred when a mixture of cadmium and hydrogen was irradiated with 3261Å light. Since HgH bands had not been observed in the $Hg^* + H_2$ system early workers concluded that there was a fundamental difference between Hg^* and Cd^* photosensitization. Steacie and LeRoy (56) showed that with paraffins the analogous reaction

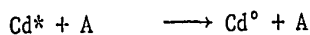


also occurred. The formation of CdH is energetically necessary since in hydrogen and paraffins containing only primary and secondary hydrogens, the H-R bond strengths are of the order of 100 kcal/mole, while the Cd* can only supply 87 kcal/mole. To make hydrogen abstraction energetically feasible, the 15.5 kcal/mole bond strength of CdH (57) must be utilized. In the case of mercury, energetic considerations do not necessitate the formation of HgH, and in fact HgH was not detected in the mercury photosensitization of hydrogen or paraffins until recently (31,32). CdH was not observed in the sensitization of ethylene although ethylene quenched Cd* very efficiently.

The first quantitative study of Cd* quenching was undertaken by Lipson and Mitchell (58) who applied the Stern-Volmer relation to fluorescence measurements. Although quenching measurements can not be extended to mechanistic interpretations, they discussed the possibility of a primary process in Cd* + H₂ leading to vibrationally excited H₂ rather than to bond cleavage:



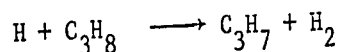
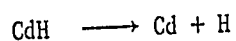
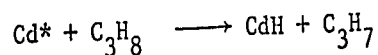
Lipson and Mitchell also discussed the possibility of spin-orbit relaxation from the Cd(³P₁) to the Cd(³P₀) states:



Should this reaction occur, the observed rate of quenching of Cd* would be faster than that of deactivation to the ground state. They concluded that it may be important as the reverse reaction would be slow.

Steacie and LeRoy (59) repeated Lipson and Mitchell's experiments, and extended this work to a greater range of compounds. Their results, together with those of Lipson and Mitchell, and some results for Hg* and Na(²P) are listed in Table I-II. Similar trends in quenching efficiency with the nature of the quencher are seen with all three sensitizers.

Agius and Darwent (60) studied the Cd* photosensitization of propane and found the quantum yield of hydrogen to be near unity over a wide range of pressures implying, along with other experimental data, the reactions:



They also discussed the possible role of Cd° concluding that since only 1.6 kcal/mole separate the spin states, any Cd* quenched to the Cd° state could be rapidly reactivated, and thus quenching by Cd° should be of little importance.

Sato and co-workers have carried out a systematic investigation on cadmium photosensitization reactions. In the Cd* photosensitization of acetylene (61), acetone (62), as well as some olefins (63,64) they found that the modes of decomposition generally paralleled those of Hg*, with minor discrepancies consistent with the smaller amount of energy available in Cd*. Relative rates of Cd* quenching (65-67) were measured using the butene-2 technique outlined earlier and the results, along with some for Hg*, triplet benzene, and triplet acetone, included for

TABLE I-II
Some Quenching Cross Sections for Cd, Hg, and Na (\AA^2)

Substrate	Cd(3P_1) ^a	Cd(3P_1) ^b	Hg(3P_1) ^c	Na(2P) ^d
H ₂	3.54	0.67	11.6	7.4
D ₂	1.80	0.19	16.1	
NH ₃	0.052	0.041	5.68	
C ₂ H ₄	24.9		27.3	44.0
C ₃ H ₆	29.1			52.0
1-C ₄ H ₈	35.2			58.0
2-C ₄ H ₈	30.6			58.0
C ₆ H ₆	28.4			75.0
C ₂ H ₂	22.0			
cyclo-C ₃ H ₆	0.71		2.16	

^aFrom reference (59).

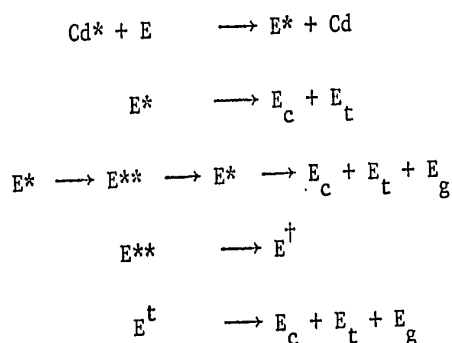
^bFrom reference (58).

^cFrom reference (7).

^dR. G. W. Norrish and W. MacF. Smith, Proc. Roy. Soc., A176,
295 (1940).

comparison, are shown in Table I-III. Sato et al. noted that trends in the quenching efficiency of Cd* follow those of Hg* but the absolute values are significantly different from those of triplet benzene or acetone despite the fact that the energies of Cd* and triplet benzene are very similar. They concluded that chemical and physical properties of the donor and acceptor such as electronic states and chemical affinities are the significant factors determining the properties of a sensitizer, rather than the amount of energy available in the sensitizer.

Sato et al. (63) studied the Cd* photosensitized interconversion of *cis*, *trans*, and *geminal* ethylene-d₂. These authors proposed three intermediates in the reaction of Cd* + ethylene, contrary to the situation in the analogous Hg* reaction where only two intermediates were necessary to satisfactorily explain the observed kinetics of the reaction (68). The mechanism proposed is:



where E represents any one of ethylene-d₂ isomers and E_c, E_t and E_g represent the *cis*, *trans*, and *geminal* ethylene-d₂ respectively. By analogy with the results for mercury, the authors identified E* and E** as triplet ethylene and triplet ethylidene and proposed that E[†]

TABLE I-III
Some Relative Quenching Efficiencies

Substrate	Cd(3P_1) ^a	Hg(3P_1) ^b	Benzene ^c	Acetone ^d
Ethylene	1.03	0.90	0.25	0.16
Propylene	1.18	0.93	0.47	0.33
1-Butene	1.08	0.51	0.33	
2-Butene	(1.00)*	(1.00)	(1.00)	(1.00)
Isobutene	1.11	0.95	1.27	0.66
Butadiene	1.13	0.93	15.	870.
Acetylene	1.03	0.83		0.015

* Quenching efficiencies are expressed relative to 2-butene.

^aFrom reference (65).

^bFrom reference (3), p. 67.

^cA. Morikawa and R. J. Cvetanovic, *Can. J. Chem.*, 46, 1813
(1968).

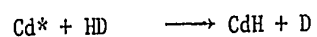
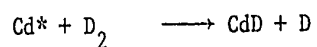
^dR. E. Rebbert and P. Ausloos, *J. Amer. Chem. Soc.*, 87, 5569
(1965).

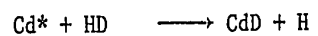
may be vibrationally excited ground state ethylene. The products of an extended photolysis are the three possible isomers produced in equal amounts regardless of the geometry of the starting dideuteroethylene. A similar study of Hunziker (69) largely confirmed the results of Sato et al., and lead to the postulation of the same three intermediates.

The quantum yield of ethylene decomposition in the Cd* photo-sensitization reaction is very small, of the order of 10^{-3} (64) since the excitation energy of Cd* is not high enough to produce triplet ethylidene with sufficient internal energy to undergo decomposition to any extent. The minor products detected; ethane, acetylene, and n-butane, are accounted for by the small degree of decomposition of triplet ethylidene to give acetylene and hydrogen, and subsequent reactions of these with Cd*.

Kalra and Knight (70,71) have studied the Cd* photosensitization of acetone and cyclohexane. The reaction with acetone produces a triplet acetone molecule which decomposes either directly or in two steps to give CO and two methyl radicals. As with other paraffins studied, the primary step in the Cd* photosensitization of cyclohexane is hydrogen abstraction, with a primary quantum yield of unity.

Breckenridge and Callear (26,27) have studied some reactions of Cd* and Cd° by flash photolysis and kinetic spectroscopy, and found that the relative rates of the reactions:

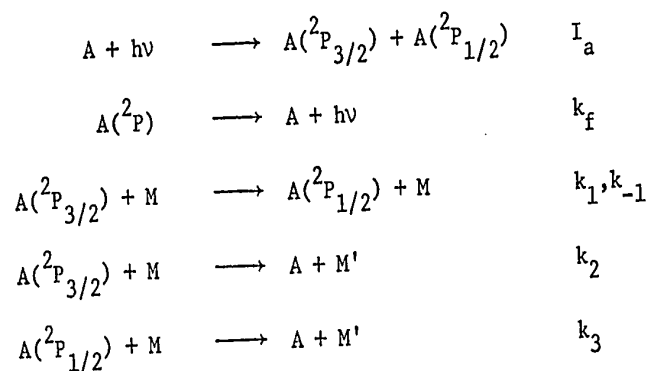




correlate very well with $\exp(-\Delta E_0/RT)$ where ΔE_0 is the change in internal energy of the reaction at 0°K. Since the results of this study are pertinent to the present work, they will be discussed in parallel, in Chapter V.

5. Other Metal Atoms Studied

Jenkins has carried out extensive studies on the quenching of alkali metals, thallium, and lead, in flames (72-76). The results of these physical measurements, obtained at temperatures between 1400 and 1800°K, are listed in Table I-IV. A kinetic analysis of the probable reaction mechanism for alkali metal atoms (A) was presented (77):



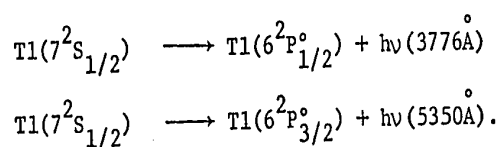
Jenkins showed that unless both the $^2P_{3/2}$ and $^2P_{1/2}$ emissions were separately monitored, the quenching rate obtained from the slope of Stern-Volmer plots would be a complex average of k_2 and k_3 , often including k_1 or k_{-1} . The exact form of this complex average would depend on the means of excitation, and the methods used to monitor the emission. If k_1 and k_{-1} are large compared to k_2 and k_3 , a valid assumption for measurements in flames, the data obtained from Stern-Volmer plots correspond to k_2 , or to the average value $(k_2 k_1 + k_3 k_{-1}) / (k_1 + k_{-1})$, if k_2 equals k_3 or not, respectively, regardless of the transition used to excite or monitor the metal. The author discussed the results in terms of Laidler's theory of ionic potential surfaces (41) but admitted that the lack of data allowing critical evaluation of

TABLE I-IV
 Quenching Cross Sections (\AA^2) from Jenkins (76)

Substrate	Li(^2P)	Na(^2P)	K(^2P)	Rb(^2P)	Cs(^2P)	Tl($^2\text{S}_{1/2}$)	Pb($^3\text{P}_1^0$)
H ₂	5.2	2.87	1.03	0.61	1.7	0.03	0.4
O ₂		12.3	15.5	25.		13.2	15.
N ₂	6.75	6.95	5.6	6.1	25.	6.4	5.7
CO	12.6	11.9	12.4	11.8		13.4	13.
CO ₂	9.2	17.0	21.4	24.0		32.5	29.
H ₂ O	1.9	0.5	0.9	1.27	5.5	1.75	8.
Ar	Small in all cases.						
He	Small in all cases.						

this theory severely restrict such interpretations.

Jenkins explained some of the large quenching cross sections in Table I-IV in terms of a chemical reaction between the excited metal atom and the substrate, for example $\text{Na}(^2\text{P}) + \text{CO}$, but this makes the small cross section observed for $\text{Tl}(^2\text{S}_{1/2}) + \text{H}_2$ exceptional in that reaction between $\text{Tl}(^2\text{P}_{1/2})$ and H_2 to form TlH is known (78). The $\text{Tl}(^2\text{P}_{1/2})$ state may undergo two radiative transitions:



Jenkins monitored only the 3776\AA transition and it will be shown that collisional effects which cannot be detected unless both transitions are monitored may cause erroneous results.

The measurements of Bellisio et al. (79) and those of McGillis and Krause (80) on Cs and Rb, obtained at much lower temperatures, confirmed Jenkins results.

Brus (28) has studied the quenching of $\text{Na}(^2\text{P})$ and of $\text{Tl}(^2\text{S}_{1/2})$ by I, I_2 , Br, Br_2 , and the respective metal halides at different velocities of the colliding species. He found that the quenching rate of $\text{Na}(^2\text{P})$ with I_2 decreases with increasing relative velocity, and discusses some of the results in terms of the molecular beam "harpooning" mechanism, a mechanism similar to the one proposed by Laidler (41). Brus pointed out that not all of his results were consistent with a harpooning mechanism, and discussed several of the quenching processes, for example $\text{Tl}^* + \text{TlI}$ where a stable complex is known to occur, in terms of chemical affinities. He concluded that no large activation energy is involved in the quenching process.

6. Flash Photolysis

Flash photolysis is an experimental technique for the rapid initiation of change and direct observation of the transient intermediates involved. It utilizes an intense flash of visible or ultraviolet radiation whose duration is short compared with that of the changes which are to be observed. By this means, a material of short lifetime may be produced in quantities large enough to be detected by absorption spectroscopy and other physical methods.

A typical flash photolysis arrangement consists of three parts:

1. A photolysis flash for producing a short pulse of light of very high intensity along with associated energy storage units - usually condensers - and equipment for charging and initiating the discharge (triggering).
2. A reaction vessel with associated thermostats and filters, and a reflector to condense light from the photolysis flash.
3. Some arrangement for physical detection and estimation of transient intermediates. Absorption spectroscopy is the method commonly adopted and the two principal techniques are as follows:
 - (a) A second spectroflash, of short duration, timed to fire at any required interval after the photolysis flash, and a spectrograph. The spectroflash gives essentially continuous light which records the absorption spectra of reaction intermediates photographically in a single flash of a few microseconds duration.
 - (b) A monochromatic source (e.g. a tungsten lamp and monochromator), the light from which is collimated and passed through the reaction vessel, an electronic

detector and a rapid recorder (e.g. photomultiplier cell and oscillograph).

Flash photolysis was developed by Porter and Norrish in 1947 (81,82) and since then has been used in a great many fields of chemistry and physics. A detailed account of the method and of the many hundreds of publications which describe its applications is beyond the scope of this introduction, and several reviews of flash photolysis have appeared recently (83,84). A brief outline demonstrating some types of applications of flash photolysis follows.

Flash photolysis has two major applications. (a) With this technique it is possible to record spectra of the excited states of molecules, and of unstable radical species generated by the photolysis flash. An example of the first is the determination of energies of the upper triplet levels of benzene, a problem which had eluded solution before the application of flash photolysis (85). Spectra of unstable species observed by means of flash photolysis include CH_2 and NH_2 , as well as many others, discussed in detail by Herzberg (57). In some instances these transient species can be produced by other means such as electric discharge or flames, but usually much better spectra and therefore much more information can be obtained under the mild conditions encountered in a flash system since relatively few reactive intermediates are produced.

(b) Flash photolysis has seen its greatest use in the study of fast reaction kinetics. A great variety of species, such as the excited states of stable molecules and atoms, as well as those of free radicals, have been studied by this method (83,84). Callear and

co-workers have studied many atomic species in the gas phase, generating them by flash photolysing some suitable parent compound. For example, the rates of spin-orbit relaxation of Fe, Se, and As have been measured, the metal atoms being produced by the flashing of $\text{Fe}(\text{CO})_5$, COSe , and AsCl_3 respectively. Davidovits (79) and Brus (28) studied the quenching of excited Na and Tl via the flash photolysis of the appropriate metal halide. Basco and Yee (86,87) generated metal atoms in their ground and excited states, and recorded the spectra of free radical intermediates from the flash photolysis of phosphine, arsine, and stibene, as well as the halides of these metals. The use of flash photolysis to study the quenching of mercury and cadmium has been mentioned, although in these cases the metal vapours were irradiated.

Techniques and instrumentation of flash photolysis are constantly improving. Time resolution is now well into the nanosecond region and rapidly proceeding into the picosecond range (88). Knowledge of fast reaction kinetics will continue to increase with the development of this technique to the theoretical limit of 10^{-14} sec.

7. Objectives of the Present Study

The quenching reactions of mercury are well documented and a comprehensive mechanism for the energy transfer process with paraffins and noble gases has emerged. Similarly, much work has been reported on the quenching reactions of cadmium and the alkali metals, but since the measurements were carried out at elevated temperatures, mechanistic interpretations cannot be derived with certainty. For similar reasons, only scattered reports on the gas phase quenching reactions of other metal atoms are available. In studies where metal vapour was created in the gas phase by flash photolysis, high temperatures were also necessary to produce sufficient vapour pressure of the parent compound and in these cases interference from unphotolyzed parent compound and other photolysis products often complicate the evaluation of experimental data.

Many metals form stable, volatile, alkyl-metal compounds. Their absorption spectra, usually a continuum in the far UV, are well known (89-91), and it has long been known that these metal-alkyls readily photodissociate to produce the metal atom and alkyl radicals (89). Studies of free radicals produced by the photodecomposition of zinc, cadmium, mercury, and lead alkyls have been extensively reported (92).

The photolysis of metal alkyls therefore appeared to be an excellent method of generating metal atoms in the gas phase; because of their high vapour pressures, experiments could be conducted at ambient temperatures and relatively simple kinetics should obtain.

Another interesting facet to this system is that the reactions of ground state atoms, about which little is known, can be examined.

It was therefore decided to begin a systematic study of the room temperature quenching reactions of Cd^* atoms produced by the flash photolysis of dimethylcadmium, to assess the role of Cd^0 atoms, and to elucidate the nature of the quenching processes within the framework of the Hg^* system.

Since the method proved successful, it was applied to the study of the quenching reactions of other metal atoms such as antimony and bismuth. Since this would have been the first systematic study of the gas phase quenching reactions of a variety of metal atoms measured under identical conditions, it was hoped that the energy transfer process could be rationalized in terms of such variables as electronic states of the metal atoms and physical parameters of the quenching atom.

CHAPTER II

EXPERIMENTAL

1. Materials

The materials used without purification, their sources and stated purities are listed in Table II-I. The alkyl-metal compounds were tested spectroscopically and found to be free of metal impurities. Argon was analyzed mass spectrometrically and found to be 99.8 mole % pure, the major impurity being nitrogen, with negligible amounts of water and oxygen. Materials which were purified, their sources and details of purification are listed in Table II-II.

Hydrogen and nitrogen were purified by passing the gas over hot copper turnings and then through a molecular sieve at -78°C . Oxygen in the H_2 or N_2 stream reacts to form water or copper oxide at the copper surface and water is removed by the molecular sieve. Mass spectrometric analysis showed both gases to be 99.9 mole % pure.

All gases condensable at -196°C were passed through repeated freeze-pump-thaw cycles.

TABLE II-I
Source and Purity of Materials Used

Compound	Source	Purity
$\text{Cd}(\text{CH}_3)_2$	Alfa Inorganics	See text
$\text{Zn}(\text{CH}_3)_2$	Alfa Inorganics	See text
$\text{Sb}(\text{CH}_3)_3$	Alfa Inorganics	See text
$\text{Bi}(\text{CH}_3)_3$	Alfa Inorganics	See text
Methane	Matheson	99.99 mole %
Ethylene	Phillips	99.98
Isobutane	Phillips	99.99
Propylene	Phillips	99.97
Hydrogen	Airco	Assayed Reagent Grade
Nitrogen	Airco	Assayed Reagent Grade
Oxygen	Airco	Assayed Reagent Grade
Ethane	Airco	Assayed Reagent Grade
CO	Airco	Assayed Reagent Grade
CO_2	Airco	Assayed Reagent Grade
Xe	Airco	Assayed Reagent Grade
Kr	Airco	Assayed Reagent Grade
Acetylene	Airco	Assayed Reagent Grade
D_2	Matheson	99.8%

TABLE II-II

Source and Purification of Materials

Compound	Source	Purification Method
<i>cis</i> and <i>trans</i> butene-2	Phillips	Separated by preparative gas chromatography
C_2H_3F	Matheson	Distilled from an isopentane slush
<i>cis</i> and <i>trans</i> $C_2H_2F_2$	Peninsular	Distilled from an isopentane slush and separated by preparative gas chromatography
1,1- $C_2H_2F_2$	Matheson	Distilled from an isopentane slush
C_2HF_3	Peninsular	Distilled from an n-pentane slush
C_2F_4	Matheson	Distilled from a methyl- cyclohexane slush
SiH_3CH_3	Merke, Sharp and Dohme	Distilled from an isopentane slush
Hydrogen	Canadian Liquid Air	See text
Nitrogen	Canadian Liquid Air	See text

2. Apparatus

a) Vacuum System

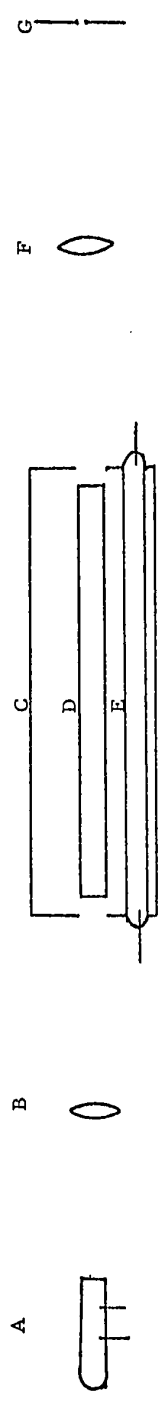
A conventional high vacuum system evacuated to 10^{-6} torr by a two-stage mercury diffusion pump was used for some gas handling and for evacuation of the cell. A mercury free high vacuum system evacuated to less than 10^{-6} torr by a three-stage oil diffusion pump was used for filling the flash lamps and handling the alkyl-metal compounds. Mercury manometers, a McLeod gauge, and Pirani tubes were used to measure pressures in the conventional vacuum system, and a Wallace and Tiernan absolute pressure gauge and Pirani tubes were used on the mercury-free system.

b) Flash Photolysis Apparatus

The flash photolysis apparatus consists of a thermostated reactor housing lined with aluminum, a flash photolysis lamp (photo-lamp), a flash spectroscopic lamp (spec-lamp) and the associated optical and electronic components.

i. Optical System

The optical system, illustrated in Figure 2-1, consists of the photo-lamp parallel to the cell; the spec-lamp, a collimating lens, the reaction cell, a focusing lens, and a Hilger-Watts large quartz spectrograph positioned along the optical axis. A Hilger-Watts medium quartz spectrograph was used for some determinations. The photo-lamp, 750 mm long and 22 mm in diameter, was filled with 50 torr of xenon. It was powered by a 60 μ F capacitor charged to 10 kilovolts or by a 15 μ F capacitor charged to 20 kV, both capacitors containing 3000 joules of energy. The spec-lamp, designed to approximate a point



- A. Spec-lamp
- B. Collimating lens
- C. Reaction housing
- D. Cell
- E. Photo-lamp
- F. Focusing lens
- G. Entrance slit of spectrograph

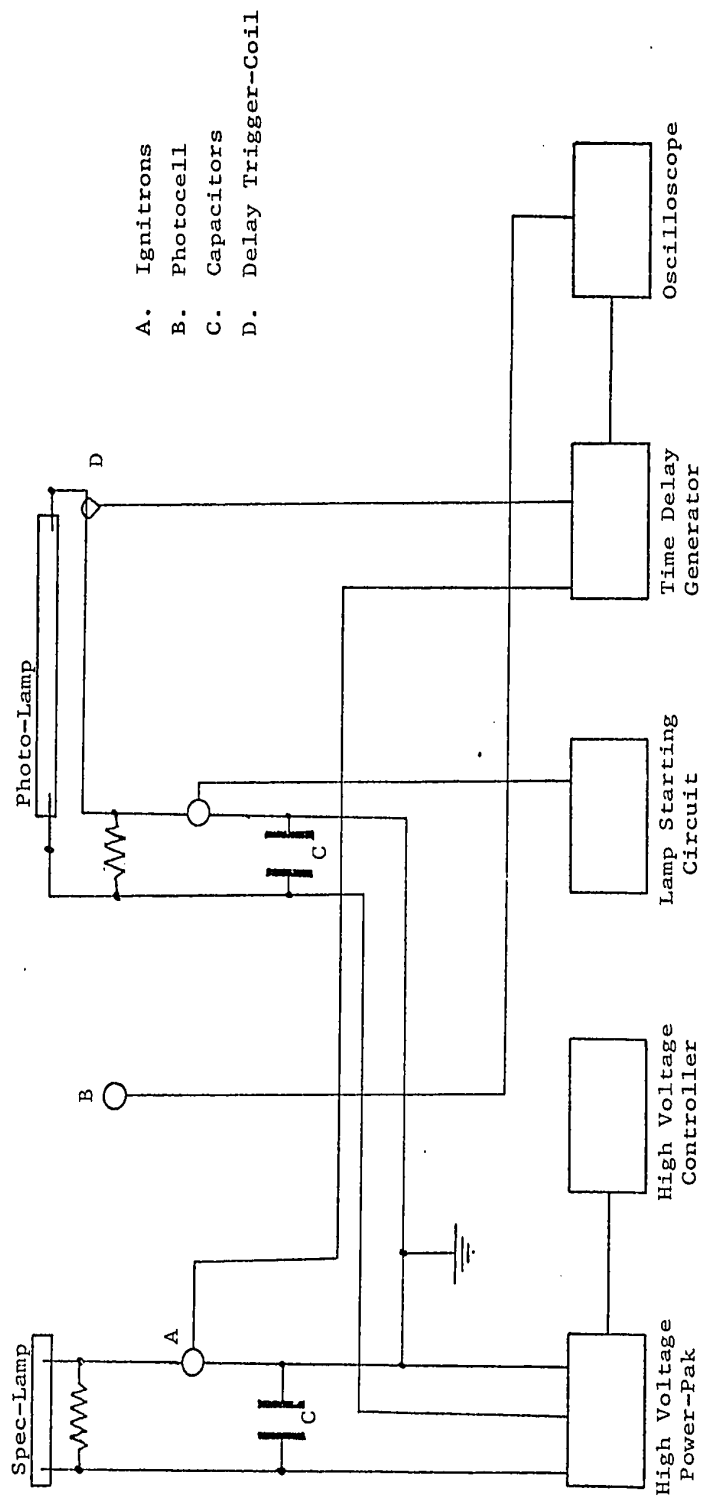
FIGURE 2-1: The Optical System.

source, was filled with 90 torr of xenon and powered by a 2.5 μF capacitor charged to 10 kV (125J). The spec-lamp output had a half-life of 11 μsec . The photo-lamp had a half-life of 23 or 12 μsec when operated at 10 or 20 kV respectively.

Spectra were recorded on Kodak 103a-0 plates. These were developed in Kodak D-19 developer according to the directions supplied. Numerical data were obtained by plate photometry employing a Joyce-Loebl Mark III recording microdensitometer.

ii. Electronics

The electronic components are illustrated schematically in Figure 2-2. This system can best be explained by describing the series of events occurring during one flash. The high voltage controller, consisting of switches, meters and safety devices, causes the power-pak to selectively charge the capacitors to the desired voltage. Closing a microswitch fires the ignitron in the photo-lamp circuit causing the capacitor to discharge through the photo-lamp. It is the light from this lamp which causes the physical and chemical changes being studied. The initiation of a current pulse in the photo-lamp circuit is detected by the delay trigger-coil which simultaneously triggers the delay generator and the horizontal sweep of the oscilloscope. After a selected period of time, the delay generator fires the ignitron in the spec-lamp circuit, and the spec-lamp fires. The continuum from this lamp passes through the cell and enters the spectrograph. A photocell monitors both flash lamps and its output is fed into the vertical axis of the oscilloscope; thus delay times can be checked. A camera with a Polaroid Land Camera back mounted on the oscilloscope allows a photographic record of delay times.



- A. Ignitrons
- B. Photocell
- C. Capacitors
- D. Delay Trigger-Coil

FIGURE 2-2: Schematic of the Electronic Components of the Flash Photolysis Apparatus.

3. Experimental Procedure

Gas mixtures were made up in storage bulbs at least eight hours before use. In some experiments where a different composition of gases was required for each flash, mixtures were made up in a calibrated mixing vessel, stirred for five minutes, and expanded into a cell of known volume. After each photolysis the cell was evacuated to less than 10^{-4} torr.

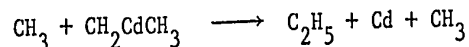
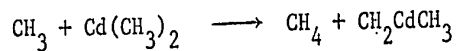
CHAPTER III

THE PHOTOLYSIS OF DIMETHYLCADMIUM

Dimethylcadmium (DMCd) exhibits a broad absorption continuum in the UV, with an absorption onset at approximately 2600\AA , depending on the pressure (91). The first and second carbon-cadmium bond strengths of DMCd are 46 and 22 kcal/mole respectively (93).

1. Reaction Products and Primary Process

Flash photolysis of DMCd produces ground state cadmium atoms (Cd) and methyl radicals, detected spectroscopically by their 3261\AA ($3P_1 \leftarrow 1S_0$) and 2160\AA (B + X) transitions respectively. The major products of the flash photolysis of large amounts of DMCd (>5 torr) were H_2 , CH_4 , C_2H_6 , and C_2H_4 ; some higher olefins and paraffins were produced to a minor extent. Similar results were reported for the conventional photolysis of DMCd (94). Ethylene and higher paraffins may be produced by the reaction sequence:



or by



and subsequent reactions of methylene and ethyl radicals with substrate or other photoproducts. When smaller amounts of DMCd (~ 0.5 torr) were photolysed in the presence of an inert diluent (100 - 700 torr), the

only product detected was ethane.

The production of Cd was shown to be a one photon process, as a plot of relative Cd concentration against flash energy is linear (Figure 3-1). The concentration of Cd was constant for more than one millisecond after reaching its maximum, the main mode of decay of the Cd being the formation of a particulate cadmium fog which was detectable after two milliseconds. Spectral bands attributable to Cd₂ (95) were not observed which is to be expected as the Cd-Cd bond strength is only 3 kcal/mole.

When more than two torr DMCD were flashed in the presence of more than 200 torr diluent, a new absorption spectrum, described in Tables III-I and III-II and shown in Figures 3-2 and 3-3 was detected. This spectrum appeared regardless of the nature of the diluent and therefore arises from DMCD photolysis. The concentration profile showed a maximum with flash energy (Figure 3-4) which indicated secondary photodecomposition and the pressure stabilization effects (Figure 3-5) suggested that the carrier is initially produced in a vibrationally excited state. Hydrocarbon diluents enhanced the intensity compared to that observed in inert diluents (Ar or CO₂), consistent with the relative deactivation efficiencies of these gases (96). An increase in intensity was also observed upon using longer wavelength irradiation, accomplished by replacing the quartz vessel ($\lambda > 2000\text{\AA}$) with a Vycor 790 cell ($\lambda > 2550\text{\AA}$). These facts are consistent with the assignment of this spectrum to CdCH₃.

Further justification for the assignment of this spectrum comes from the fact that in the flash photolysis of dimethylzinc a

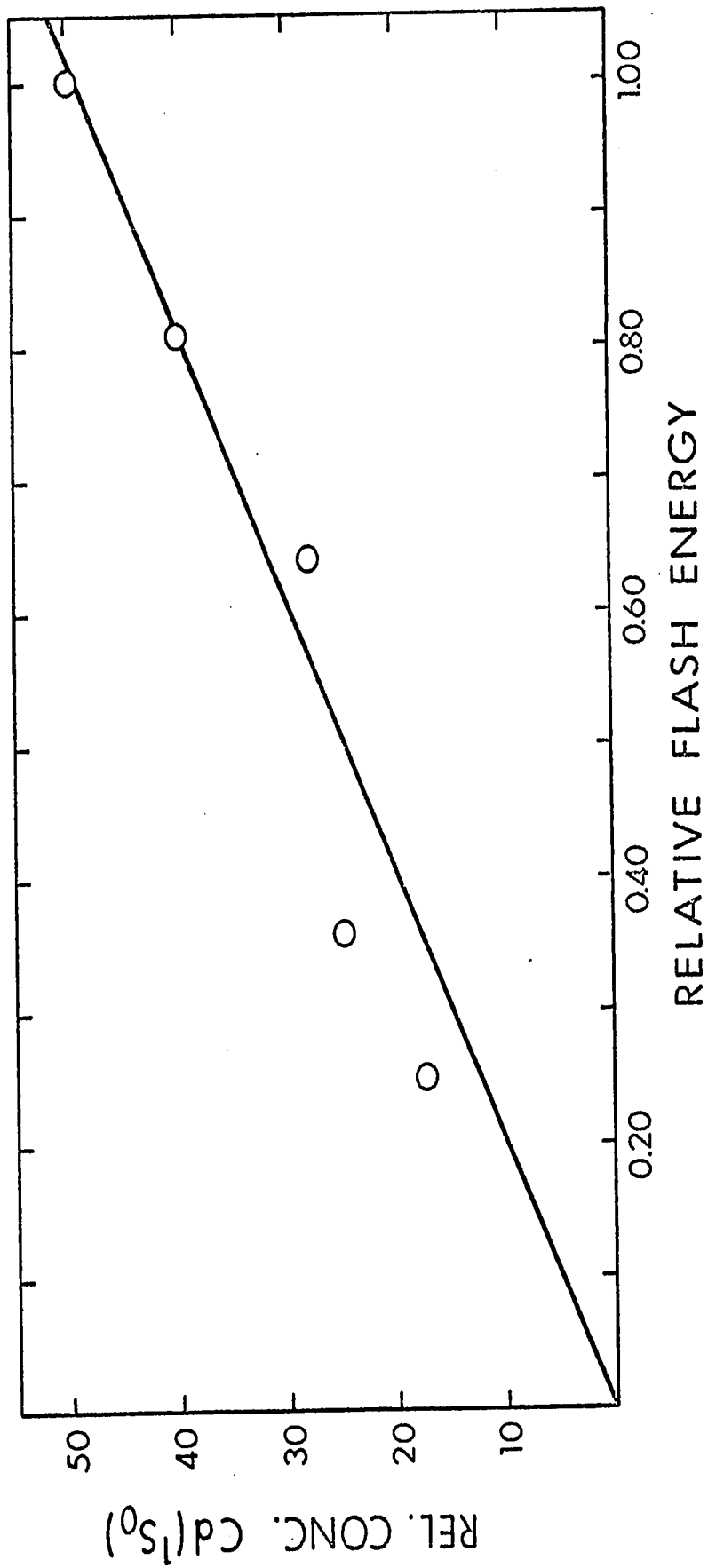


FIGURE 3-1: A Plot of Cd($1S_0$) vs Flash Energy.

TABLE III-I

The CdCH₃ (A + X) Spectrum

λ (Å)	Relative Intensity	ν (cm ⁻¹)	$\Delta\nu(\nu_3')$	$\Delta\nu(\nu_2')$
4443	10	22,507] 1022
4442	3	22,512		
4421	0.6	22,619(?)	403	
4365	3	22,910] 1019
4250	7	23,529	400] 999
4179	1.4	23,929		
4077	1.6	24,528] 984
4014	0.4	24,913	395	

TABLE III-II
The CdCH₃ (B ← X) Spectrum

$\lambda(\text{\AA})$	Relative Intensity	$\nu(\text{cm}^{-1})$	$\Delta\nu(\nu'_3)$	$\Delta\nu(\nu'_2)$
2864	10	24,916		
2863	5	34,928		
2858	2	24,990(?)	345	952
2836	0.5	35,261		

2788	8	35,868		984
2787	5	35,881		
2780	1.4	35,971(?)	377	
2759	0.5	36,245		

2715	4	36,832		964
2714	3	36,846		
2708	0.5	36,928(?)		

2646	2	37,793		961

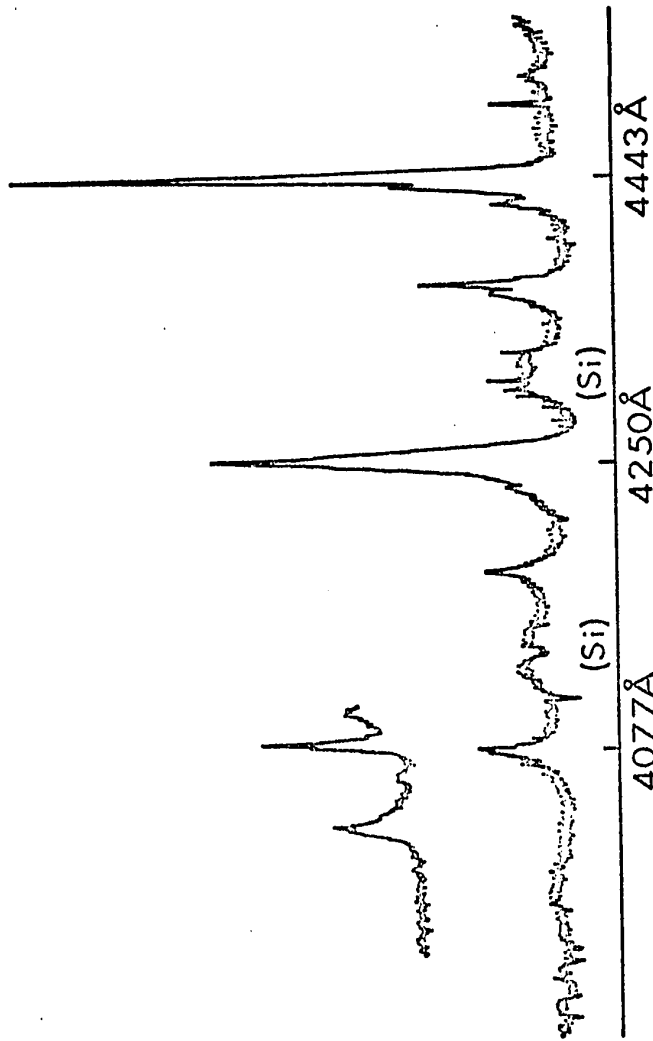


FIGURE 3-2: The CdCH₃ (A + X) Spectrum.

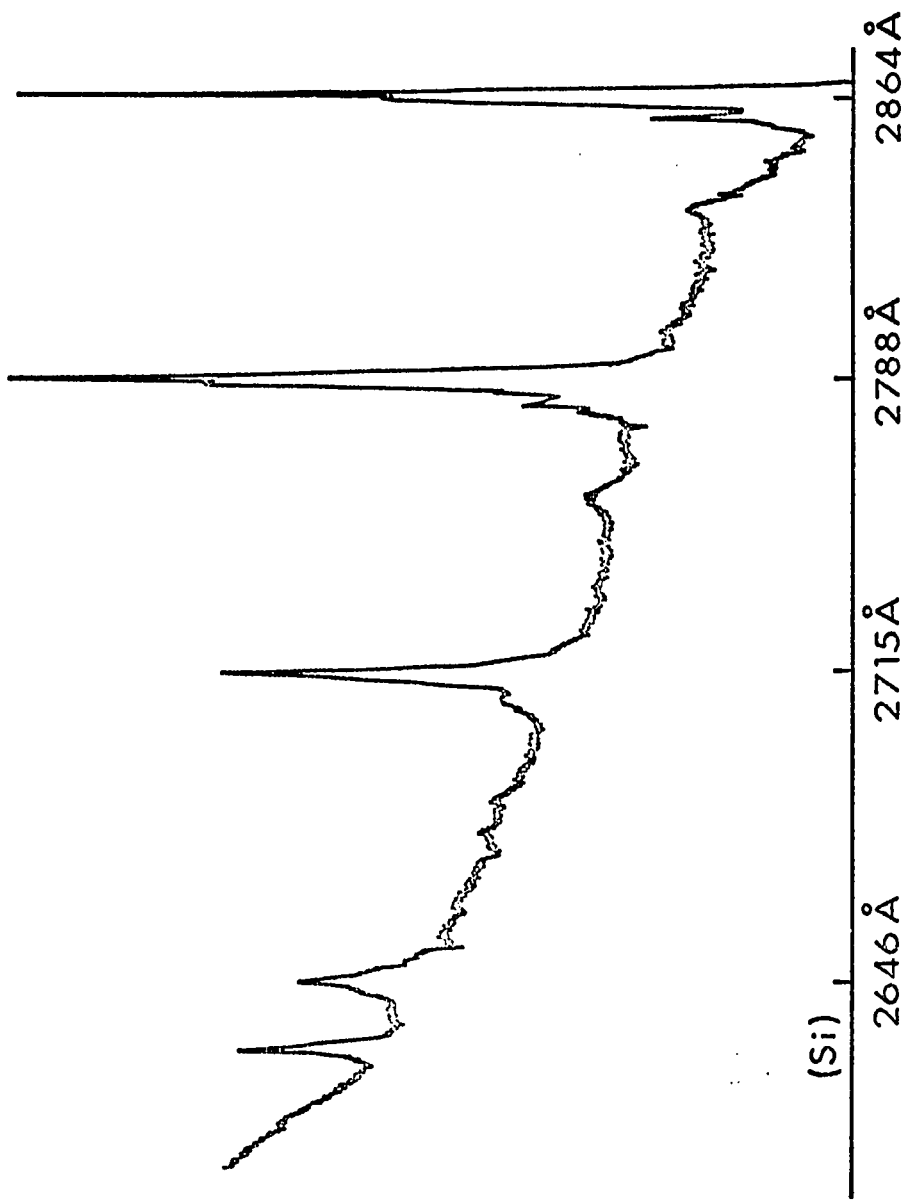


FIGURE 3-3: The CdCH₃ (B + X) Spectrum.

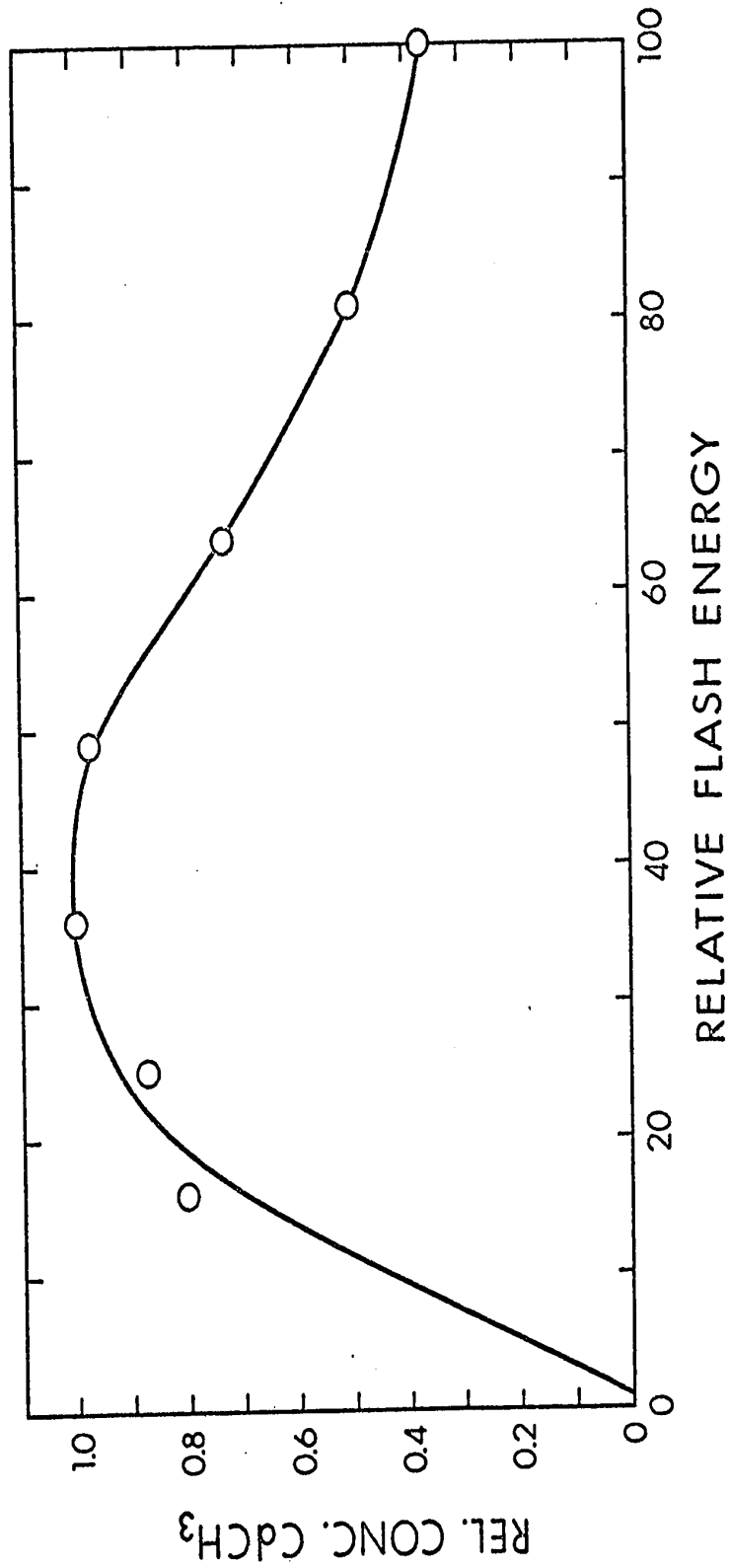


FIGURE 3-4: A Plot of [CdCH₃] vs Flash Energy.

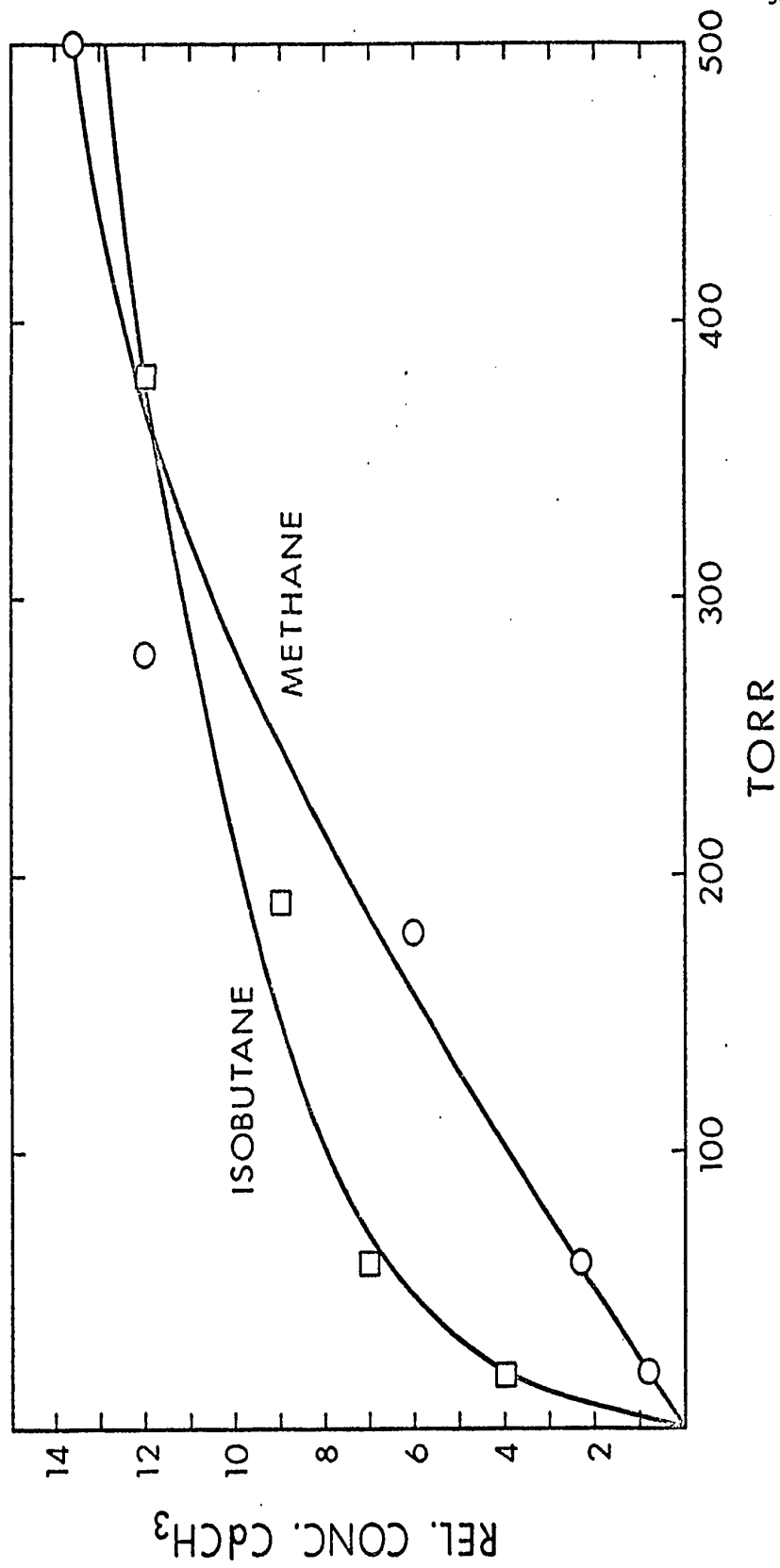


FIGURE 3-5: A Plot of $[CdCH_3]$ vs Pressure.

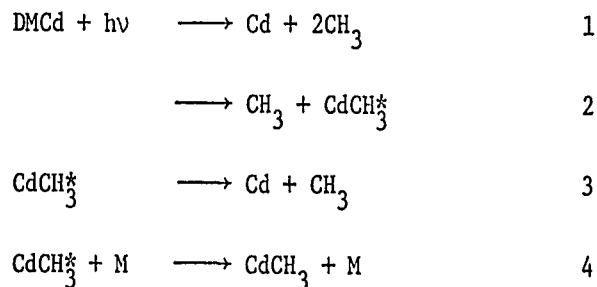
completely analogous spectrum, described in Tables III-III and III-IV and shown in Figures 3-6 and 7, was observed. The ZnCH_3 spectrum is more intense than that of CdCH_3 , consistent with the stronger Zn-C bond strength (93). Furthermore, the vibrational spacings of these spectra can be assigned to the usual CH_3 symmetric deformation modes (ν_2) and the X-C stretching modes (ν_3) observed in the spectra of other methyl containing compounds such as CH_3I (97).

There is no evidence for reactions such as:



since the addition of NO, an excellent radical scavenger, to the reaction mixture caused no change in the intensity of the CdCH_3 spectrum. Furthermore, in the photolysis of DMCd in the presence of radical (e.g. CF_3 , C_2H_5) sources no new spectra were observed.

The following mechanism satisfactorily explains the observed characteristics of the photolysis of DMCd :



It is not possible to establish whether step 1 or steps 2 + 3 is the primary mode of decomposition of DMCd . Reaction 2 does occur at least to a small extent. The minimum energy of radiation the DMCd absorbs corresponds to 111 kcal/mole. If the primary step were the

TABLE III-III
The ZnCH_3 (A \leftarrow X) Spectrum

$\lambda(\text{\AA})$	Relative Intensity	$\nu(\text{cm}^{-1})$	$\Delta\nu(\nu'_3)$	$\Delta\nu(\nu'_2)$
4175.6	10	23,949		
4174.3	9	23,956		
4157.0	0.5	24,056(?)		1070
			278	
4127.6	8	24,227		
4126.3	7	24,235		1057
4095.0	1	24,420(?)		

3997.0	3.5	24,019		
3996.0	2.5	24,025		
3983.0	<0.5	25,107(?)		
			265	
3956.7	2	25,274		
3955.0	1.75	25,284		1061

3834.4	0.5	26,080		1059
			263	
3796.1	<0.5	26,343		

TABLE III-IV
The ZnCH_3 (B + X) Spectrum

$\lambda(\text{\AA})$	Relative Intensity	$\nu(\text{cm}^{-1})$	$\Delta\nu(\nu'_2)$
2739	10	36,510	929
2671	8	37,439	978
2603	3	38,417	

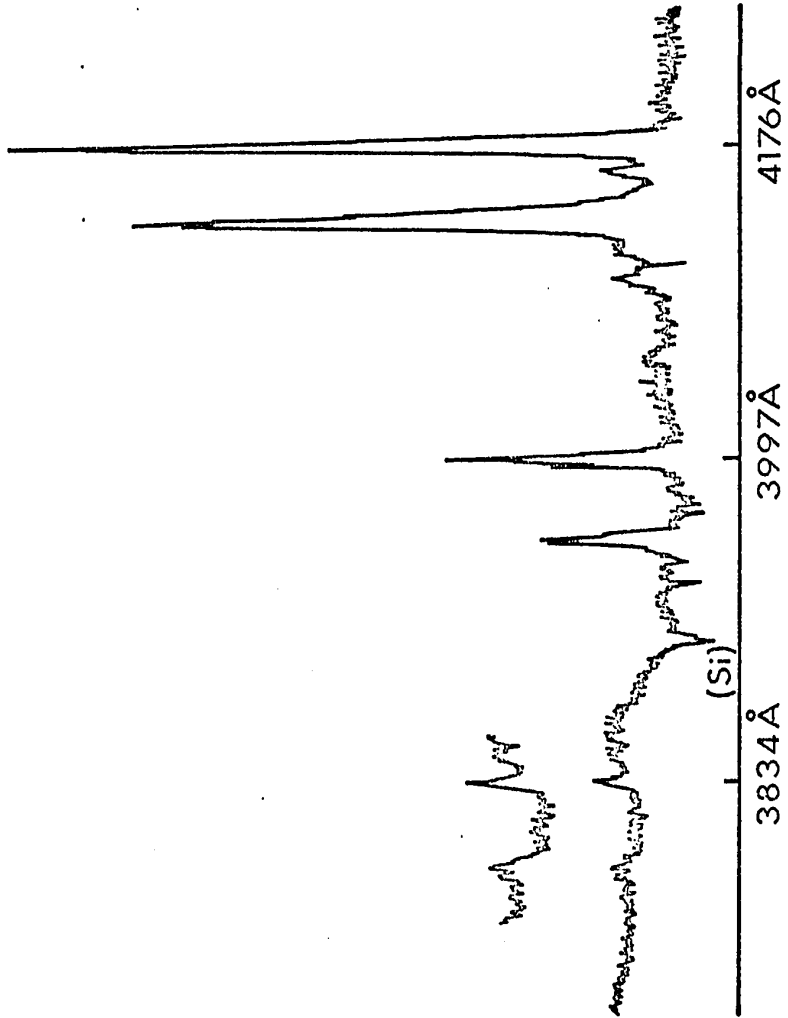


FIGURE 3-6: The ZnCH₃ (A + X) Spectrum.

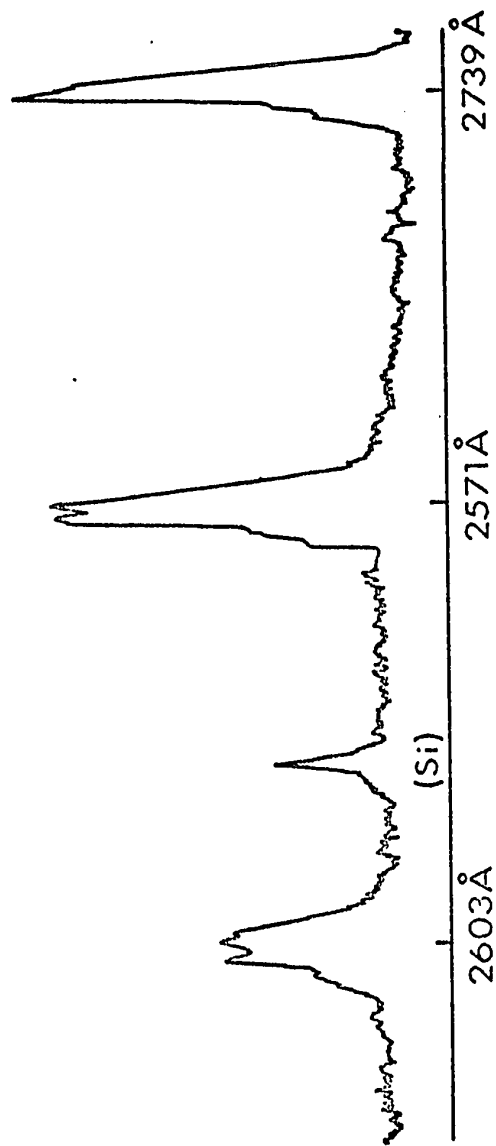
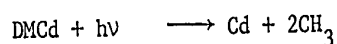


FIGURE 3-7: The ZnCH₃ (B + X) Spectrum.

rupture of one Cd-C bond, the fragments would contain more than 65 kcal/mole of excess energy and it is likely that CdCH_3 , with a Cd-C bond energy of 22 kcal/mole, would dissociate in a few vibrations. Whether step 1 is the major mode of decomposition or step 2 followed immediately by step 3, the net result is the same and the overall reaction is:



In the majority of experiments with DMCD, 0.5 torr of DMCD in 300 torr of a diluent was used. The diluent serves two purposes in flash photolysis experiments. It acts as a thermal buffer, preventing a rapid increase in temperature which could initiate pyrolysis of the reaction mixture; it also pressure broadens atomic lines, making them more readily detectable by absorption spectroscopy. Under these conditions the Cd concentration reaches a maximum 7 μsec after the initiation of the photo-flash, well before the photo-lamp reaches maximum intensity. This, together with the fact that no DMCD could be recovered from the photolysed mixture, indicates that the DMCD is completely dissociated in one flash. Since the rate of methyl radical recombination is very rapid (98), the only species present in the reaction cell in significant quantities within microseconds after the onset of the photoflash are Cd, C_2H_6 , and diluent.

Flashing a mixture of large amounts of DMCD (>5 torr) in an inert diluent, or normal mixtures of 0.5 torr DMCD in 300 torr of a hydrocarbon or hydrogen caused the 0,0 bands of the CdH ($A^2\Pi_{1/2,3/2} + X^3\Sigma$) spectrum (57) to appear. When mixtures of DMCD and a hydrocarbon

were photolysed the $\text{Cd}(^3\text{P}_{2,1,0})(\text{Cd}^3)$ states could be detected by their 3611, 3466 and 3404A transitions, respectively. See Figure 3-8. Whereas the collisional deactivation of $\text{Cd}(^3\text{P}_1)(\text{Cd}^*)$ to $\text{Cd}(^3\text{P}_0)(\text{Cd}^\circ)$ has been inferred from fluorescence measurements (99), this is the first system in which Cd° has been detected by absorption spectroscopy. The relative concentrations of the three spin states were in the order $^3\text{P}_2 \ll ^3\text{P}_1 < ^3\text{P}_0$. The maximum concentration of Cd° was formed when the diluent was methane; $\text{Cd}(^3\text{P}_{2,1,0})$ atoms were also formed in the presence of N_2 but in much lesser amounts. The photolysis of DMCd in the presence of D_2 or $n\text{-C}_4\text{D}_{10}$ also produced the analogous CdD spectrum. This again indicates that cadmium photosensitization is occurring since CdD could only be formed by the abstraction of deuterium by an excited cadmium atom.

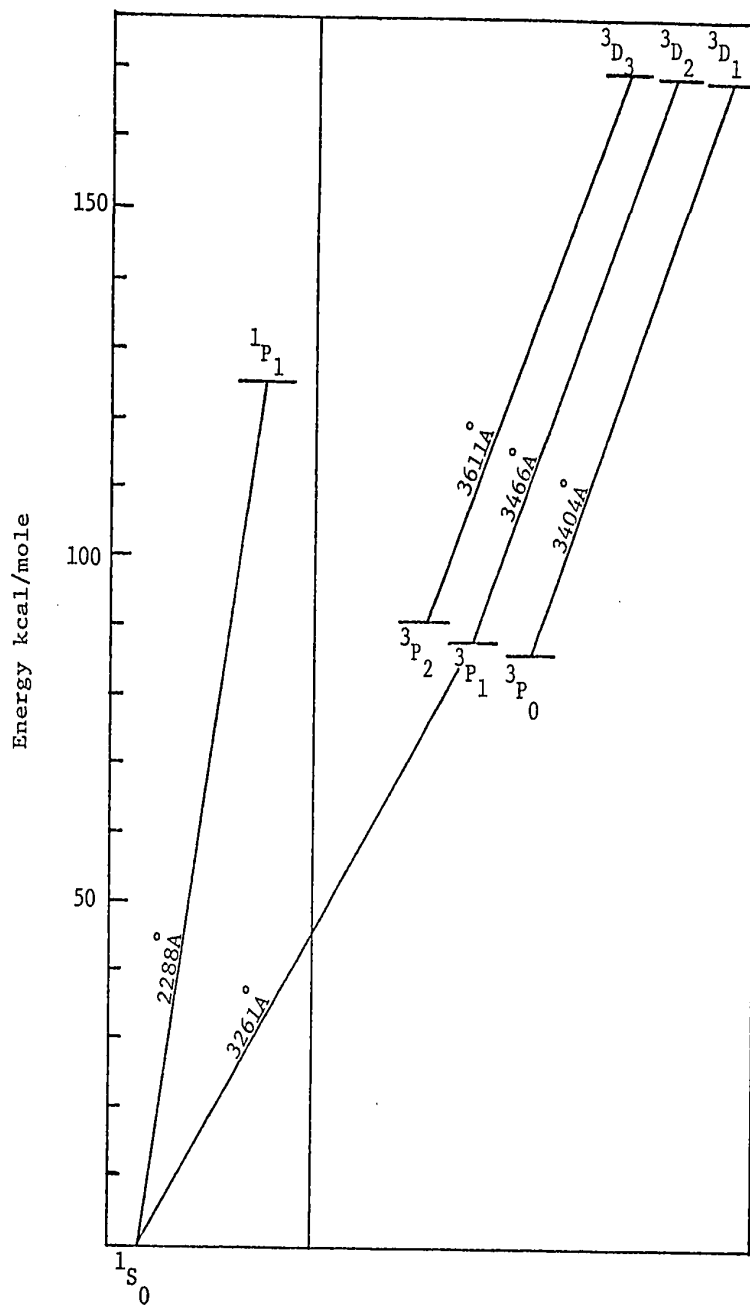


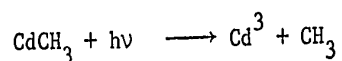
FIGURE 3-8: A Partial Grotrian Diagram for Cadmium.

2. Electronic States of Cadmium Atoms

Since electronically excited cadmium atoms were produced in the system, it was necessary to devise a series of auxiliary experiments which could characterize their mode of formation and subsequent decay.

a) It can be shown from energetic considerations that excited cadmium atoms are not produced in the primary photodecomposition of DMCD. The maximum energy absorbed by DMCD is 140 kcal/mole, corresponding to $2000\overset{\circ}{\text{A}}$, the effective quartz transmission limit. If energy is not lost into translational, rotational, or vibrational modes of the fragments, only 72 kcal/mole are available after rupture of both Cd-C bonds, and the lowest excited state of cadmium, the 3P_0 state, lies 86 kcal/mole above the ground state. Direct production of excited cadmium is therefore impossible.

b) Excited cadmium could be formed by secondary photolysis of CdCH_3 :



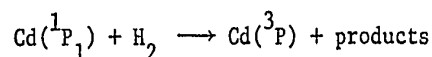
but this is unlikely as the concentration of CdCH_3 in these experiments is very small.

c) The excited cadmium is most likely produced by secondary absorption of light by ground state cadmium atoms.

When mixtures of DMCD (5 torr) in methane (300 torr) were flashed in a Pyrex cell ($\lambda > 3200\overset{\circ}{\text{A}}$) no Cd^3 was seen. (Under identical conditions, photolysis in a quartz vessel ($\lambda > 2000\overset{\circ}{\text{A}}$) produces substantial amounts of Cd^3 .) Next, absorption of $3261\overset{\circ}{\text{A}}$ radiation was eliminated by means of a concentric quartz jacket around the quartz cell filled with

a 50 mg/l water solution of 2,7-dimethyl-3,6-diazacyclohepta-1,6-diene perchlorate (UV dye). This solution has two strong absorption bands centered about 3200 and 2550Å and a window which transmits at 2288Å. Photolysis through this filter also yielded large amounts of Cd³. Thus Cd³ must be produced via the ¹P₁ state.

Breckenridge and Callear (27) propose an identical mechanism for formation of Cd³ in their experiments utilizing a cadmium resonance flash-lamp. They estimate the rate of the reaction



to be approximately $3 \times 10^{-10} \text{ cm}^3 \text{ molecules}^{-1} \text{ sec}^{-1}$. Analogous quenching of the ¹P₁ state of mercury to the ³P₁ level by H₂ and CO has been observed (100). It is therefore likely that the triplet state plays an important role in the Hg(¹P₁) photosensitization reactions of hydrocarbons as well (101,102).

Modes of decay of Cd³ will be discussed in conjunction with the results of quenching experiments described in Chapter V.

Table III-V summarizes all species observed in the flash photolysis of DMcd-hydrocarbon mixtures, and a mechanism consistent with all the experimental data follows:

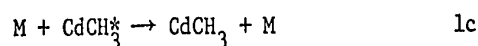
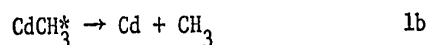
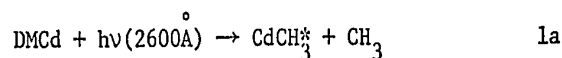
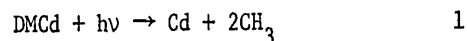
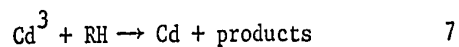
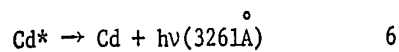
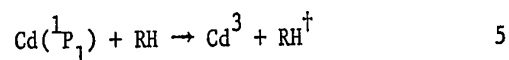
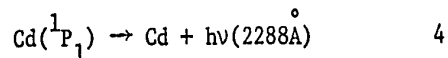
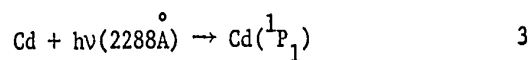


TABLE III-V
Species Observed in Flashed DMCD-CH₄ Mixtures

Species	Transition (Å)	Comments
Cd(¹ S ₀)	³ P ₁ ← ¹ S ₀ (3261)	Also ¹ P ₁ ← ¹ S ₀ (2288)
Cd(³ P ₀)	³ D ₁ ← ³ P ₀ (3404)	Also ⁷ S ₁ ← ³ P ₀ (3080)
Cd(³ P ₁)	³ D ₂ ← ³ P ₁ (3466)	Also ³ D ₁ ← ³ P ₁ (3468), weak
Cd(³ P ₂)	³ D ₃ ← ³ P ₂ (3611)	Very weak, only observed with high conc. of DMCD
CH ₃	B ← X (2160)	
CdH	A ← X (~4500)	See text
CdCH ₃	See Tables III-I, II	See text



The photolysis of DMCD produces ground state cadmium atoms and methyl radicals, the production of CdCH_3 being insignificant under most conditions. The ground state cadmium can be excited to the ${}^1\text{P}_1$ state by absorption of 2288Å light. $\text{Cd}({}^1\text{P}_1)$ may fluoresce; in the presence of a hydrocarbon or hydrogen, or to a lesser extent in nitrogen, it can be quenched to the ${}^3\text{P}$ states. The Cd^* may then fluoresce and the Cd^3 may be physically or chemically quenched.

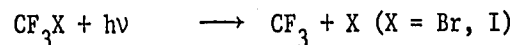
CHAPTER IV

THE UV SPECTRA OF CdBr, CdI, ZnBr, AND ZnI

In a series of publications from this laboratory the rates of combination of atomic mercury with chlorine, bromine, and iodine atoms, and the subsequent dimerization of the mercury halide molecules were reported. Their $A^2\Pi-X^2\Sigma$ spectra were analysed (103). It was decided to extend this investigation to cover the analogous reactions of zinc and cadmium atoms produced by the flash photolysis of DMCd and DMZn.

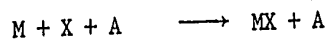
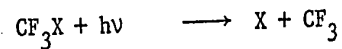
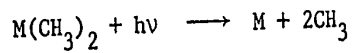
Weiland (104) investigated the emission spectra of CdBr, CdI, and ZnI some 40 years ago and analysed one component of the $2\Pi-2\Sigma$ system in each case. Recently Patel et al. (105) reported the analysis of the other $2\Pi-2\Sigma$ component of CdI. Ramasastry and Sreeramarty (105) observed the ZnBr ($A^2\Pi-X^2\Sigma$) system. These studies used flames or high voltage discharges as a source of the metal halide radicals. Under these harsh conditions poorer spectra with much more interference from other species were obtained.

In this work the source of halogen atoms was the photolysis of the appropriate trifluoromethyl halide:

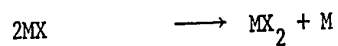


The co-photolysis of $M(CH_3)_2$ where M is Cd or Zn and CF_3X where X is a halogen leads to the appearance of the MX spectra. Under the conditions necessary for the spectra to be detected the formation and

decay of MX was too rapid to allow quantitative kinetic analysis in all cases studied. However, the following reactions were indicated by the experimental data:



Under conditions of excess metal atoms the decay was second order in MX



and with excess halogen it was first order:



Although quantitative analyses were impossible, the UV spectra of the four metal halides were recorded. In all cases the spectra obtained were more complete than those from any previous investigation, and much more accurate and complete vibrational analysis could thus be done. The ${}^2\Pi_{1/2} - {}^2\Sigma$ systems of CdBr and ZnI were observed and analysed for the first time. In all four metal halides examined, a Boltzmann distribution of states was observed.

1. The UV Spectra of Cadmium and Zinc Halides

a) The Absorption Spectrum of CdBr

Two band systems for CdBr lying in the regions 3114 - 3247Å and 3241 - 3374Å have been analysed (Tables IV-I and IV-II, Figure 4-1). The analysis of this spectrum leads to the following equations:

$${}^2\Pi_{3/2} - {}^2\Sigma$$

$$\begin{aligned} \nu = & 31,467.15 + 253.00(v'+1/2) - 0.70(v'+1/2)^2 \\ & - 233.80(v''+1/2) + 0.50(v''+1/2)^2 \dots \end{aligned}$$

$${}^2\Pi_{1/2} - {}^2\Sigma$$

$$\begin{aligned} \nu = & 30,301.31 + 253.00(v'+1/2) - 2.30(v'+1/2)^2 \\ & - 233.80(v''+1/2) + 2.25(v''+1/2)^2 \dots \end{aligned}$$

Calculated and observed band position are in agreement within $\pm 3 \text{ cm}^{-1}$ for these and all other spectra reported here.

The ${}^2\Pi_{3/2} - {}^2\Sigma$ component is the same as that observed by Wieland in emission and the values of upper and lower state vibrational frequencies obtained by the present analysis are in good agreement. The ${}^2\Pi_{1/2} - {}^2\Sigma$ component, observed here for the first time, is very similar in terms of ω_e' and ω_e'' , and the ${}^2\Pi$ splitting constant obtained, 1165.8 cm^{-1} , is close to the expected value of 1140 cm^{-1} (106).

b) The Absorption Spectrum of CdI

Vibrational analysis of the many bands observed in the CdI spectrum, listed in Tables IV-III and IV-IV and shown in Figure 4-2, yielded the following equations:

TABLE IV-I
The ${}^2\Pi_{3/2}-{}^2\Sigma$ System of CdBr

λ (Å)	Int	ν_{vac} (cm $^{-1}$)		(v', v'')
		Obs	Calc	
3246.9	1	30,789.8	30,791.1	(0,3)
3243.9	0	30,818.2	30,815.7	(1,4)
3241.8	<1	30,838.2	30,839.9	(2,5)
3239.6	0	30,859.1	30,863.7	(3,6)
3236.5	<1	30,888.7	30,887.1	(4,7)
3234.0	0	30,912.6	30,910.1	(5,8)
3231.6	1	30,935.5	30,932.7	(6,9)
3229.1	0	30,959.5	30,954.9	(7,10)
3227.9	<1	30,971.0	30,976.7	(8,11)
3225.2	0	30,996.9	30,998.1	(9,12)
3223.1	0	31,017.1	31,019.1	(0,2)
3220.7	<1	31,040.2	31,042.7	(1,3)
3217.9	<1	31,067.2	31,065.9	(2,4)
3215.9	0	31,086.5	31,088.7	(3,5)
3213.0	0	31,114.6	31,111.1	(4,6)
3210.8	0	31,135.9	31,133.1	(5,7)
3208.4	<1	31,159.2	31,154.7	(6,8)
3206.2	<1	31,180.6	31,175.9	(7,9)
3204.4	0	31,198.1	31,198.1	(8,10)
3201.8	0	31,223.4	31,217.1	(9,11)
3199.3	4	31,247.8	31,248.1	(0,1)
3197.0	4	31,270.3	31,270.7	(1,2)
3194.8	3	31,291.8	31,292.9	(2,3)
3192.5	1	31,314.4	31,314.7	(3,4)
3190.3	1	31,336.0	31,336.1	(4,5)
3188.3	<1	31,355.6	31,357.1	(5,6)
3186.3	0	31,375.3	31,377.7	(6,7)
3183.9	0	31,399.0	31,397.9	(7,8)
3182.4	0	31,413.8	31,417.7	(8,9)
3175.9	10	31,478.1	31,478.1	(0,0)
3173.7	9	31,499.9	31,499.7	(1,1)
3171.4	4	31,522.7	31,520.9	(2,2)
3169.6	1	31,540.6	31,541.7	(3,3)
3167.6	1	31,560.5	31,562.1	(4,4)
3165.6	0	31,580.5	31,582.1	(5,5)
3163.7	1	31,599.4	31,601.7	(6,6)
3161.4	1	31,622.4	31,620.9	(7,7)
3159.8	1	31,638.4	31,639.7	(8,8)
3157.2	2	31,664.5	31,658.1	(9,9)
3150.8	7	31,728.8	31,729.7	(1,0)
3148.7	7	31,750.0	31,749.9	(2,1)
3146.6	5	31,771.2	31,769.7	(3,2)

TABLE IV-I (cont'd)
 The $^2\Pi_{3/2}-^2\Sigma$ System of CdBr

$\lambda(\text{\AA})$	Int	$\nu_{\text{vac}} (\text{cm}^{-1})$		(ν', ν'')
		Obs	Calc	
3145.0	3	31,787.3	31,789.1	(4,3)
3142.5	3	31,812.6	31,808.1	(5,4)
3141.2	1	31,825.8	31,826.7	(6,5)
3139.3	0	31,845.0	31,844.9	(7,6)
3137.7	1	31,861.3	31,862.7	(8,7)
3135.7	1	31,881.6	31,880.1	(9,8)
3126.2	1	31,978.5	31,979.9	(2,0)
3124.4	1	31,998.9	31,998.7	(3,1)
3122.4	0	32,017.4	32,017.1	(4,2)
3120.4	0	32,037.9	32,035.1	(5,3)
3118.8	0	32,054.3	32,052.7	(6,4)
3117.1	0	32,071.8	32,069.9	(7,5)
3115.6	0	32,087.3	32,086.7	(8,6)
3114.3	0	32,100.7	32,103.1	(9,7)

TABLE IV-II
The $2\Pi_{1/2}-2\Sigma$ System of CdBr

$\lambda(\text{\AA})$	Int	$\nu_{\text{vac}}(\text{cm}^{-1})$		(v', v'')
		Obs	Calc	
3373.2	<1	29,637.0	29,636.5	(0,3)
3369.1	0	29,673.0	29,669.1	(1,4)
3365.4	0	29,705.6	29,701.6	(2,5)
3362.0	<1	29,735.7	29,734.0	(3,6)
...	29,856.8	(0,2)
3345.3	<1	29,884.1	29,884.9	(1,3)
3342.1	0	29,912.7	29,912.9	(2,4)
3338.7	0	29,943.2	29,940.8	(3,5)
3335.4	0	29,972.8	29,968.6	(4,6)
3334.0	0	29,994.4	29,996.3	(5,7)
3330.1	<1	30,020.5	30,023.9	(6,8)
3326.8	<1	30,050.3	30,051.4	(7,9)
3323.4	2	30,081.0	30,081.6	(0,1)
3319.7	1	30,114.6	30,105.2	(1,2)
3317.7	1	30,132.7	30,128.7	(2,3)
3315.7	1	30,150.9	30,152.1	(3,4)
3311.9	<1	30,185.5	30,175.4	(4,5)
3310.6	<1	30,197.3	30,198.6	(5,6)
3308.4	1	30,217.4	30,221.7	(6,7)
3305.1	2	30,247.6	30,244.7	(7,8)
3303.5	2	30,262.2	30,267.6	(8,9)
3300.1	3	30,293.4	30,290.4	(9,10)
3298.2	10	30,310.9	30,310.9	(0,0)
3295.7	7	30,331.1	30,330.0	(1,1)
3294.2	4	30,347.7	30,349.0	(2,2)
3292.0	2	30,368.0	30,367.9	(3,3)
3289.7	1	30,389.2	30,386.7	(4,4)
3288.0	<1	30,404.9	30,405.4	(5,5)
3286.1	0	30,422.5	30,424.0	(6,6)
3284.5	0	30,437.3	30,442.5	(7,7)
3282.0	<1	30,460.5	30,460.9	(8,8)
3280.3	<1	30,476.3	30,479.2	(9,9)
3271.4	<1	30,559.2	30,559.3	(1,0)
3270.4	<1	30,568.5	30,573.8	(2,1)
3268.6	1	30,585.4	30,588.2	(3,2)
3267.3	1	30,597.5	30,602.5	(4,3)
3265.4	1	30,615.3	30,616.7	(5,4)
3263.5	2	30,633.1	30,630.8	(6,5)
3262.0	4	30,647.2	30,644.8	(7,6)
3245.6	0	30,802.1	30,803.1	(2,0)
3244.1	0	30,816.3	30,813.0	(3,1)
3243.3	<1	30,823.9	30,822.8	(4,2)
3242.4	<1	30,832.5	30,832.5	(5,3)
3241.0	<1	30,845.8	30,842.1	(6,4)

TABLE IV-III
 The $2\Pi_{3/2}-2\Sigma$ System of CdI^a

$\lambda(\text{\AA})$	Int	$\nu_{\text{vac}}(\text{cm}^{-1})$		(ν', ν'')
		Obs	Calc	
3567.7	1	28,021.3	28,021.4	(0,9)
3562.8	5	28,059.8	28,057.4	(1,10)
3558.1	2	28,096.9	28,093.4	(2,11)
3554.1	1	28,128.5	28,129.4	(3,12)
3549.9	0	28,161.8	28,165.4	(4,13)
3544.3	1	28,206.3	28,201.4	(5,14)
3547.4	0	28,181.6	28,182.4	(0,8)
3542.6	1	28,219.8	28,216.4	(1,9)
3538.5	(6)	28,252.5	28,250.4	(2,10)
3535.2	1	28,278.9	28,284.4	(3,11)
3529.6	0	28,323.8	28,318.4	(4,12)
3526.3	1	28,350.3	28,352.4	(5,13)
3521.5	2	28,388.9	28,386.4	(6,14)
3527.1	1	28,343.8	28,345.4	(0,7)
3522.7	2	28,379.2	28,377.4	(1,8)
3519.0	3	28,409.1	28,409.4	(2,9)
3515.3	2	28,439.0	28,441.4	(3,10)
3510.8	1	28,475.4	28,473.4	(4,11)
3506.9	<1	28,507.1	28,510.4	(0,6)
3503.3	0	28,536.4	28,540.4	(1,7)
3499.0	0	28,571.4	28,570.4	(2,8)
3495.8	<1	28,597.6	28,600.4	(3,9)
3491.3	0	28,634.5	28,630.4	(4,10)
3487.9	0	28,662.4	28,660.4	(5,11)
3483.8	0	28,696.1	28,690.4	(6,12)
3480.7	<1	28,721.7	28,720.4	(7,13)
3477.2	2	28,750.6	28,750.4	(8,14)
3473.9	1	28,777.9	28,780.4	(9,15)
3470.1	2	28,809.4	28,810.4	(10,16)
3485.8	<1	28,679.6	28,677.4	(0,5)
3483.0	<1	28,702.7	28,705.4	(1,6)
3479.0	1	28,735.7	28,733.4	(2,7)
3475.8	2	28,762.2	28,761.4	(3,8)
3471.6	2	28,796.9	28,789.4	(4,9)
3468.9	<1	28,819.4	28,817.4	(5,10)
3465.4	<1	28,848.5	28,846.4	(0,4)
3462.4	0	28,873.5	28,872.4	(1,5)
3458.8	<1	28,903.5	28,898.4	(2,6)
3456.2	1	28,925.3	28,924.4	(3,7)
3453.4	2	28,948.7	28,950.4	(4,8)
3449.9	3	28,978.1	28,976.4	(5,9)
3446.7	1	29,005.0	29,002.4	(6,10)
3444.2	<1	29,026.0	29,028.4	(7,11)

TABLE IV-III (cont'd)
 The $^2\Pi_{3/2}-^2\Sigma$ System of CdI^a

λ (Å)	Int	ν_{vac} (cm ⁻¹)		(v',v'')
		Obs	Calc	
3440.7	1	29,055.6	29,054.4	(8,12)
3437.7	0	29,080.9	29,080.4	(9,13)
3434.6	1	29,107.2	29,106.4	(10,14)
3431.9	1	29,130.1	29,132.4	(11,15)
3444.9	<1	29,020.1	29,017.4	(0,3)
3442.4	1	29,041.2	29,041.4	(1,4)
3439.2	1	29,068.2	29,065.4	(2,5)
3437.0	0	29,086.8	29,089.4	(3,6)
3433.7	1	29,114.8	29,113.4	(4,7)
3430.7	1	29,140.2	29,137.4	(5,8)
3428.3	<1	29,160.6	29,161.4	(6,9)
3425.2	1	29,187.0	29,185.4	(7,10)
3424.8	1	29,190.4	29,190.4	(0,2)
3422.4	1	29,210.1	29,212.4	(1,3)
3420.0	2	29,231.4	29,234.4	(2,4)
3417.5	1	29,252.8	29,256.4	(3,5)
3414.4	<1	29,279.4	29,278.4	(4,6)
3411.7	<1	29,302.5	29,300.4	(5,7)
3409.6	0	29,320.6	29,322.4	(6,8)
3406.8	<1	29,344.7	29,344.4	(7,9)
3403.9	(4)	29,369.7	29,366.4	(8,10)
3401.8	(4)	29,387.8	29,388.4	(9,11)
3398.7	2	29,416.3	29,410.4	(10,12)
3396.3	1	29,435.4	29,432.4	(11,13)
3394.2	1	29,453.6	29,454.4	(12,14)
3391.6	1	29,476.2	29,476.4	(13,15)
3389.2	1	29,497.1	29,498.4	(14,16)
3404.5	5	29,364.5	29,365.4	(0,1)
3402.2	5	29,384.3	29,385.4	(1,2)
3400.3	4	29,400.8	29,405.4	(2,3)
3397.5	2	29,425.0	29,425.4	(3,4)
3395.0	1	29,446.7	29,445.4	(4,5)
3393.5	1	29,459.7	29,465.4	(5,6)
3390.9	1	29,482.3	29,485.4	(6,7)
3387.9	1	29,508.4	29,505.4	(7,8)
3386.2	<1	29,523.2	29,525.4	(8,9)
3383.4	(8)	29,547.6	29,545.4	(9,10)
3381.3	(5)	29,566.0	29,565.4	(10,11)
3378.6	2	29,589.6	29,585.4	(11,12)
3384.0	10	29,542.4	29,542.4	(0,0)
3381.9	7	29,560.7	29,560.4	(1,1)
3379.8	3	29,579.1	29,578.4	(2,2)
3377.2	<1	29,601.9	29,596.4	(3,3)

TABLE IV-III (cont'd)
 The $2\Pi_{3/2}-2\Sigma$ System of CdI^a

$\lambda(\text{\AA})$	Int	$\nu_{\text{vac}}(\text{cm}^{-1})$		(v',v'')
		Obs	Calc	
3375.8	<1	29,614.1	29,614.4	(4,4)
3374.1	<1	29,629.1	29,632.4	(5,5)
3371.9	<1	29,648.4	29,650.4	(6,6)
3370.1	<1	29,664.2	29,668.4	(7,7)
3367.9	<1	29,683.6	29,686.4	(8,8)
3366.0	0	29,700.4	29,704.4	(9,9)
3363.6	0	29,721.5	29,722.4	(10,10)
3361.8	6	29,737.5	29,737.4	(1,0)
3360.1	7	29,752.5	29,753.4	(2,1)
3358.4	5	29,767.6	29,769.4	(3,2)
3356.3	4	29,786.2	29,785.4	(4,3)
3354.3	2	29,803.9	29,801.4	(5,4)
3352.7	<1	29,818.2	29,817.4	(6,5)
3351.5	<1	29,828.8	29,833.4	(7,6)
3349.3	0	29,848.4	29,849.4	(8,7)
3348.0	0	29,860.0	29,865.4	(9,8)
3345.4	0	29,883.2	29,881.4	(10,9)
3343.5	0	29,900.2	29,897.4	(11,10)
3341.7	0	29,816.3	29,813.4	(12,11)
3340.0	1	29,931.5	29,930.4	(2,0)
3337.9	3	29,950.4	29,944.4	(3,1)
3336.8	3	29,960.2	29,958.4	(4,2)
3335.2	3	29,974.6	29,972.4	(5,3)
3333.8	2	29,987.2	29,986.4	(6,4)
3332.2	2	30,001.6	30,000.4	(7,5)
3330.7	1	30,015.1	30,014.4	(8,6)
3329.4	<1	30,026.8	30,028.4	(9,7)
3327.7	<1	30,042.2	30,042.4	(10,8)
3326.7	0	30,051.2	30,056.4	(11,9)
3324.7	0	30,069.3	30,070.4	(12,10)
3322.9	0	30,085.6	30,084.4	(13,11)
3321.7	0	30,096.4	30,098.4	(14,12)
3320.1	<1	30,110.9	30,112.4	(15,13)
3317.0	1	30,139.1	30,140.4	(17,15)
3315.3	1	30,154.5	30,154.4	(18,16)
3319.2	<1	30,119.1	30,121.4	(3,0)
3318.7	<1	30,132.7	30,133.4	(4,1)
3316.6	1	30,142.7	30,145.4	(5,2)
3314.7	2	30,160.0	30,157.4	(6,3)
3314.2	2	30,164.5	30,169.4	(7,4)
3312.7	2	30,178.2	30,181.4	(8,5)
3311.4	2	30,190.0	30,193.4	(9,6)
3310.0	1	30,202.8	30,205.4	(10,7)

TABLE IV-III (cont'd)
 The $2\Pi_{3/2}-2\Sigma$ System of CdI^a

$\lambda(\text{\AA})$	Int	$\nu_{\text{vac}}(\text{cm}^{-1})$		(v',v'')
		Obs	Calc	
3308.0	<1	30,221.1	30,217.4	(11,8)
3307.2	<1	30,228.4	30,229.4	(12,9)
3306.0	1	30,259.4	30,241.4	(13,10)
3304.3	<1	30,254.9	30,253.4	(14,11)
3303.3	<1	30,264.1	30,265.4	(15,12)
3301.7	<1	30,278.7	30,277.4	(16,13)
3300.6	0	30,288.8	30,289.4	(17,14)
3299.2	0	30,301.7	30,301.4	(18,15)
3298.1	0	30,311.8	30,310.4	(4,0)
3296.9	0	30,322.8	30,320.4	(5,1)
3296.4	0	30,327.4	30,330.4	(6,2)
3294.6	<1	30,344.0	30,340.4	(7,3)
3294.0	0	30,349.5	30,350.4	(8,4)
3292.9	0	30,359.7	30,360.4	(9,5)
3291.4	<1	30,373.5	30,370.4	(10,6)
3290.5	<1	30,381.8	30,380.4	(11,7)
3289.6	1	30,390.1	30,390.4	(12,8)
3288.3	<1	30,402.1	30,400.4	(13,9)
3287.4	<1	30,410.4	30,410.4	(14,10)
3286.4	1	30,419.7	30,420.4	(15,11)
3285.1	1	30,431.7	30,430.4	(16,12)
3284.0	1	30,411.9	30,440.4	(17,13)
3283.2	<1	30,449.3	30,450.4	(18,14)
3281.9	<1	30,461.4	30,460.4	(19,15)
3280.8	<1	30,471.6	30,470.4	(20,16)

^a Intensities given in parentheses are shoulders.

TABLE IV-IV
The $2\Pi_{1/2}-2\Sigma$ System of CdI^a

$\lambda(\text{\AA})$	Int	$\nu_{\text{vac}}(\text{cm}^{-1})$		(ν', ν'')
		Obs	Calc	
3629.9	<1	27,541.1	27,542.2	(0,4)
3627.4	0	27,560.1	27,561.2	(1,5)
3624.7	0	27,580.7	27,580.2	(2,6)
3621.5	1	27,605.0	27,599.2	(3,7)
3619.6	1	27,619.5	27,618.2	(4,8)
3617.4	<1	27,636.3	27,637.2	(5,9)
...	27,656.2	(6,10)
3612.8	<1	27,671.5	27,675.2	(7,11)
3609.8	0	27,694.5	27,694.2	(8,12)
3607.2	0	27,714.5	27,713.2	(0,3)
3604.7	<1	27,733.7	27,730.2	(1,4)
3602.4	<1	27,751.4	27,747.2	(2,5)
3601.2	<1	27,760.6	27,764.2	(3,6)
3598.5	0	27,781.5	27,781.2	(4,7)
3596.4	0	27,797.7	27,798.2	(5,8)
3594.3	<1	27,813.9	27,815.2	(6,9)
3592.3	<1	27,829.4	27,832.2	(7,10)
3590.0	<1	27,847.2	27,849.2	(8,11)
3587.7	<1	27,865.1	27,866.2	(9,12)
3585.3	1	27,883.1	27,883.2	(10,13)
3585.0	1	27,886.1	27,886.2	(0,2)
3583.3	1	27,900.1	27,901.2	(1,3)
3582.0	1	27,909.4	27,916.2	(2,4)
3578.8	<1	27,934.3	27,931.2	(3,5)
3578.0	1	27,940.6	27,946.2	(4,6)
3575.5	1	27,960.2	27,961.2	(5,7)
3573.1	2	27,978.9	27,976.2	(6,8)
3572.1	<1	27,986.8	27,991.2	(7,9)
3569.8	1	28,004.8	28,006.2	(8,10)
3567.7	1	28,021.3	28,021.2	(9,11)
3565.7	2	28,037.0	28,036.2	(10,12)
3563.9	3	28,051.2	28,051.2	(11,13)
3561.9	(5)	28,066.9	28,066.2	(12,14)
3562.5	5	28,062.2	28,061.2	(0,1)
3561.2	4	28,072.4	28,074.2	(1,2)
3559.4	3	28,086.6	28,087.2	(2,3)
3557.5	2	28,101.6	28,100.2	(3,4)
3555.6	1	28,116.6	28,113.2	(4,5)
3554.1	1	28,128.5	28,126.2	(5,6)
3553.1	<1	28,136.4	28,139.2	(6,7)
3551.1	<1	28,152.3	28,152.2	(7,8)
3549.9	0	28,161.8	28,165.2	(8,9)
3547.8	0	28,178.5	28,178.2	(9,10)

TABLE IV-IV (cont'd)
 The $^2\Pi_{1/2}-^2\Sigma$ System of CdI^a

λ (Å)	Int	ν_{vac} (cm ⁻¹)		(v',v'')
		Obs	Calc	
3546.1	<1	28,192.0	28,191.2	(10,11)
3544.3	<1	28,206.3	28,204.2	(11,12)
3542.6	1	28,219.8	28,217.2	(12,13)
3540.3	10	28,238.2	28,238.2	(0,0)
3538.9	6	28,249.3	28,249.2	(1,1)
3537.1	3	28,263.7	28,260.2	(2,2)
3536.0	2	28,272.5	28,271.2	(3,3)
3535.2	1	28,278.9	28,282.2	(4,4)
3533.6	<1	28,291.7	28,293.2	(5,5)
3531.9	0	28,305.3	28,304.2	(6,6)
3531.0	0	28,312.5	28,315.2	(7,7)
3529.6	0	28,323.8	28,326.2	(8,8)
3528.2	0	28,335.0	28,337.2	(9,9)
3526.3	1	28,350.3	28,348.2	(10,10)
3524.7	1	28,363.1	28,359.2	(11,11)
3523.9	2	28,369.6	28,370.2	(12,12)
3522.1	2	28,384.1	28,381.2	(13,13)
3520.5	2	28,397.0	28,392.2	(14,14)
3516.9	3	28,426.0	28,426.2	(1,0)
3515.3	2	28,439.0	28,435.2	(2,1)
3514.5	2	28,445.4	28,444.2	(3,2)
3513.3	2	28,455.2	28,453.2	(4,3)
3511.9	2	28,466.5	28,462.2	(5,4)
3510.9	2	28,474.6	28,471.2	(6,5)
3510.4	1	28,478.7	28,480.2	(7,6)
3509.2	1	28,488.4	28,489.2	(8,7)
3508.0	1	28,498.2	28,498.2	(9,8)
3506.9	<1	28,507.1	28,507.2	(10,9)
3505.1	0	28,521.7	28,525.2	(12,11)

^a Intensities given in parentheses are shoulders.

$${}^2\Pi_{3/2}-{}^2\Sigma$$

$$\begin{aligned} \nu &= 29,533.40 + 197.00(\nu'+1/2) - 1.00(\nu'+1/2)^2 \\ &\quad - 170.00(\nu''+1/2) + 1.00(\nu''+1/2)^2 \dots \end{aligned}$$

$${}^2\Pi_{1/2}-{}^2\Sigma$$

$$\begin{aligned} \nu &= 28,232.70 + 190.00(\nu'+1/2) - 1.00(\nu'+1/2)^2 \\ &\quad - 179.00(\nu''+1/2) + 1.00(\nu''+1/2)^2 \dots \end{aligned}$$

This analysis confirms that the bands observed by Ramasastry and Rao (107), originally thought to be a new system, are in fact an extension of the ${}^2\Pi_{3/2}-{}^2\Sigma$ system. The ${}^2\Pi$ splitting for CdI is 1300.7 cm^{-1} .

c) The Absorption Spectrum of ZnBr

The spectrum, listed in Tables IV-V and IV-VI and shown in Figure 4-3, was analysed as belonging to the two overlapping components of the system of ZnBr. The following equations were derived:

$${}^2\Pi_{3/2}-{}^2\Sigma$$

$$\begin{aligned} \nu &= 32,533.70 + 354.00(\nu'+1/2) - 2.00(\nu'+1/2)^2 \\ &\quad - 318.00(\nu''+1/2) + 2.00(\nu''+1/2)^2 \dots \end{aligned}$$

$${}^2\Pi_{1/2}-{}^2\Sigma$$

$$\begin{aligned} \nu &= 32,124.90 + 350.00(\nu'+1/2) - 2.00(\nu'+1/2)^2 \\ &\quad - 318.00(\nu''+1/2) + 2.00(\nu''+1/2)^2 \dots \end{aligned}$$

Definite assignments for the ${}^2\Pi_{1/2}-{}^2\Sigma$ bands have been made for the first time. Previously only 5 bands were known (106) and no assignments

TABLE IV-V
The ${}^2\Pi_{3/2}-{}^2\Sigma$ System of ZnBr

λ (Å)	Int	ν_{vac} (cm $^{-1}$)		(v', v'')
		Obs	Calc	
3147.5	1	31,762.1	31,758.7	(8,12)
3142.7	<1	31,810.6	31,814.7	(9,13)
3146.5	1	31,772.2	31,768.7	(3,6)
3141.1 ^a	<1	31,826.6	31,820.7	(4,7)
3136.8	<1	31,870.4	31,872.7	(5,8)
3131.0	1	31,929.5	31,924.7	(6,9)
3126.1	1	31,979.5	31,976.7	(7,10)
3121.1	1	32,030.7	32,028.7	(8,11)
3116.6	2	32,077.0	32,080.7	(9,12)
3111.0	3	32,134.7	32,132.7	(10,13)
3127.6	1	31,964.2	31,966.7	(1,3)
3122.2	<1	32,019.4	32,014.7	(2,4)
3118.3	1	32,059.5	32,062.7	(3,5)
3113.4	1	32,109.9	32,110.7	(4,6)
3108.8	2	32,157.5	32,158.7	(5,7)
3103.9	1	32, 08.2	32,206.7	(6,8)
3099.6	1	32,252.9	32,254.7	(7,9)
3095.1 ^a	1	32,299.8	32,302.7	(8,10)
3090.2	1	32,351.0	32,350.7	(9,11)
3085.9	2	32,396.1	32,398.7	(10,12)
3081.3	1	32,444.4	32,446.7	(11,13)
3102.0	2	32,227.9	32,228.7	(0,1)
3097.9	1	32,270.6	32,272.7	(1,2)
3093.9	1	32,312.3	32,316.7	(2,3)
3089.4	3	32,359.4	32,360.7	(3,4)
3084.9	2	32,406.6	32,404.7	(4,5)
3080.7	1	32,450.8	32,448.7	(5,6)
3077.2 ^a	2	32,487.7	32,492.7	(6,7)
3072.6	33	32,536.3	32,536.7	(7,8) or p branch of (0,0)
3072.0	10	32,542.7	32,542.7	(0,0)
3068.2	3	32,583.0	32,582.7	(1,1)
3063.9	2	32,628.7	32,622.7	(2,2)
3060.5	2	32,664.9	32,662.7	(3,3)
3057.1	1	32,701.3	32,702.7	(4,4)
3053.2	1	32,743.0	32,742.7	(5,5)
3049.5	2	32,782.8	32,782.7	(6,6)
3045.8	2	32,822.6	32,822.7	(7,7)
3042.2	1	32,861.4	32,862.7	(8,8)
3038.4 ^a	1	32,902.5	32,902.7	(9,9)
3035.1	2	32,938.3	32,942.7	(10,10)
3030.6	2	32,987.2	32,982.7	(11,11)

TABLE IV-V (cont'd)
 The ${}^2\Pi_{3/2}-{}^2\Sigma$ System of ZnBr

$\lambda(\text{\AA})$	Int	$\nu_{\text{vac}}(\text{cm}^{-1})$		(ν', ν'')
		Obs	Calc	
3039.0	2	32,896.0	32,896.7	(1,0)
3035.6	2	32,932.9	32,932.7	(2,1)
3032.3 ^a	2	32,968.7	32,968.7	(3,2)

^a These bands are common to both systems.

TABLE IV-VI
The ${}^2\Pi_{1/2}-{}^2\Sigma$ System of ZnBr

λ (Å)	Int	ν_{vac} (cm $^{-1}$)		(v', v'')
		Obs	Calc	
3141.1 ^a	<1	31,826.8	31,826.9	(0,1)
3134.7	1	31,891.8	31,898.9	(2,3)
3130.1	2	31,938.6	31,934.9	(3,4)
3123.3	1	32,008.2	32,006.9	(5,6)
3120.0	<1	32,042.0	32,042.9	(6,7)
3110.4	8	32,140.9	32,140.9	(0,0)
3107.4	1	32,171.9	32,172.9	(1,1)
3104.6	2	32,201.0	32,204.9	(2,3)
3101.1	1	32,237.3	32,236.9	(3,3)
3098.2	1	32,267.5	32,268.9	(4,4)
3095.1 ^a	1	32,299.8	32,300.9	(5,5)
3092.2	1	32,330.1	32,332.9	(6,6)
3088.4	3	32,369.9	32,364.9	(7,7)
3077.2 ^a	2	32,487.7	32,486.9	(1,0)
3074.8	2	32,513.0	32,514.9	(2,1)
3071.7	4	32,545.8	32,542.9	(3,2)
3069.5	1	32,569.2	32,570.9	(4,3)
3061.7	2	32,652.1	32,654.9	(7,6)
3059.0	1	32,680.9	32,682.9	(8,7)
3044.8	2	32,833.4	32,828.9	(2,0)
3043.0	1	32,852.8	32,852.9	(3,1)
3041.2	1	32,872.2	32,876.9	(4,2)
3038.4 ^a	1	32,902.5	32,900.9	(5,3)
3036.2	1	32,926.4	32,924.9	(6,4)
3034.0	1	32,950.2	32,948.9	(7,5)
3032.3 ^a	2	32,968.7	32,972.9	(8,6)

^aThese bands are common to both systems.

were possible. The $^2\Pi$ splitting from the present analysis is 397.8 cm^{-1} which is close to the predicted value of 386 cm^{-1} (106).

d) The Absorption Spectrum of ZnI

From the analysis of the observed spectrum (Tables IV-VII and IV-VIII, Figure 4-4) the following equations were derived:

$$^2\Pi_{3/2} - ^2\Sigma$$

$$\begin{aligned} \nu = & 30,125.80 + 248.20(\nu'+1/2) - 0.72(\nu'+1/2)^2 \\ & - 223.40(\nu''+1/2) + 0.75(\nu''+1/2)^2 \dots \end{aligned}$$

$$^2\Pi_{1/2} - ^2\Sigma$$

$$\begin{aligned} \nu = & 29,498.90 + 272.00(\nu'+1/2) - 0.50(\nu'+1/2)^2 \\ & - 223.40(\nu''+1/2) + 0.50(\nu''+1/2)^2 \dots \end{aligned}$$

Again, results of this analysis agree with previous work on the known $^2\Pi_{3/2} - ^2\Sigma$ component (106), and several previously unassigned bands can now be shown to belong to this system (104). The $^2\Pi_{1/2} - ^2\Sigma$ system has not previously been reported in the literature. The $^2\Pi$ splitting calculated is 626.9 cm^{-1} , higher than the 386 cm^{-1} predicted (106) from the 3P splitting of the Zn atom.

TABLE IV-VII
The $2\Pi_{3/2}-2\Sigma$ System of ZnI

λ (Å)	Int	ν_{vac} (cm ⁻¹)		(v', v'')
		Obs	Calc	
3463.6	<1	28,863.5	28,863.2	(1,7)
3459.1	<1	28,901.8	28,897.1	(2,8)
3455.1	<1	28,934.5	28,931.1	(3,9)
3451.9 ^a	1	28,961.3	28,965.1	(4,10)
3447.1	0	29,001.6	28,999.2	(5,11)
3430.9	0	29,138.5	29,141.0	(3,8)
3426.4	1	29,176.8	29,173.5	(4,9)
3423.2	1	29,204.1	29,206.1	(5,10)
3418.7	<1	29,242.5	29,238.8	(6,11)
3415.6 ^a	1	29,269.1	29,271.5	(7,12)
3411.0	1	29,308.5	29,304.3	(8,13)
3407.7	1	29,336.9	29,337.1	(9,14)
3413.2	1	29,289.6	29,290.5	(1,5)
3409.6	1	29,320.6	29,321.4	(2,6)
3405.8	2	29,353.3	29,352.4	(3,7)
3402.1 ^a	1	29,385.2	29,383.4	(4,8)
3398.9	2	29,412.9	29,414.5	(5,9)
3395.4	1	29,443.2	29,445.7	(6,10)
3388.7 ^a	1	29,501.4	29,506.4	(1,4)
3384.4	(7)	29,538.9	29,535.8	(2,5)
3381.4	3	29,565.1	29,565.3	(3,6)
3378.2 ^a	2	29,593.1	29,594.8	(4,7)
3369.8	3	29,624.7	29,624.4	(5,8)
3371.7 ^a	1	29,650.1	29,654.1	(6,9)
3367.7	1	29,685.4	29,683.8	(7,10)
3364.8	1	29,710.9	29,713.6	(8,11)
3366.5 ^a	1	29,695.9	29,695.9	(0,2)
3363.7 ^a	1	29,720.7	29,723.8	(1,3)
3360.4 ^a	1	29,749.8	29,751.7	(2,4)
3357.3	1	29,777.3	29,779.7	(3,5)
3354.0	3	29,806.6	29,807.7	(4,6)
3351.0	3	29,833.3	29,835.8	(5,7)
3348.0 ^a	2	29,860.0	29,864.0	(6,8)
3344.5	2	29,891.3	29,892.2	(7,9)
3340.9	3	29,923.5	29,920.5	(8,10)
3337.8	3	29,951.3	29,948.8	(9,11)
3334.8	3	29,978.2	29,977.2	(10,12)
3332.2	1	30,001.6	30,005.7	(11,13)
3341.7	4	29,916.3	29,916.3	(0,1)
3338.8	5	29,942.3	29,942.7	(1,2)
3335.8	4	29,969.2	29,969.1	(2,3)
3332.9	3	29,995.3	29,995.6	(3,4)
3330.1	1	30,020.5	30,022.1	(4,5)
3327.0	1	30,048.5	30,048.7	(5,6)

TABLE IV-VII (cont'd)
 The ${}^2\Pi_{3/2}-{}^2\Sigma$ System of ZnI

λ (Å)	Int	$\nu_{\text{vac}}(\text{cm}^{-1})$		(v',v'')
		Obs	Calc	
3320.8	0	30,104.6	30,102.1	(7,8)
3318.3 ^a	1	30,127.3	30,128.9	(8,9)
3315.2 ^a	(6)	30,155.4	30,155.7	(9,10)
3312.4	3	30,180.9	30,182.6	(10,11)
3317.1	10	30,138.2	30,138.2	(0,0)
3314.7	7	30,160.0	30,163.1	(1,1)
3311.7	3	30,187.3	30,188.0	(2,2)
3308.4 ^a	1	30,217.4	30,213.0	(3,3)
3306.2	<1	30,237.5	30,238.0	(4,4)
3303.3	<1	30,264.1	30,263.1	(5,5)
3300.8	1	30,287.0	30,288.3	(6,6)
3298.0	0	30,312.7	30,313.5	(7,7)
3295.2	0	30,338.5	30,338.8	(8,8)
3292.6	1	30,362.4	30,364.1	(9,9)
3289.5 ^a	1	30,391.0	30,389.5	(10,10)
3286.9	1	30,415.1	30,415.0	(11,11)
3284.4 ^a	1	30,438.2	30,440.5	(12,12)
3281.3	1	30,467.0	30,466.1	(13,13)
3278.4	1	30,493.9	30,491.7	(14,14)
3290.3	5	30,383.6	30,385.0	(1,0)
3287.8	6	30,406.7	30,408.4	(2,1)
3284.9	5	30,433.6	30,431.9	(3,2)
3282.4	4	30,456.8	30,455.4	(4,3)
3280.1	3	30,478.1	30,479.0	(5,4)
3277.3	1	30,504.2	30,502.7	(6,5)
3274.9	0	30,526.5	30,526.4	(7,6)
3272.3	0	30,550.8	30,550.2	(8,7)
3269.8	<1	30,574.1	30,574.0	(9,8)
3267.1	1	30,599.4	30,597.9	(10,9)
3264.7	1	30,621.9	30,621.9	(11,10)
3262.5	0	30,642.5	30,645.9	(12,11)
3259.9	1	30,667.0	30,670.5	(13,12)
3257.0	<1	30,694.3	30,694.1	(14,13)
3263.9	<1	30,629.4	30,630.3	(2,0)
3261.6	1	30,651.0	30,652.3	(3,1)
3259.1	1	30,674.5	30,674.3	(4,2)
3256.4	<1	30,699.9	30,696.4	(5,3)
3254.2	0	30,720.7	30,718.6	(6,4)
3252.4	0	30,737.7	30,740.8	(7,5)
3249.3	1	30,767.0	30,763.1	(8,6)
3245.1	<1	30,806.8	30,807.8	(9,7)
3242.1	<1	30,835.3	30,830.3	(10,8)

TABLE IV-VII (cont'd)
 The ${}^2\Pi_{3/2}^- - {}^2\Sigma$ System of ZnI

$\lambda(\text{\AA})$	Int	$\nu_{\text{vac}} (\text{cm}^{-1})$		(ν', ν'')
		Obs	Calc	
3240.0	1	30,855.3	30,852.8	(11,9)
3237.5	1	30,879.2	30,874.2	(3,0)
3235.6	<1	30,897.3	30,894.7	(4,1)
3233.6	0	30,916.4	30,915.3	(5,2)
3231.8	<1	30,933.6	30,936.0	(6,3)
3228.9	0	30,961.4	30,956.7	(7,4)

^aThese bands are common to both systems, the ${}^2\Pi_{3/2}^- - {}^2\Sigma$ and ${}^2\Pi_{1/2}^- - {}^2\Sigma$. Intensities in parentheses are shoulders.

TABLE IV-VIII
The $^2\Pi_{1/2}-^2\Sigma$ System of ZnI

λ (Å)	Int	ν_{vac} (cm ⁻¹)		(v', v'')
		Obs	Calc	
3465.2	<1	28,850.1	28,850.0	(4,8)
3459.1	<1	28,901.8	28,902.6	(5,9)
3452.7	0	28,954.6	28,955.2	(6,10)
3445.8	1	29,012.6	29,007.8	(7,11)
3439.9	<1	29,062.3	29,060.4	(8,12)
3433.8	0	29,113.9	29,113.0	(9,13)
3427.2	<1	29,170.0	29,165.6	(10,14)
3464.3	<1	28,857.6	28,859.0	(0,3)
3457.9	1	28,911.0	28,910.6	(1,4)
3451.9 ^a	1	28,961.3	28,962.2	(2,5)
3445.8	1	29,012.6	29,013.8	(3,6)
3439.4	0	29,066.5	29,065.4	(4,7)
3433.5	<1	29,116.5	29,117.0	(5,8)
3427.2	<1	29,170.0	29,168.6	(6,9)
3420.8	1	29,224.6	29,220.2	(7,10)
3415.6 ^a	1	29,269.1	29,271.8	(8,11)
3409.3	1	29,323.2	29,323.4	(9,12)
3403.1	1	29,376.6	29,375.0	(10,13)
3438.4	<1	29,075.0	29,079.4	(0,2)
3432.3	<1	29,126.7	29,130.0	(1,3)
3425.8	1	29,181.9	29,180.6	(2,4)
3420.2	1	29,229.7	29,231.2	(3,5)
3408.3	<1	29,331.8	29,332.4	(5,7)
3402.1 ^a	<1	29,385.2	29,383.0	(6,8)
3397.2	2	29,427.6	29,433.6	(7,9)
3390.0	1	29,490.1	29,484.2	(8,10)
3385.4	(8)	29,530.2	29,534.8	(9,11)
3379.0	3	29,586.1	29,585.4	(10,12)
3372.9	1	29,639.6	29,636.0	(11,13)
3367.3	1	29,688.9	29,686.6	(12,14)
3411.9	3	29,300.8	29,300.8	(0,1)
3406.1	2	29,350.7	29,350.4	(1,2)
3400.3	2	29,400.8	29,400.0	(2,3)
3394.7	1	29,449.3	29,449.6	(3,4)
3388.7 ^a	1	29,501.4	29,499.2	(4,5)
3383.8	1	29,551.1	29,548.8	(5,6)
3378.2 ^a	2	29,593.1	29,598.4	(6,7)
3371.7 ^a	1	29,650.1	29,648.0	(7,8)
3366.5 ^a	1	29,695.9	29,697.6	(8,9)
3360.4 ^a	1	29,749.8	29,747.2	(9,10)
3349.5	4	29,846.7	29,846.4	(11,12)

TABLE IV-VIII (cont'd)
 The ${}^2\Pi_{1/2}-{}^2\Sigma$ System of ZnI

λ (Å)	Int	ν_{vac} (cm ⁻¹)		(v', v'')
		Obs	Calc	
3343.7	1	29,898.4	29,896.0	(12,13)
3386.2	10	29,523.2	29,523.2	(0,0)
3380.6	6	29,572.1	29,571.8	(1,1)
3375.1	3	29,620.3	29,620.4	(2,2)
3368.9	1	29,674.8	29,669.0	(3,3)
3363.7 ^a	1	29,720.7	29,717.3	(4,4)
3359.5	1	29,757.8	29,766.2	(5,5)
3353.0	1	29,815.5	29,814.8	(6,6)
3348.0 ^a	2	29,860.0	29,863.4	(7,7)
3342.2	2	29,811.8	29,912.0	(8,8)
3336.3	3	29,964.7	29,960.6	(9,9)
3326.1	1	30,056.6	30,057.8	(11,11)
3355.4	4	29,794.2	29,794.2	(1,0)
3350.0	4	29,842.2	29,841.8	(2,1)
3345.0	3	29,886.8	29,889.4	(3,2)
3339.1	4	29,939.6	29,937.0	(4,3)
3334.6	2	29,980.0	29,984.6	(5,4)
3328.6	1	30,034.1	30,032.2	(6,5)
3323.4	1	30,081.0	30,079.8	(7,6)
3318.3 ^a	1	30,127.3	30,127.4	(8,7)
3313.3	5	30,172.7	30,175.0	(9,8)
3308.4 ^a	1	30,217.4	30,222.5	(10,9)
3302.4	1	30,272.3	30,270.2	(11,10)
3297.5	1	30,317.3	30,317.8	(12,11)
3325.3	1	30,063.9	30,064.2	(2,0)
3320.4	<1	30,108.2	30,110.8	(3,1)
3315.2 ^a	(6)	30,155.4	30,157.4	(4,2)
3309.9	2	30,203.7	30,204.0	(5,3)
3305.4	0	30,244.8	30,250.6	(6,4)
3299.4	1	30,299.8	30,297.2	(7,5)
3294.6	0	30,344.0	30,343.8	(8,6)
3289.5 ^a	1	30,391.0	30,390.4	(9,7)
3284.4 ^a	1	30,438.2	30,437.0	(10,8)
3279.5	0	30,483.7	30,483.6	(11,9)
3295.8	0	30,332.9	30,333.2	(3,0)
3285.7	2	30,426.2	30,424.4	(5,2)
3280.6	1	30,473.5	30,470.0	(6,3)
3276.1	1	30,515.3	30,515.6	(7,4)
3270.7	0	30,565.7	30,561.2	(8,5)
3266.5	1	30,605.0	30,606.8	(9,6)

^aThese bands are common to both the ${}^2\Pi_{3/2}-{}^2\Sigma$ and ${}^2\Pi_{1/2}-{}^2\Sigma$ systems. Intensities in parentheses are shoulders.

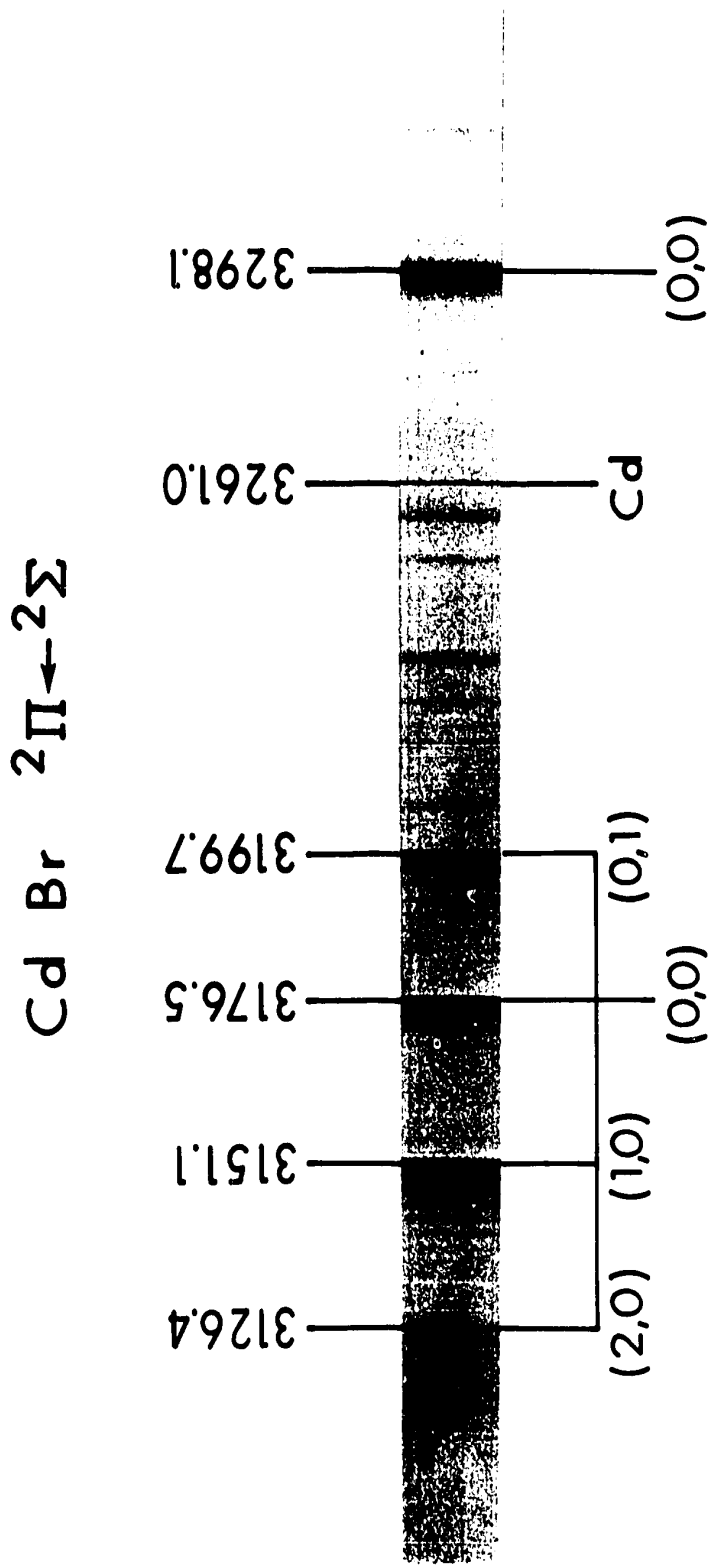


FIGURE 4-1: The UV Spectrum of CdBr.

$\Sigma_2 \rightarrow \Pi_2$
Cd I \rightarrow P D

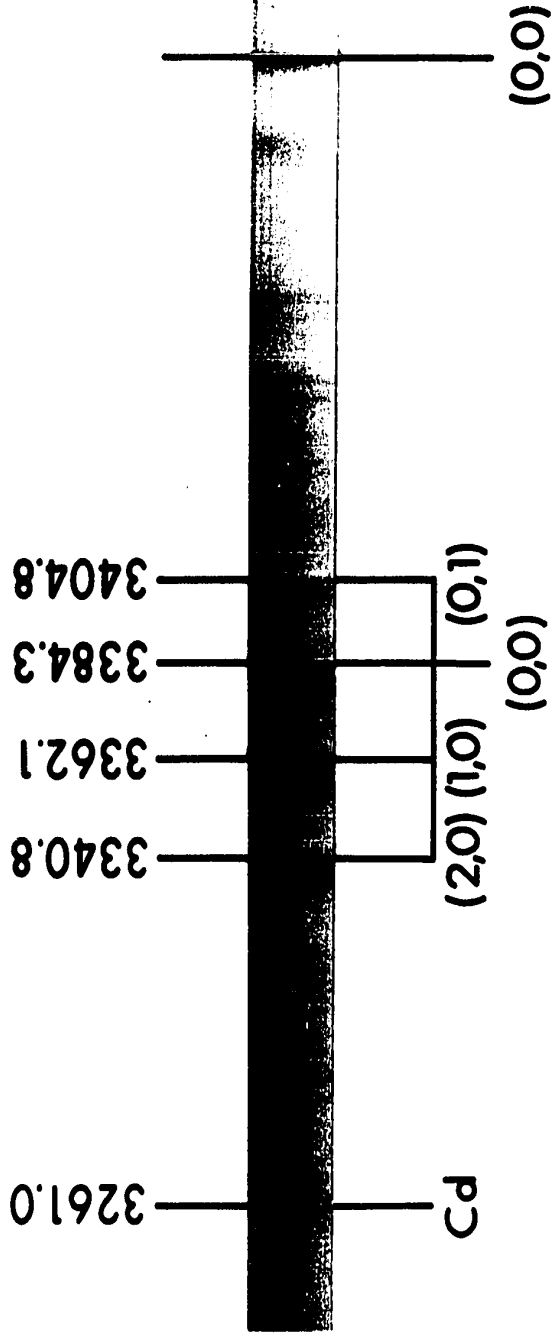


FIGURE 4-2: The UV Spectrum of CdI.

Zn Br $2\Pi \leftarrow 2\Sigma$

Zn(3076 Å)

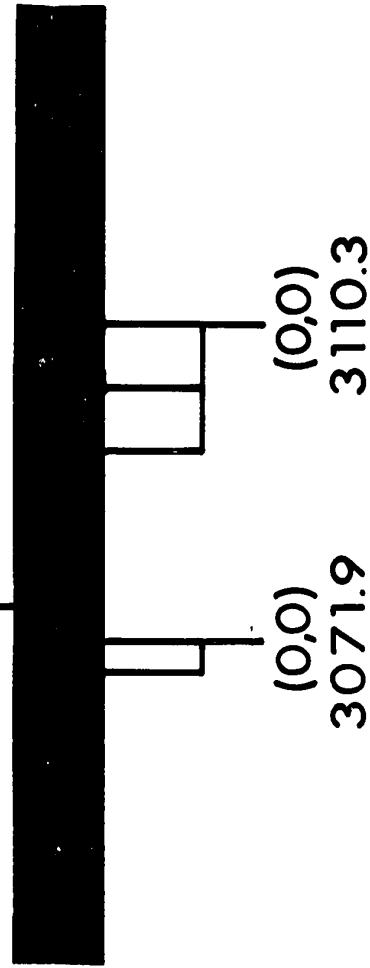


FIGURE 4-3: The UV Spectrum of ZnBr.

Zn I $2\Pi \leftarrow 2\Sigma$

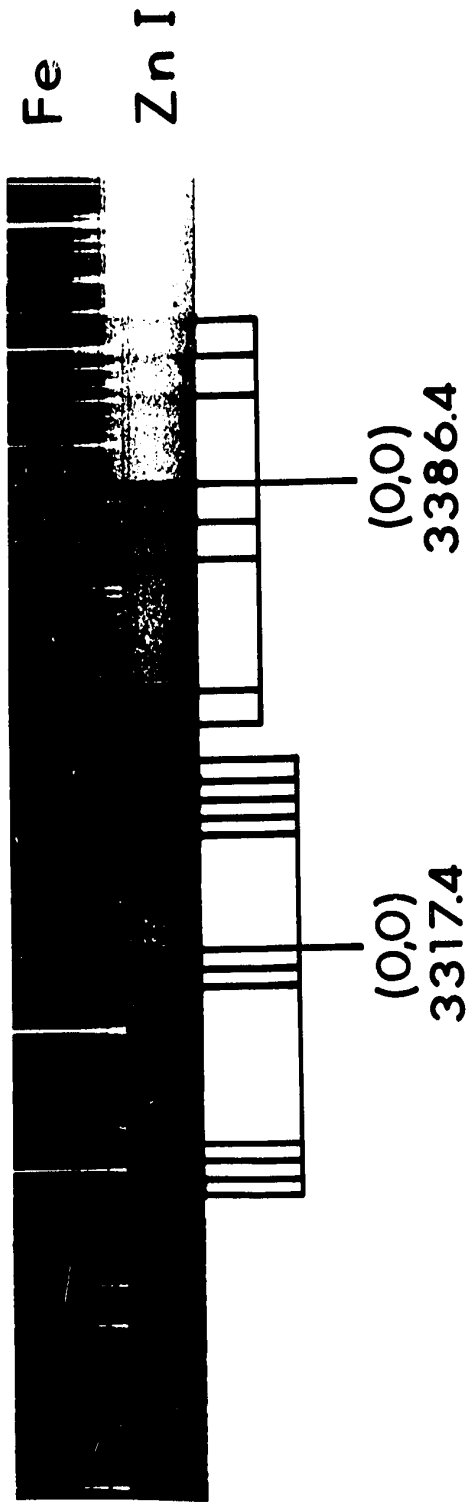


FIGURE 4-4: The UV Spectrum of ZnI.

2. The Doublet Pi Splittings

The observed $^2\Pi$ splittings for cadmium, mercury, and zinc halides are summarized in Table IV-V. Howell (106), in his work on the $^2\Pi-^2\Sigma$ system of HgF, found that the molecular coupling constant for the $^2\Pi$ state is approximately given by two-thirds of the atomic coupling constant for the 3P state of mercury. Therefore he argued that the optically excited electron in HgF($^2\Pi$) is a relatively unperturbed mercury electron and he predicted little change in the molecular coupling constants for the $^2\Pi$ states of other mercury halides. It is evident from Table IV-V that this hypothesis holds well for HgCl and HgBr. However there is a significant discrepancy in the case of HgI. This is probably related to the stronger perturbations caused by the heavier iodine atom on the excited state. The values from the present study of the $^2\Pi$ splittings in the case of CdBr and ZnBr are also in agreement with Howell's hypothesis. The splittings observed for CdI and ZnI deviate significantly along the series, and in a direction opposite to that observed for HgI. Thus it can be concluded that in the fluorides, chlorides, and bromides of mercury, cadmium, and zinc, the excited electron is an almost unchanged electron of the metal atom, whereas in the iodides the perturbation of the optical electron is more severe.

TABLE IV-IX

 $^2\Pi$ Splittings^a of Zn, Cd, and Hg Halides

M	MF	MCl	MBr	MI
Zn	370.0 ^b	384.9 ^c	397.8	626.9
Cd	1179.0 ^d	1115.0 ^d	1165.8	1300.7
Hg	3940.0 ^d	3920.0 ^e	3833.0 ^f	3538.0 ^g

^aIn cm^{-1} .^bG. D. Rochester and E. Olsson, Z. Physik., 114, 495 (1939).^cS. D. Cornell, Phys. Rev., 54, 341 (1938).^dFrom reference (106).^{e,f,g}From references (103a,b,c) respectively.

CHAPTER V

THE QUENCHING OF CADMIUM (3P) ATOMS

The flash photolysis of DMCD in methane produces Cd^3 in sufficient quantities to allow kinetic studies of its decay. Since all the DMCD is decomposed by the photoflash, and C_2H_6 is the only product of the photolysis, decay of Cd^3 is not influenced by parent compound or photo-products. Ethane is a very inefficient quencher of Cd^3 .

The most intense absorption from the first cadmium triplet observed was the $^3D_1 \leftarrow ^3P_0$ line at $3404\overset{\circ}{A}$, and this transition was monitored for kinetic determinations. Wherever possible, the $3466\overset{\circ}{A}$ ($^3D_2 \leftarrow ^3P_1$) transition was also monitored but under most conditions used here, this line was too weak to allow quantitative measurements. In those few cases where both transitions could be observed the first order plot of Cd^* decay paralleled that of Cd° within experimental error, and after the termination of the photolysis flash, the ratio of the concentrations of the two states was constant. This indicates that the components of the cadmium triplet are in equilibrium, as shown by Breckenridge and Callear (27). Thus it is possible to follow the concentration of Cd^3 by monitoring the intensity of the Cd° absorption line at $3404\overset{\circ}{A}$.

Before quantitative work could be undertaken, the Beer-Lambert coefficient for the $3404\overset{\circ}{A}$ line had to be determined. The relationship between optical density, OD, the extinction coefficient, ϵ ,

concentration of absorber, c , and path length, l , is found empirically to be

$$OD = \epsilon(c l)^n$$

where n is the Beer-Lambert coefficient; n is found to lie between 0.5 and 1, and depends on resolving power of the monochromator used. For most molecular absorption bands in solution, which are fairly broad, $n = 1$ and Beer's law is usually written $OD = \epsilon c l$. Atomic lines and sharp molecular bands in gas phase absorption spectroscopy often give rise to a Beer-Lambert factor of less than unity and for atomic lines $n = 0.5$.

In order to determine n for this system, mixtures of DMGd in methane were flashed at several delay times and the procedure was repeated with one half of the photo-lamp and cell shielded. Assuming that the shielding does not affect the concentration of Cd^3 in the exposed portion of the cell, the following equations apply:

i. no shielding $OD = \epsilon(c l)^n$

ii. shielding $OD_{1/2} = \epsilon(c \times l/2)^n$

which in turn lead to

$$\frac{OD}{OD_{1/2}} = \frac{1}{0.5^n} = 2^n$$

and a plot of OD vs $OD_{1/2}$ has a slope of 2^n . Several determinations were made and a Beer-Lambert factor of 0.7 ± 0.1 was measured for the 3404\AA line. A typical plot is shown in Figure 5-1. An attempt to determine n for the 3466\AA ($^3D_2 \leftarrow ^3P_1$) line was inconclusive due to the low intensity of this transition and resulting scatter in the data.

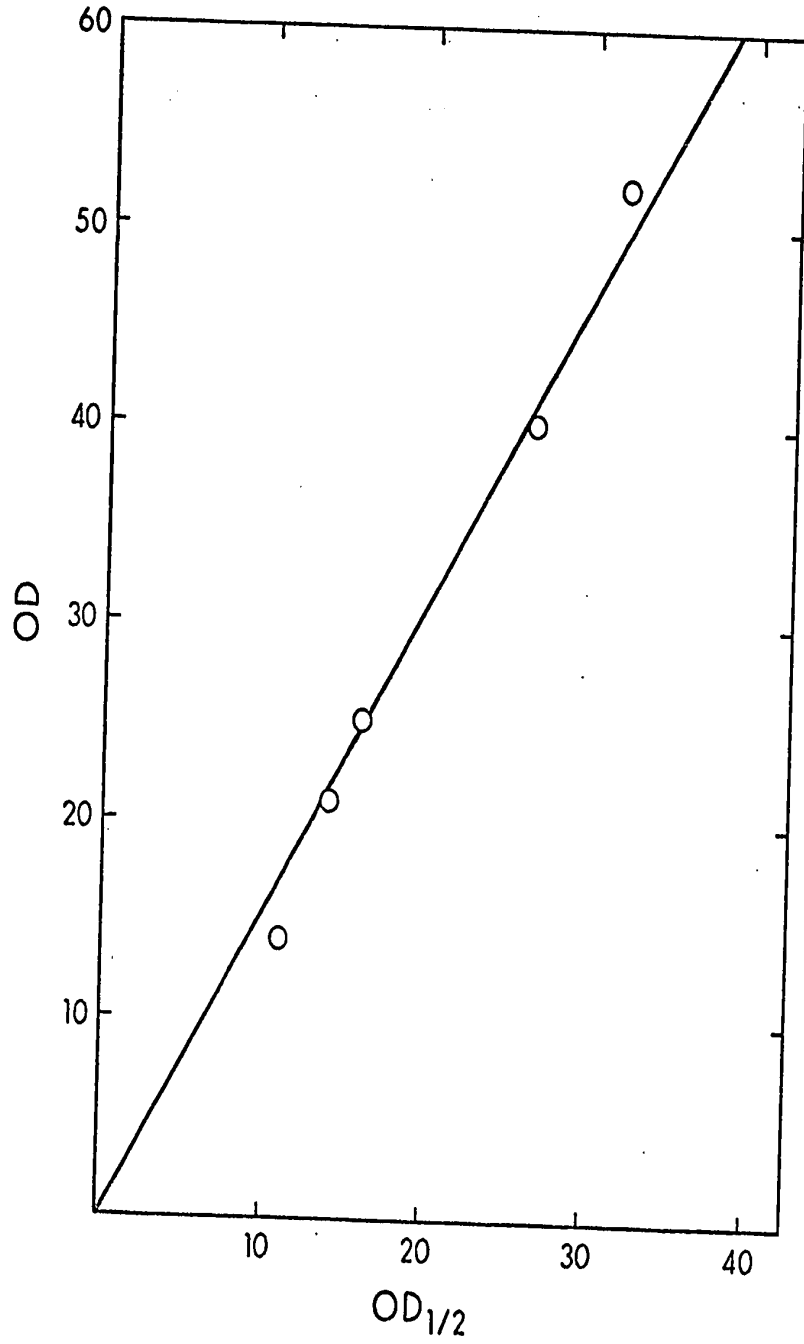


FIGURE 5-1: A Plot of OD vs $OD_{1/2}$.

1. Rate Constants for the Deactivation of Cd(³P)

The rate of decay of Cd° in CH₄ was found to be independent of methane pressure in the range 200 - 650 torr, and of temperature in the range 27 - 110°C. The rate constant for decay of Cd° under these conditions was found to be $3.3(\pm 0.5) \times 10^4 \text{ sec}^{-1}$, corresponding to a lifetime of 3.0×10^{-5} seconds. The data are given in Tables V-I through V-IV, and a typical first order plot is shown in Figure 5-2.

The rate of decay of Cd° was also measured in the presence of olefins and other substrates. In these experiments mixtures of 0.5 torr of DMCD and quencher were made up to a total pressure of 300 torr with methane. The pressure of quencher could not be varied greatly as the slope of the first order plots with quencher must be significantly different from that in methane alone; large pressures of quenchers could not be used since the concentration of Cd° would be too low to allow quantitative measurements. The kinetic data are given in Tables V-V through V-XIX and an example of a first order plot is shown in Figure 5-3. That Cd* quenching is second order for all gases studied here, and that the pseudo-first order approximation is valid for these conditions has been well established in the previous work on cadmium quenching (65). The absolute rate coefficients for the decay of Cd° in various substrates are summarized in Table V-XX. Table V-XXI lists relative rates of decay of Hg* and Cd* from this and other work.

The experimental data, that is microdensitometer peak heights and delay times, were processed by computer to give a least squares slope which was adjusted for fluorescent decay and divided by the

TABLE V-I

Data for Cd(³P) Decay in 300 torr CH₄ at Room Temperature

Time μsec	Relative Concentration of Cd°								
30	132	158	166		157	119	162	123	
40	99	116	129	155	119	96	130	87	
50	76	104	102	127	95	72	116	75	134
60	56	70	85	92	70	59	74	63	100
70	59	52	74	80	54	47	62	50	81
80	36	42	64	63	40	39	56	34	67
90	21	31	42	60	31	33		25	53
100	20		33		22	25	30		46
110	15		27		20	18	28	20	38
120	12					15			29
slope (x10 ⁴)	3.71	3.83	3.00	2.90	3.79	3.23	3.29	3.33	2.91

Average slope = $3.33 \times 10^4 \text{ sec}^{-1}$.

TABLE V-II
 Data for the Decay of Cd(³P) in 300 torr CH₄ at 110°C

Time μsec	Relative Concentration of Cd°					
	30	122	119	128	105	102
40	90	78	82	80	82	65
50	64	60	57	53	61	43
60	42	44	41	42	37	32
70	29	33	27	31	32	25
80	22	22	21	19	23	17
slope (x10 ⁴)	3.55	3.20	3.60	3.23	3.07	3.05

Average slope = 3.28×10^4 .

TABLE V-III
 Data for Cd^3 Decay in 650 torr CH_4 at
 Room Temperature

Time sec	Relative Concentration of Cd^0				
	30	58	54	56	128
40	49	41	46	101	102
50	37	30	39	79	85
60	29	20	33	60	74
70	22	19	26	39	64
80	19	15	18	39	42
90					33
slope ($\times 10^4$)	3.36	3.85	2.94	3.78	3.00

Average slope = $3.38 \times 10^4 \text{ sec}^{-1}$.

TABLE V-IV
 Data for the Fluorescent Decay of
 $\text{Cd}(^3\text{P}_1)$ at Room Temperature

Time μsec	Relative Concentration of Cd*		
	30	54	57
40	38	48	56
50	30	38	34
60	21	25	31
70	17	21	18
80	14	15	14
slope ($\times 10^4$)	3.41	3.71	4.10

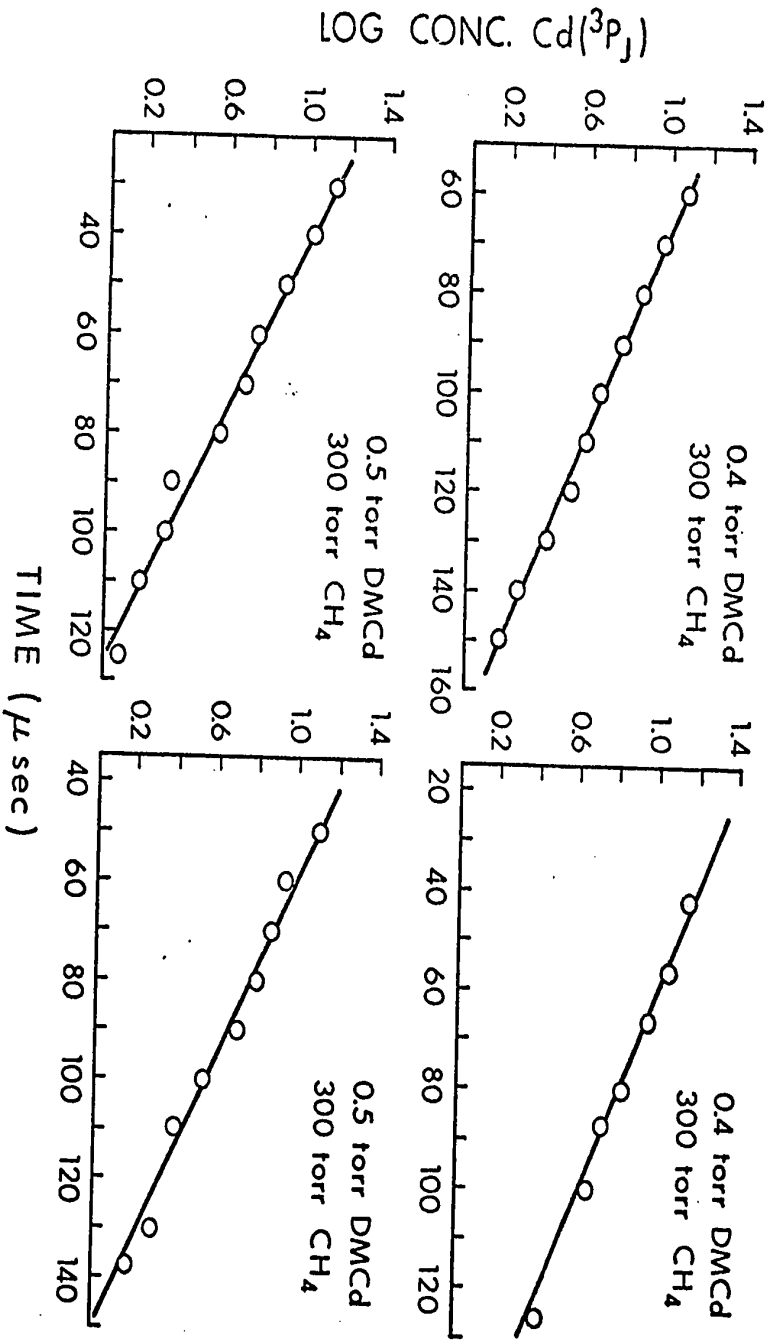


FIGURE 5-2: First Order Plots for Fluorescent Decay of Cd³.

TABLE V-V
Data for Cd^3 Decay in C_2H_4 at Room Temperature

Time μsec	Relative Concentration of Cd°									
	99	95	167	92	132	139	73	82	90	90
30	99	95	167	92	132	139	73	82	90	90
40	66	68	114	63	85	105	58	57	68	68
50	45	48	91	49	63	79	46	44	47	47
60	33	34	54	31	48	59	31	31	37	37
70	20	25	43	20	36	35	24	24	27	27
80	16	18	31	16	25	29	19	19	20	20
90			19		15	21				
slope ($\times 10^4$)	5.08	4.77	5.04	4.98	4.50	4.62	3.99	4.19	4.30	4.30
torr C_2H_4	0.50	0.50	0.50	0.32	0.51	0.51	0.21	0.21	0.21	0.21
rate $\times 10^8$ $\text{l mole}^{-1}\text{sec}^{-1}$	6.56	5.40	6.41	6.20	4.30	4.74	5.89	7.68	8.66	8.66
Average rate = $6.24 \times 10^8 \text{ l mole}^{-1}\text{sec}^{-1}$.										

TABLE V-VI
Data for Cd³ Decay in C₃H₆ at Room Temperature

Time l:sec	Relative Concentration of Cd°											
	141	105	105	108	75	84	75	90	73	79		
30												
40	102	82	74	70	56	57	48	57	48	63		
50	62	55	51	55	43	45	37	42	34	44		
60	46	38	42	40	27	30	25	28	24	30		
70	36	34	28	31	24	25	19	25	14	26		
80	21		24	25	16	20	11	15	9	16		
slope (x10 ⁴)	5.27	4.39	4.40	4.51	4.36	4.25	5.13	4.97	5.73	4.41		
torr C ₃ H ₆	0.32	0.32	0.32	0.32	0.32	0.39	0.39	0.43	0.43	0.43		
rate x 10 ⁸ l mole ⁻¹ sec ⁻¹	11.4	6.21	6.27	6.91	6.04	4.42	8.65	7.15	10.5	4.71		

Average rate constant = 7.22 x 10⁸ l mole⁻¹sec⁻¹.

TABLE V-VII
Data for Cd^3 Decay in $\text{c-C}_4\text{H}_8$ at Room Temperature

Time μsec	Relative Concentration of Cd^3									
	102	67	76	126	118	104	93	90	90	68
30										
40	67	50	60	92	74	78	69	61	61	68
50	43	32	43	68	54	60	48	41	41	47
60	32	21	38	49	34	50	36	24	24	33
70	18	15	27	36	23	30	21	18	18	23
80	13	9	16	29	19		15	12	12	22
slope (10^4)	5.87	5.59	3.95	4.34	5.52	4.01	5.09	5.86	4.46	4.46
torr $\text{c-C}_4\text{H}_8$	0.43	0.43	0.43	0.32	0.32	0.32	0.32	0.32	0.32	0.32
rate const. $1 \text{ mole}^{-1}\text{sec}^{-1}$	11.1	9.85	2.70	5.92	12.8	3.98	10.3	14.8	14.8	6.62

Average rate constant = $8.68 \times 10^8 \text{ l mole}^{-1}\text{sec}^{-1}$.

TABLE V-VIII
Data for Cd^3 Decay in $t\text{-C}_4\text{H}_8$ at Room Temperature

Time μsec	Relative Concentration of Cd°									
	91	95	92	87	74	83	78	59	73	
30	61	60	61	51	54	51	43	53		
40	46	49	49	47	34	42	41	37	42	
50	23	35	31	23	23	23	29	21	30	
60	20	20	23	12	16	19	18	13	13	
70	17	15	13	10	10	10	13	10	10	
80	5.25	5.13	5.15	6.28	5.60	5.64	4.98	5.03	5.29	
slope ($\times 10^4$)										
rate const. $1 \text{ mole}^{-1} \text{ sec}^{-1}$ $\times 10^9$	1.13	1.05	1.07	1.29	0.99	1.01	0.83	0.85	0.98	
torr $t\text{-C}_4\text{H}_8$	0.32	0.32	0.32	0.43	0.43	0.43	0.38	0.38	0.38	

Average rate constant = $1.02 \times 10^9 \text{ l mole}^{-1} \text{ sec}^{-1}$.

TABLE V-IX
 Data for Cd^3 Decay in C_2H_2 at Room Temperature

Time μsec	Relative Concentration of Cd°					
30	88	79	102	105	132	132
40	59	51	68	74	85	100
50	43	37	56	52	63	77
60	21	32	42	37	48	46
70	18	13	28	27	36	35
80	11	12	16	20	27	28
slope ($\times 10^4$)	5.94	5.31	4.71	4.71	4.60	4.63
torr C_2H_2	0.86	0.86	0.43	0.43	0.43	0.43
rate const. $1 \text{ mole}^{-1} \text{ sec}^{-1}$ $\times 10^8$	5.69	4.32	7.61	7.61	5.45	5.67

Average rate constant = $6.06 \times 10^8 \text{ l mole}^{-1} \text{ sec}^{-1}$.

TABLE V-X
Data for Cd³ Decay in H₂ at Room Temperature

	t ^a	h ^b	t	h	t	h	t	h	t	h
	36	111	24	138	26	89	28	85	30	122
	47	82	38	95	39	63	38	65	43	80
	54	67	51	60	50	35	46	43	54	68
	64	41	62	50	60	25	58	25	61	31
	82	26	71	30	68	16	70	16	77	14
	92	20	27	110			46	32		
	107	14	98	15						
slope ^c	4.73		4.12		5.56		5.96		5.57	
torr	2.9		4.4		9.4		7.0		7.7	
rate ^e	6.08		3.37		4.45		7.04		5.45	
	18	157	20	114	28	120	30	90	24	95
	42	92	31	80	42	85	40	78	28	70
	29	118	42	50	50	54	50	42	42	42
	65	45	56	33	62	41	60	32	53	32
	33	99	64	22	68	24	72	20	22	81
	33	99	24	100					82	13
	98	13	91	8					84	13
slope	4.02		5.26		5.13		5.25		4.62	
torr	3.4		7.7		9.4		7.0		7.7	
rate	3.81		4.70		3.59		5.14		4.65	

Average rate constant = 4.83×10^7 l mole⁻¹sec⁻¹.

^aTime in μ sec. ^bRelative concentration of Cd°. ^c $\times 10^4$. ^dConcentration of H₂.

^eRate constant in l mole⁻¹sec⁻¹ $\times 10^7$.

TABLE V-XI
Data for Cd^3 Decay in D_2 at Room Temperature

Time μsec	Relative Concentration of Cd^0					
30	83	85	70	118	86	74
40	57	63	51	74	62	51
50	45	48	34	54	56	34
60	30	36	24	34	29	23
70	25	27	16	23	20	16
80	21	16	13	19	12	10
slope ($\times 10^4$)	4.24	4.60	5.06	5.52	5.17	5.60
torr D_2	15.	15.	15.	25.	25.	25.
rate const. $1 \text{ mole}^{-1} \text{sec}^{-1}$ $\times 10^7$	1.11	1.58	2.15	1.65	1.38	1.70

Average rate constant = $1.58 \times 10^7 \text{ l mole}^{-1} \text{sec}^{-1}$.

TABLE V-XII
Data for Cd^3 Decay in $\text{C}_2\text{H}_3\text{F}$ at Room Temperature

Time μsec	Relative Concentration of Cd^3									
	72	66	63	73	68	78	83	85	85	85
30										
40	43	45	48	50	52	48	43	61	61	64
50	25	28	28	37	35	34	41	37	37	45
60	17	20	18	24	27	22	24	23	23	28
70	14	13	15	14	15	13	22	17	17	21
80	12	8	9	8	15	10	12			14
slope ($\times 10^4$)	5.73	5.90	5.59	5.80	4.69	6.15	5.21	5.98	5.98	4.99
torr $\text{C}_2\text{H}_3\text{F}$	3.4	3.4	3.4	2.6	2.6	2.6	3.0	3.0	3.0	3.0
rate const. $1 \text{ mole}^{-1} \text{ sec}^{-1}$ $\times 10^8$	1.32	1.41	1.24	1.79	0.98	2.04	1.17	1.64	1.64	1.03

Average rate constant = $1.40 \times 10^8 \text{ l mole}^{-1} \text{ sec}^{-1}$.

TABLE V-XIII
Data for Cd^3 Decay in $t\text{-C}_2\text{H}_2\text{F}_2$ at Room Temperature

Time μsec	Relative Concentration of Cd°									
	70	67	55	71	68	74	92	90	69	
30										
40	47	49	38	53	47	50	72	58	44	
50	28	29	29	31	39	34		41	32	
60	20	17	18	20	17	24	35	29	22	
70	13	13	11	14	14	12	20	22	19	
80	7	8	7	12	11	10	17	14	12	
slope ($\times 10^4$)	6.25	6.16	5.61	5.61	5.48	5.84	5.02	5.18	4.85	
torr $t\text{-C}_2\text{H}_2\text{F}_2$	5.0	5.0	5.0	4.0	4.0	4.0	3.1	3.1	3.1	
rate const. $1 \text{ mole}^{-1} \text{ sec}^{-1}$ $\times 10^8$	1.10	1.07	0.86	1.08	1.02	1.18	1.02	1.11	0.91	

Average rate constant = $1.04 \times 10^8 \text{ l mole}^{-1} \text{ sec}^{-1}$.

TABLE V-XIV
Data for Cd^3 Decay in $c\text{-C}_2\text{H}_2\text{F}_2$ at Room Temperature

Time μsec	Relative Concentration of Cd°									
	64	54	47	66	57	62	57	60	63	63
30	64	54	47	66	57	62	57	60	63	63
40	44	38	36	47	37	41	44	43	42	42
50	31	31	20	33	25	28	25	27	26	26
60	20	20	12	23	18	22	20	25	24	24
70	14	15	10	15	11	15	9	11	18	18
80	9	13	5	7	7	11	8	9	9	9
slope ($\times 10^4$)	5.43	4.34	6.19	5.54	5.90	5.07	5.76	5.34	4.93	4.93
torr $c\text{-C}_2\text{H}_2\text{F}_2$	5.0	5.0	5.0	4.5	4.5	4.5	4.0	4.0	4.0	4.0
rate const. $1 \text{ mole}^{-1} \text{sec}^{-1}$ $\times 10^7$	7.91	3.80	10.8	9.23	10.7	7.27	11.4	9.47	7.53	7.53

Average rate constant = 8.68×10^7 .

TABLE V-XV
Data for Cd^3 Decay in $1,1\text{-C}_2\text{H}_2\text{F}_2$ at Room Temperature

Time μsec	Relative Concentration of Cd°																									
	63	51	59	51	57	60	54	46	47	42	34	44	36	30	40	25	26	25	17	15	15	12	7	12		
30	63	51	59	51	57	60	54	46	47																	
40	42	32	44	34	43	44	36	30	40																	
50	27	35	32	20	29	30	31	26	25																	
60	20	21	22	21	19	18	18	16	17																	
70	14	11	17	10	17	15	15	11	15																	
80	8	14	10	11	10	12	12	7	12																	
slope ($\times 10^4$)	5.62	4.14	4.76	4.75	4.81	4.95	4.46	5.06	3.7																	
torr $g\text{-C}_2\text{H}_2\text{F}_2$	4.9	4.9	4.9	5.5	5.5	5.5	4.5	4.5	4.5																	
rate const. $1 \text{ mole}^{-1}\text{sec}^{-1}$ $\times 10^7$	8.73	3.09	5.45	4.84	5.05	5.53	4.69	7.18	1.66																	
Average rate constant = $5.13 \times 10^7 \text{ l mole}^{-1}\text{sec}^{-1}$.																										

TABLE V-XVI
Data for Cd^3 Decay in C_2HF_3 at Room Temperature

Time μsec	Relative Concentration of Cd°										
30	71	81	80	62	64	54	73	63	83		
40	49	49	59	47	45	37	48	39	47		
50	28	27	36	26	25	18	34	28	39		
60	19	23	24	18	19	19	24	25	20		
70	18	18	18	12	14	10	14	18	13		
80	16	12	15	8	9	6	10	10	12		
slope ($\times 10^4$)	4.84	5.60	5.23	5.89	5.71	6.02	5.71	4.70	6.00		
torr C_2HF_3	8.4	8.2	8.4	8.2	8.2	8.2	10.	10.	10.		
rate const. $1 \text{ mole}^{-1} \text{sec}^{-1}$ $\times 10^7$	3.36	5.05	4.23	5.86	5.45	6.16	4.49	2.57	5.02		

Average rate constant = $4.69 \times 10^7 \text{ l mole}^{-1} \text{sec}^{-1}$.

TABLE V-XVII
 Data for Cd^3 Decay in C_2F_4 at Room Temperature

Time μsec	Relative Concentration of Cd^0											
	71	90	68	76	66	66	70	60	75	51	40	26
30	71	90	68	76	66	66	70	60	75			
40	53	59	47	48	45	51	61	46	51			
50	31	49	32	29	38	34	41	35	40			
60	25	33	29	24	27	25	30	30	26			
70		23	23	13	22	21	19	20	25			
80	13	18	15	11	15	15		14	12			
slope ($\times 10^4$)	5.03	4.63	4.08	4.80	4.04	4.31	4.48	3.90	4.52			
torr C_2F_4	9.2	9.2	9.2	10.	10.	10.	10.	10.	10.			
rate const. $1 \text{ mole}^{-1}\text{sec}^{-1}$ $\times 10^7$	3.19	2.59	1.36	4.29	1.33	1.69	2.65	1.35	2.83			
Average rate constant = $2.33 \times 10^7 \text{ l mole}^{-1}\text{sec}^{-1}$.												

TABLE V-XVIII
 Data for Cd³ Decay in SiH₃CH₃ at Room Temperature

Time μsec	Relative Concentration of Cd ^o									
	30	40	50	60	70	80	slope (x10 ⁴)	torr SiH ₃ CH ₃	rate constant l mole ⁻¹ sec ⁻¹ x 10 ⁹	
	109	79	49	38	32	20	4.69	0.21	1.23	
	136	99	72	53	44	22	4.71	0.21	1.23	
	94	67	42	30		12	5.72	0.21	2.14	
	89	73	45	34	27	18	4.40	0.21	0.96	
	106	74	37	36	21	27	5.26	0.21	1.73	
	93	60	54	34	35	12	4.87	0.21	1.38	
	106	74	54	34	25	18	5.06	0.21	1.55	
	92	67	34	23	19		6.30	0.21	2.66	

Average rate constant = 1.59×10^9 l mole⁻¹sec⁻¹.

TABLE V-XIX
Data for Cd* Decay in C₂H₄ and H₂ at Room Temperature

	C ₂ H ₄		H ₂	
	Time	[Cd*]	Time	[Cd*]
	30	82	18	91
	40	65	42	44
	50	31	29	64
	60	22	65	17
	70	13	33	52
	80	7	33	54
slope (x10 ⁴)		4.78	5.26	4.50
rate constant 1 mole ⁻¹ sec ⁻¹		0.50	0.50	3.4
torr quencher		5.40	7.59 (x10 ⁸)	5.85 x 10 ⁷
				3.92 x 10 ⁷
				4.48
				4.4
				76
				43
				30
				23
				10
				59

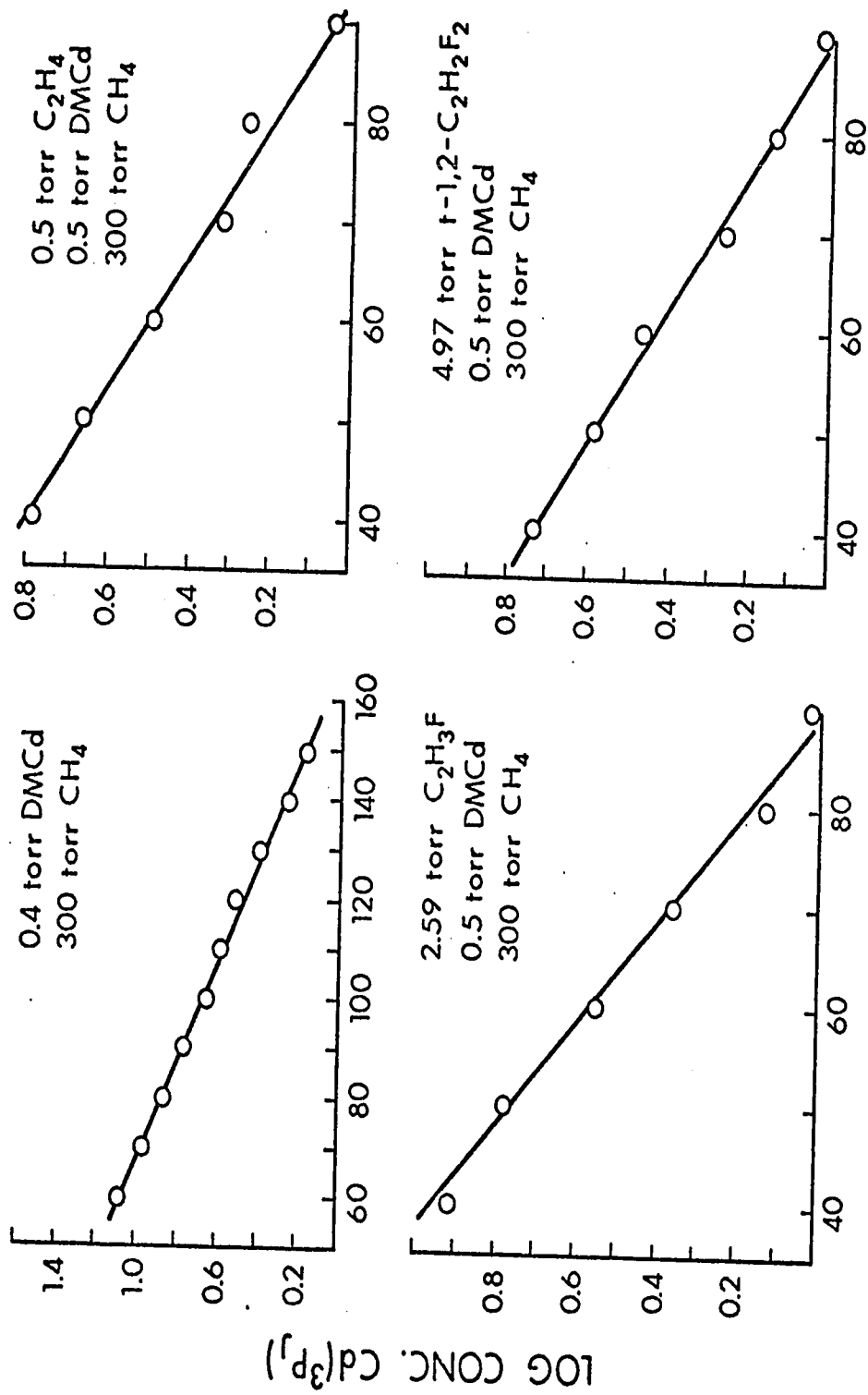


FIGURE 5-3: Typical First Order Plots for the Decay of Cd^{3+} .

TABLE V-XX
 Quenching Rate Constants for Cd(3P)

Quencher	Rate Constant (l. mole ⁻¹ sec ⁻¹)	
	(3P_0)	(3P_1)
C ₂ H ₄	6.2(±1.5) 10 ⁸	6.5 x 10 ⁸
C ₃ H ₆	7.2(±2.3) 10 ⁸	
<i>c</i> -C ₄ H ₈	8.7(±4.1) 10 ⁸	
<i>t</i> -C ₄ H ₈	1.0(±0.1) 10 ⁹	
C ₂ H ₂	6.1(±1.3) 10 ⁸	
H ₂	4.8(±1.2) 10 ⁷	4.9 x 10 ⁷
D ₂	1.6(±0.4) 10 ⁷	
C ₂ H ₃ F	1.4(±0.3) 10 ⁸	
<i>t</i> -C ₂ H ₂ F ₂	1.0(±0.1) 10 ⁸	
<i>c</i> -C ₂ H ₂ F ₂	8.7(±2.2) 10 ⁷	
1,1-C ₂ H ₂ F ₂	5.5(±1.0) 10 ⁷	
C ₂ HF ₃	4.7(±1.3) 10 ⁷	
C ₂ F ₄	2.3(±1.1) 10 ⁷	
SiH ₃ CH ₃	1.6(±0.5) 10 ⁹	

TABLE V-XXI

Relative Rates of Cadmium and Mercury Quenching

Temp. °K Quencher	Cd(³ P) ^a	Cd(³ P)	Cd(³ P) ^d	Hg(³ P ₁) ^e
	300	550	485	300
C ₂ H ₄	(1.00)*	(1.00) ^b	(1.00)	(1.00)
C ₃ H ₆	1.16	1.15 ^b	1.00	1.10
<i>c</i> -C ₄ H ₈	1.40	0.97 ^b	0.97	1.18
<i>t</i> -C ₄ H ₈	1.61	0.97 ^b	0.97	
C ₂ H ₂	0.98	1.00 ^b	0.91	0.98
H ₂	0.08	0.79 ^b	0.47	0.80
D ₂	0.03		0.18	1.16
C ₂ H ₃ F	0.23	0.80 ^c		0.82
<i>t</i> -C ₂ H ₂ F ₂	0.16	0.69 ^c		
<i>c</i> -C ₂ H ₂ F ₂	0.14	0.60 ^c		
1,1-C ₂ H ₂ F ₂	0.09	0.58 ^c		0.65
C ₂ HF ₃	0.08	0.31 ^c		0.44
C ₂ F ₄	0.04	0.18 ^c		0.20
SiH ₃ CH ₃	2.59			1.80

* Values in parenthesis used as standards.

^a Results of this study. ^b From reference (64).^c S. Tsunashima and O. P. Strausz, unpublished results.^d From reference (59). ^e From reference (7).

concentration of quencher to obtain a rate constant. The resulting rate constants for each quenching gas were then averaged. The errors reported are the standard deviation of the mean of the rate constants.

The standard deviations of the slopes of the individual plots were small, of the order of 1% of their value but the standard deviations of the mean of the rate constants were of the order of 25%. Although large errors may be introduced in the measurement of very small pressures where very efficient quenchers are concerned, the range of errors did not depend on the rate of quenching, and other sources of error are operative. The most probable source of random errors is the variation in photographic plate characteristics. The photographic plates themselves are not reproducible, variations in plate characteristics cannot be avoided. The error limits reported here are in the same range as those from other studies using the same technique. Metal deposition on the cell walls was shown to be insignificant since experiments performed using either increasing or decreasing order of delay times yielded the same results.

2. Activation Energy of the Cd³ + Ethylene Reaction

The rate of quenching of Cd³ by ethylene was measured at 27, 50, 80 and 110°C. Higher temperatures were not attempted as pyrolysis of DMCD becomes significant at 150°C (108). The data and rate constants are listed in Tables V-XXII through V-XXIV. The rate parameters calculated from the Arrhenius plot (Figure 5-4) are

$$k = 4 \times 10^{10} \exp(-2300/RT) \text{ l mole}^{-1} \text{ sec}^{-1}.$$

With this data the relative rates from references b and c of Table V-XXI were converted to absolute values. This data was then combined with the rate constants from this study and Arrhenius parameters for a series of reactions were obtained. The results are listed in Table V-XXV.

TABLE V-XXII

Data for Cd^3 Decay in C_2H_4 at 50°C

Time μsec	Relative Concentration of Cd°													
	120	85	73	59	70	158	152	150	101	98	70	76	55	43
30														
40	91	61	49	42	51	106	117	114	76	70				
50	61	45	35	30	34	69	83	72	55	43				
60	49	35	18	25	24	49	62	61	42	40				
70	32	28	14	20	16	34	35	48	32	25				
80	24	19	13	10	13	38	29	31	24	21				
slope ($\times 10^4$)	4.54	4.13	5.47	4.35	5.06	4.74	4.81	4.36	4.13	4.61				
torr C_2H_4	0.30	0.30	0.43	0.43	0.43	0.30	0.30	0.30	0.30	0.30				
rate const. $\text{l mole}^{-1}\text{sec}^{-1}$ $\times 10^8$	8.14	5.38	10.0	4.79	8.12	9.49	9.96	6.93	5.38	8.61				

Average rate constant = $7.69 (\pm 1.97) \times 10^8 \text{ l mole}^{-1}\text{sec}^{-1}$.

TABLE V-XXIII
 Data for Cd^3 Decay in C_2H_4 at 80°C

Time μsec	Relative Concentration of Cd°															
	80	73	146	156	136	73	75	80	78	80	81	80	78	80	81	81
30	80	73	146	156	136	73	75	80	78	80	81	80	78	80	81	81
40	54	58	94	102	110	50	51	46	55	57	62	57	55	57	62	62
50	39	39	75	79	86	36	40	37	38	39	37	38	38	39	37	37
60	29	29	56	63	61	25	26	24	25	32	34	25	25	32	34	34
70	20	21	38	44	33	17	25	20	22	23	23	20	22	23	23	23
80	11	19	29	22	35	10	13	13	12	17	19	13	12	17	19	19
slope ($\times 10^4$)	5.16	4.20	4.59	4.78	4.19	5.33	4.50	5.11	5.04	4.43	4.33	5.11	5.04	4.43	4.33	4.33
torr C_2H_4	0.26	0.26	0.26	0.26	0.26	0.32	0.32	0.26	0.26	0.21	0.21	0.26	0.26	0.21	0.21	0.21
rate const. $1 \text{ mole}^{-1} \text{sec}^{-1}$ $\times 10^9$	1.55	0.74	1.07	1.23	0.73	1.38	0.81	1.51	1.45	1.16	1.05	1.51	1.45	1.16	1.05	1.05
Average rate constant = $1.15 (\pm 0.30) \times 10^9 \text{ 1 mole}^{-1} \text{sec}^{-1}$.																

TABLE V-XXIV
Data for Cd^3 Decay in C_2H_4 at 110°C

Time μsec	Relative Concentration of Cd°									
	30	40	50	60	70	80	slope ($\times 10^4$)	torr C_2H_4	rate const. $1 \text{ mole}^{-1} \text{ sec}^{-1}$ $\times 10^9$	Average rate constant = $1.64 (\pm 0.37) \times 10^9 \text{ l mole}^{-1} \text{ sec}^{-1}$
	92	86	101	82	96	71	94	66	60	
	64	62	50	63	66	53	72	51	44	
	33	56	52	45	34	31	40	34	30	
	24	29	24	28	17	25	22	25	18	
	13	20	16	23	9		16	21	15	
	9	12	11	20	7	13	11	15	12	
	6.83	5.23	6.24	4.32	6.81	5.04	6.20	4.31	4.98	
	0.50	0.20	0.40	0.20	0.50	0.20	0.40	0.20	0.20	
	1.68	2.27	1.74	1.18	1.67	2.07	1.72	1.17	1.32	

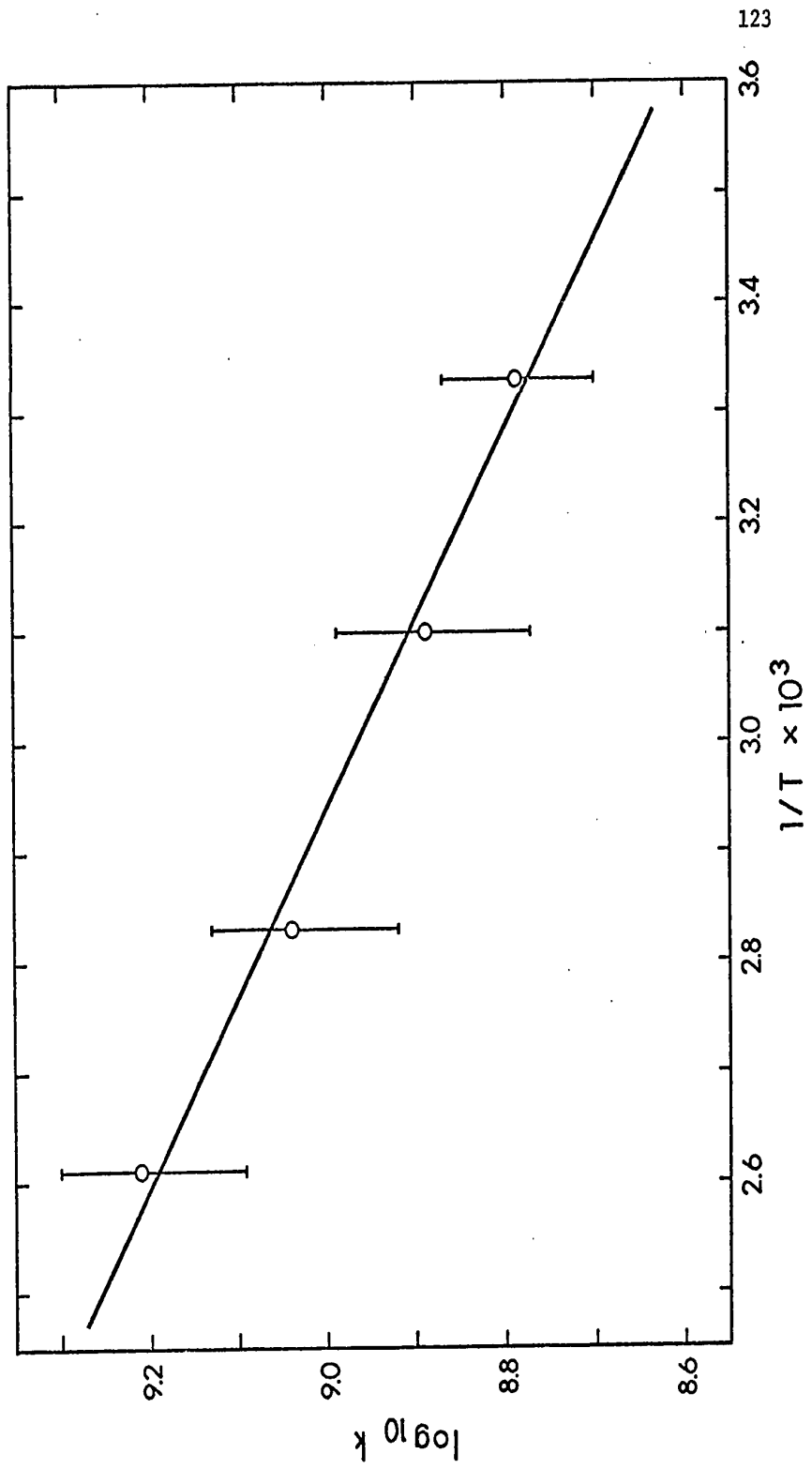


FIGURE 5-4: Arrhenius Plot.

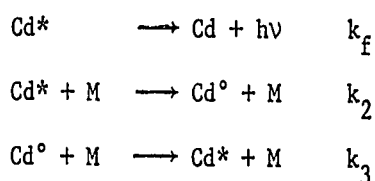
TABLE V-XXV
 Rate Constants at 275°C, and Estimated Activation
 Energies and A-factors

Quencher	k at 275°C	E _a (kcal/mole)	Log ₁₀ A
C ₂ H ₄	4.1 x 10 ⁹	2.3	10.6
C ₂ H ₃ F	3.2 x 10 ⁹	3.6	10.8
<i>trans</i> -C ₂ H ₂ F ₂	2.7 x 10 ⁹	3.8	10.8
<i>cis</i> -C ₂ H ₂ F ₂	2.4 x 10 ⁹	3.8	10.8
CH ₂ CF ₂	2.2 x 10 ⁹	4.3	10.9
C ₂ HF ₃	1.3 x 10 ⁹	3.8	10.5
C ₂ F ₄	7.4 x 10 ⁸	4.0	10.3
C ₃ H ₆	4.7 x 10 ⁹	2.2	10.4
<i>cis</i> -C ₄ H ₈	4.0 x 10 ⁹	1.8	10.2
C ₂ H ₂	4.1 x 10 ⁹	2.3	10.4
H ₂	3.2 x 10 ⁹	4.9	11.3

3. Discussion

The independence of the rate of decay of Cd^3 with methane pressure indicates that the rate of quenching by several hundred torr of methane is extremely slow compared to the rate of fluorescence and spin-orbit equilibration. The measured rate of Cd° decay under these conditions is approximately one order of magnitude slower than the natural decay rate of Cd^* , 4.5×10^5 sec (109).

Assuming the following mechanism:



the decay of Cd° is given by: (see Appendix)

$$-\frac{d[\text{Cd}^\circ]}{dt} = \frac{b \pm \sqrt{b^2 - 4c}}{2} [\text{Cd}^\circ]$$

where $b = k_f + k_2[\text{M}] + k_3[\text{M}]$ and $c = k_f k_3[\text{M}]$. Numerical evaluation of the above equation shows that $-d[\text{Cd}^\circ]/dt$ approaches a value of

$$k_f \left(\frac{k_3}{k_2 + k_3} \right)$$

The value of k_f is greater than that obtained experimentally from the decay rate of Cd° and the magnitude of the discrepancy will depend on the relative values of k_2 and k_3 . If the spin states are thermalized, the $\text{Cd}^*/\text{Cd}^\circ$ population ratio will be approximately 1/5, $k_2/k_3 = 5$ and k_f will be six times faster than the observed rate of Cd° decay at 300°K. However, the experimental ratio $\text{Cd}^*/\text{Cd}^\circ$ is 0.4 and independent of temperature, although this value is approximate as the Beer-Lambert factor is not known for Cd^* , and the error in

measuring the weak Cd* line is large.

A significant imprisonment effect is to be expected in this system as the concentration of ground state cadmium atoms is high, of the order of 0.5 torr. Until the values of k_2 and k_3 become available, the value of the fluorescence rate constant remains unspecified within the limits set by the natural lifetime and the measured rate of Cd° decay. However, this experimental decay rate of Cd° is used in evaluating the results of the quenching measurements.

In the quenching experiments the relationship between the observed rate of decay of Cd° and the rate of quenching of Cd* depends on the mechanism of quenching and on the values of k_2 and k_3 (see Appendix). If the rate constant for quenching of Cd°, k_4 , is zero, the rate of Cd* quenching will be equal to the decay rate of Cd° multiplied by $(k_2+k_3)/k_3$. If the rate constant for quenching of Cd* and Cd° are equal, the measured rate is the true rate of quenching. If k_4 lies in the range $0 - k_1$, where k_1 is the rate constant for quenching of Cd*, the rate of decay of Cd°, k_{expt} , will lie between $k_1 k_3 / (k_2 + k_3)$ and k_1 .

$$\text{If } 0 < k_4 < k_1$$

$$\text{then } k_1 k_3 / (k_2 + k_3) < k_{\text{expt}} < k_1$$

An analysis of the decay kinetics of coupled J states has been accomplished under steady state conditions and qualitatively similar results were obtained (110). The quenching rate of Hg° by ethylene is only two times less than that for Hg* (201). Since the $^3P_1 - ^3P_0$ splitting for Cd and Hg are 1.6 and 5 kcal/mole respectively, it is likely that the rates of quenching of Cd* and Cd° would be similar

since the energy difference between them is slight. Thus the discrepancy between the reported rate constants and the true values is expected to be small.

The rate constants reported here are approximately two orders of magnitude smaller than those reported by Steacie and LeRoy (59) or Lipson and Mitchell (58). The discrepancy can be attributed to the complete neglect of imprisonment effects in both of the previous studies and the omission of the intervention of the 3P_0 state in the mechanism. The present work shows that equilibration of the spin states occurs at least in hydrocarbons. Under these conditions, quenching results cannot be calculated from the Stern-Volmer plots; furthermore, the technique used to calibrate photographic plates in the previous work has been shown to be unsatisfactory. (see Chapter VI)

It is well established that the interaction of Cd^3 and ethylene produces triplet ethylene (3Et) (63,65). The energy of 3Et in the planar configuration is ~ 105 kcal/mole above that of the ground state while 3Et in the skew configuration is some 60 kcal/mole above the ground state (111). Triplet cadmium, containing only 87 kcal/mole, cannot interact with ethylene to produce 3Et without violating the Franck-Condon principle, which states that only vertical transitions are allowed. Thus the rate of reaction with Cd^3 is expected to be slow compared to that with mercury where, due to the greater energy content of Hg^* , the transition is of higher probability.

The relative rates of quenching Cd^3 by olefins depend on the electron density of the π -electron cloud of the double bond, the site of reaction. The inductive effects of fluorine atoms and methyl

groups decrease and increase this electron density respectively, and the rate constants increase and decrease correspondingly with the addition of each substituent. Thus Cd^3 , like Hg^* , displays electrophilic character in quenching reactions. However the rate of the Cd^* reactions are more sensitive to the degree of substitution than the analogous Hg^* reactions because the Cd^* reaction is energy limited.

The formation of CdH and CdD with hydrogen and paraffins shows that cadmium photosensitization is occurring. The significant decrease in the rate of Cd^3 quenching by D_2 as compared to H_2 indicates that in this near thermoneutral reaction, the zero-point energy difference between H_2 and D_2 and the CdH and CdD is a significant factor in determining the respective rates. The higher rate of Cd^* quenching by SiH_3CH_3 , compared to that by C_2H_4 may be due to the enthalpy of the respective reaction; the hydrogen abstraction reaction would be exothermic.

The existence of activation energies for Cd^3 photosensitization reactions, Table V-XXVI, explains the variations observed in the relative rates of Cd^* quenching studies listed in Table V-XXII. In fact the trends observed in the relative rates of quenching as a function of temperature can be explained by variations in E_a .

The first measurements of activation energies in mercury sensitization were reported by Campbell et al. (112) who reported the relative activation energy of formation of *n* and *iso*-propyl radicals in the Hg^* and Hg° photosensitization of propane. The present study however, describes the first absolute measurement of an activation energy for a photosensitization reaction.

A mechanistic interpretation of the measured activation energy, however, is difficult without knowledge of the microscopic details of the interaction between Cd^3 and ethylene. The activation energy may be due to the existence of a small energy barrier to crossing from the potential surface correlation with $\text{Cd}^* + \text{C}_2\text{H}_4$ to the potential surface correlation to $\text{Cd} + {}^3\text{Et}$.

CHAPTER VI

THE QUENCHING OF ANTIMONY AND BISMUTH ATOMS

1. The Quenching of Excited Bismuth Atoms

Trimethylbismuth (TMBi) exhibits a broad absorption in the UV with a maximum at 2115\AA ($\epsilon = 1.7 \times 10^4 \text{ l mole}^{-1} \text{ cm}^{-1}$) and shoulders at 2600 and 2225\AA . The spectrum, recorded on a Cary Model 14 spectrometer, is shown in Figure 6-1. The flash photolysis of TMBi in the presence of argon produces a variety of atomic and molecular species, summarized in Table VI-I. No additional spectra were observed in the presence of N_2 , H_2 , C_2H_4 , or hydrocarbons. If the spectroscopic lamp was not employed several atomic emission transitions were detected. An energy level diagram (113) for the bismuth atom showing the states detected by emission and absorption spectroscopy along with the transitions relevant to the following discussion is given in Figure 6-2.

A system, with bands at 2490 , 2555 and 2615\AA , decays rapidly during the photolysis flash but after the flash has terminated it persists for some $300 \mu\text{sec}$. Flash energy variation studies show that the intensity of the 2615\AA band decreases with increasing energy, suggesting that the carrier is photolyzed. It is a reasonable assumption that BiCH_3 or possibly $\text{Bi}(\text{CH}_3)_2$ is the carrier.

The bands at 2290 , 2330 , 3090 , and 3165\AA which appear only with added CO_2 can be resolved into two systems, the splitting in each pair being $720 \pm 20 \text{ cm}^{-1}$. A possible carrier is the previously unobserved $X_2^2 \pi_{3/2}$ state of BiO , estimated by Bridge and Howell (114) to be 8000 cm^{-1} above the $X_1^2 \pi_{1/2}$ ground state. If this is so, then the

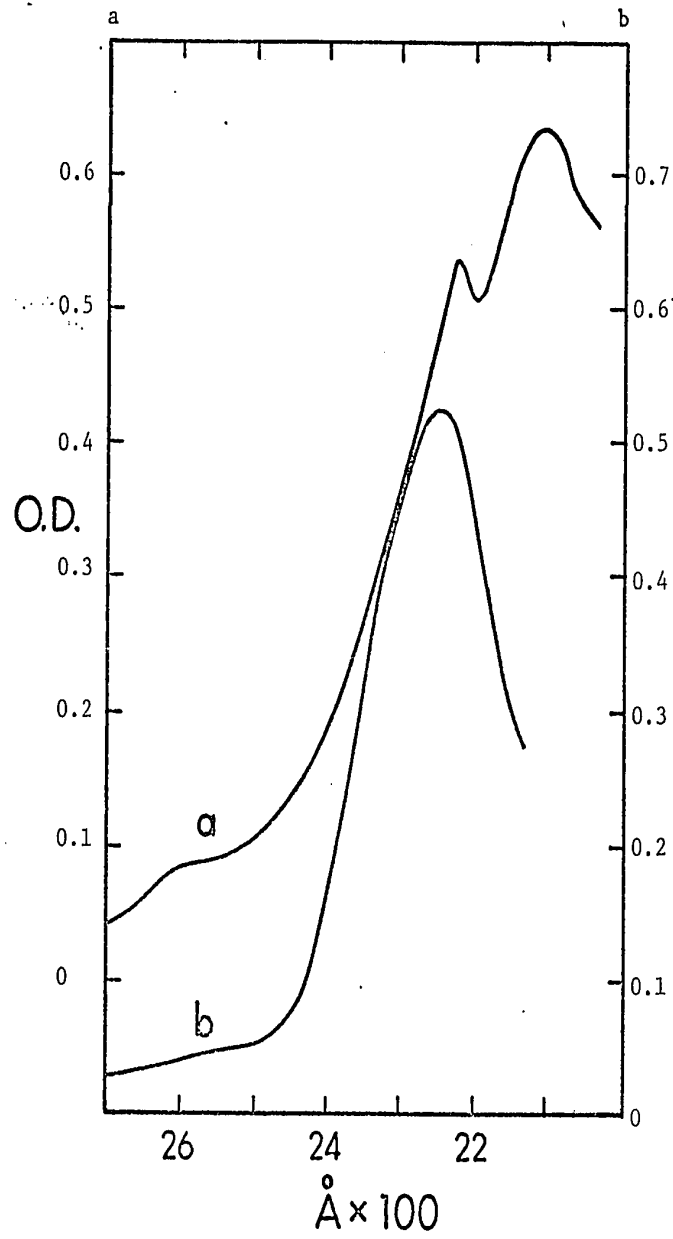


FIGURE 6-1: Absorption Spectra of TMBi and TMSb:
a 0.07 torr TMBi; b 0.05 torr TMSb.

TABLE VI-I

Species Observed in Absorption in Flashed TMBi

Species	Transition	$\lambda(\text{\AA})$	Comments
$\text{Bi}(^4\text{S}^0)$	$^4\text{P}_{1/2} \leftarrow ^4\text{S}^0$	3068	Decay not simple first or second order
$\text{Bi}(^2\text{D}_{3/2}^0)$	$^2\text{P}_{1/2} \leftarrow ^2\text{D}_{3/2}^0$	2898	
$\text{Bi}(^2\text{D}_{5/2}^0)$	$^2\text{P}_{3/2} \leftarrow ^2\text{D}_{5/2}^0$	2938	Quenched by 100 torr of H_2 , C_2H_4
$\text{Bi}(^2\text{P}_{1/2}^0)$? $\leftarrow ^2\text{P}_{1/2}^0$	2730	
$\text{Bi}_2(\text{X}^1\Sigma_g^+)$	B \leftarrow X	5000	
$\text{Bi}_2(\text{X}^1\Sigma_g^+)$	C \leftarrow X	\sim 3150	TMBi > 0.1 torr
$\text{Bi}_2(\text{X}^1\Sigma_g^+)$	D \leftarrow X	\sim 2700	
$\text{Bi}_2(\text{X}^1\Sigma_g^+)$? \leftarrow X	\sim 2150	Weak, complicated by overlap with other systems; not analyzed
CH_3	B \leftarrow X	2160	
?		2900-3100	See text
$\text{BiO}(\text{X}_1^2\Pi_{3/2})$	A \leftarrow X ₁	\sim 2591	Appears with added O_2 , CO_2
$\text{BiO}(\text{X}_2^2\Pi_{1/2})$	A \leftarrow X ₂	See text	See text
$\text{BiCH}_3(?)$		See text	See text

long wavelength bands may correspond to the (n,0) and (n+1,0) bands of the $E \leftarrow X_2$ transition (115). In this case the $X_2 - X_1$ splitting would be 6980 cm^{-1} , considerably less than Bridge and Howell's estimate. An alternative explanation that these are the (n,0) and (n,1) bands of the $E \leftarrow X_2$ transition, is unlikely since a change from $\omega_e = 692 \text{ cm}^{-1}$ to $\omega_e = 750 \text{ cm}^{-1}$ in the X_1 and X_2 states respectively could not arise from a change in spin-orbit coupling. A change in spin-orbit coupling causes at most a change of a few wavenumbers in ω_e for all spectra listed in reference (57).

The 2900 - 3100Å system observed at high TMBi pressures consists of an absorption band 100Å wide centered at 2935Å and a series of red degraded bands. Positions of the band heads and splittings between bands are given in Table VI-II. Although the spectrum appears to be typical of a heavy diatomic molecule, the rate of decay is much more rapid than that of ground state Bi_2 and the frequency differences between successive bands are larger than the vibrational frequencies of any known state of Bi_2 (57). The largest known ω_e for Bi_2 is 172.71 cm^{-1} for the $X^1\Sigma_g$ state (57). No assignment has been made.

In an attempt to determine the mode of formation of the highly excited metal atoms observed in emission, time resolved emission experiments were carried out. Under all conditions the emission from the $\text{Bi}(^4P_{1/2})$ at 3068Å ($^4P_{1/2} \rightarrow ^4S_0$), the Bi resonance line, exactly followed the photo-flash profile, indicating that all processes leading to formation of excited atoms were rapid. This method for monitoring the emission was therefore abandoned.

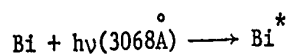
TMBi flashed through UV dye, which did not affect the extent of photolysis but greatly attenuated the incident radiation around 3068Å,

TABLE VI-II
 The 2900-3100Å System Observed in Flashed TMBi

$\lambda(\text{Å})$	$\nu(\text{cm}^{-1})$	$\Delta\nu(\text{cm}^{-1})$
2922	34230 ± 10	360
2953	33870	210
2971	33660	200
(2989)	33460	220
3008	33240	220
3028	33020	230
3949	32790	200
(3068)	32590	230
3090	32360	220
3111	32140	180
3129	31960	230
3152	31730	210
3173	31520	

Values in parentheses are uncertain because of overlap with intense atomic lines.

gave essentially the same intensity of emission from excited metal states. Excited atom formation by processes such as



can therefore be ruled out. Increasing the flash energy from 1500 to 3000 J produced an increase by a factor of 3 in the 3068 $\overset{\circ}{\text{\AA}}$ emission intensity. This observation is consistent with a multiquantum process and it is likely therefore, that excited atoms are produced in a process involving BiCH₃ and Bi(CH₃)₂.

Preliminary experiments showed that added gas could have two effects on the 3068 $\overset{\circ}{\text{\AA}}$ emission line: the gas could change its shape and/or quench it. With increasing argon pressure two distinct satellite bands to the short wavelength side of the 3068 $\overset{\circ}{\text{\AA}}$ line became apparent, with maxima approximately 12 and 18 $\overset{\circ}{\text{\AA}}$ from the resonance line. Hydrogen, C₂H₆, and CH₄ also broadened the line to shorter wavelengths. Xenon produced a single satellite band on the long wavelength side of the 3068 $\overset{\circ}{\text{\AA}}$ line. Microdensitometer traces showing the variation in the 3068 $\overset{\circ}{\text{\AA}}$ line shape with the nature and pressure of the added gas are reproduced in Figure 6-3.

Satellite bands have been observed earlier on both sides of the Bi resonance line in the presence of Xe (116) and similar bands have been seen in other systems, notably with mercury (7) and alkali metals (117).

The formation of collisionally induced satellite bands close to atomic transitions is generally attributed to the transitory formation of van der Waals molecules (7, 116). The radiative-transition probabilities for these molecules differ from those of the free atoms

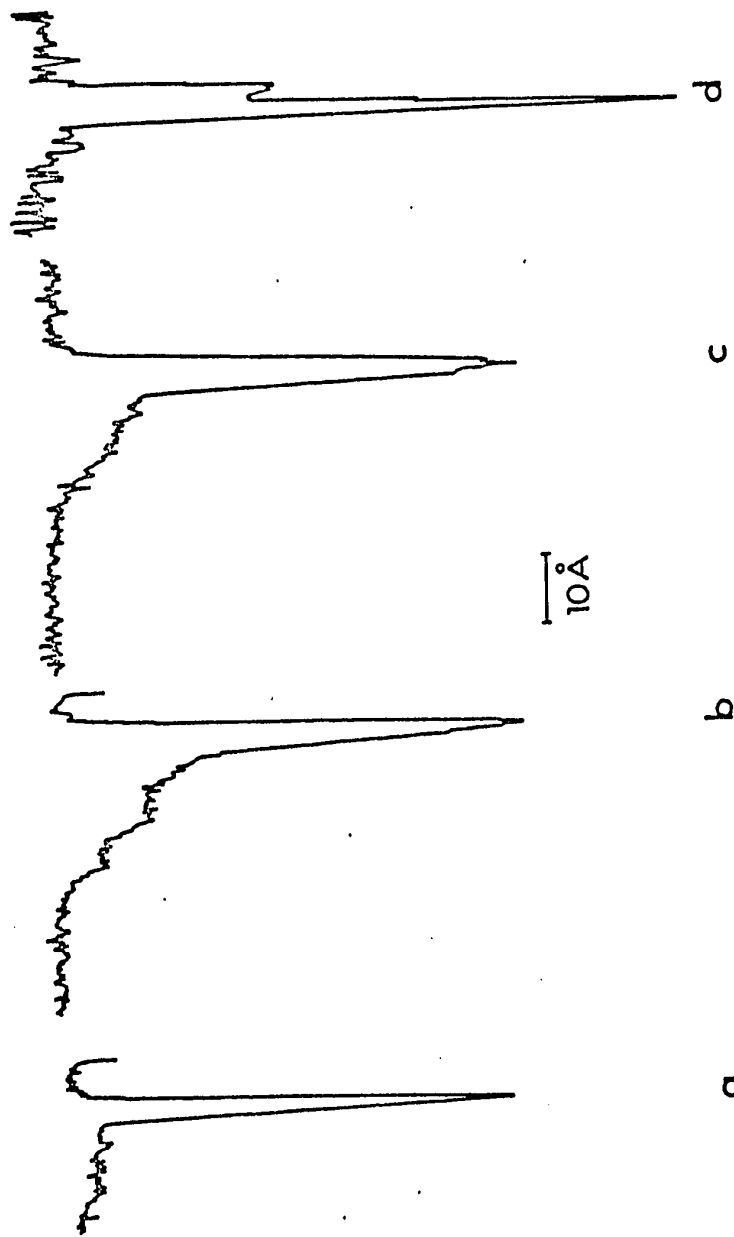


FIGURE 6-3: Emission from $\text{Bi}(^4P_{1/2})$ at 3068 Å: a, 100 torr of Ar; b, 640 torr of Ar; c, 100 torr of Ar, 500 torr of CH_4 ; d, 10 torr of Ar, 90 torr of Xe; all with 0.01 torr of TMBi.

owing to perturbations by intermolecular forces; collisionally-induced emission from metastable atomic states has been observed (118, 119).

Since all the excited states of Bi observed here have very short lifetimes neither time resolved emission nor kinetic absorption spectroscopy could be used to measure quenching rates. Therefore, fluorescence measurements were carried out and rates of quenching of excited Bi were calculated from the Stern-Volmer relationship. Quantitative quenching experiments were carried out at total pressures of 100 torr using argon as diluent. At this pressure of argon satellite band formation was negligible and it is assumed that varying the Ar pressure at a constant total pressure of 100 torr has no effect on emission intensity. All experiments were conducted with 10^{-2} torr TMBi since the emission intensity of the excited Bi states is a maximum at this pressure. Because of insufficient intensity from other states, only four of the Bi states were studied quantitatively; $\text{Bi}(^4\text{P}_{1/2})$ at 3068\AA ($^4\text{P}_{1/2} \rightarrow ^4\text{S}_0$), $\text{Bi}(^4\text{P}_{5/2})$ at 3024\AA ($^4\text{P}_{5/2} \rightarrow ^2\text{D}_{5/2}^\circ$), $\text{Bi}(^2\text{P}_{3/2})$ at 2938\AA ($^2\text{P}_{3/2} \rightarrow ^2\text{D}_{5/2}^\circ$), and $\text{Bi}(^2\text{P}_{1/2})$ at 2898\AA ($^2\text{P}_{1/2} \rightarrow ^2\text{D}_{3/2}^\circ$). Results were plotted in the form I_0/I vs p where I_0 is the emission intensity in the absence of quencher and I is the emission intensity in the presence of $100-p$ torr of argon and p torr of quencher. The data are given in Table VI-III and typical plots are shown in Figures 6-4, 5, 6.

In order to convert emission peak heights, obtained by plate photometry, into relative intensities it was necessary to determine the relationship between the intensity of light and the optical density changes on the photographic plate. The intensity of the spec-lamp, I_1 , was varied by inserting a calibrated rhodium step filter into the light path. The plate densities produced in this manner were plotted against

TABLE VI-III
Stern-Volmer Data for Excited Bi

Quencher	Pressure (torr)	3068Å		3024Å		2938Å		2898Å		
		ΔOD	$\frac{I_0}{I}$	ΔOD	$\frac{I_0}{I}$	ΔOD	$\frac{I_0}{I}$	ΔOD	$\frac{I_0}{I}$	
Xe	0	75	1	45	1	36	1	36	1	
	10	74	1	48		29	1.31	46	.73	
	20	73		47		27	1.43	50	.66	
	30	71		48		22	1.81	53	.60	
	50	74		47		17	2.43	71	.39	
	75	72		46		14	3.16	79	.33	
	90	72		45		11	3.95	86	.29	
	CO	0	80	1	43	1	39	1	42	1
		3.6	60	1.54			27	1.60	31	1.51
5.2		50	1.97	34	1.37	25	1.68			
6.5		48	2.13	34	1.37	27	1.60	24	2.00	
7.7		44	2.34	30	1.60	19	2.32	23	2.10	
10.3		38	3.81	27	1.79	19	2.32	21	2.42	
12.9				27	1.79	19	2.32	18	2.76	
15.5		32	3.50	21	2.40	14	3.26	14	3.68	

TABLE VI-III (cont'd)

Stern-Volmer Data for Excited Bi

Quencher	Pressure (torr)	3068Å		3024Å		2938Å		2898Å	
		ΔOD	$\frac{I_0}{I}$	ΔOD	$\frac{I_0}{I}$	ΔOD	$\frac{I_0}{I}$	ΔOD	$\frac{I_0}{I}$
N ₂	0	85	1	40	1	37	1	35	1
	3.5			32	1.32	23	1.81	24	1.52
	5.0			35	1.19	25	1.61	27	1.32
	10			33	1.30	17	2.52	25	1.52
	15	69	1.40	31	1.35	17	2.52	25	1.52
	20	68	1.42	36	1.16	15	2.98	24	1.48
	25			33	1.27	11	4.03	18	2.10
	30	68	1.42	35	1.19	12	3.66	23	1.63
	35			29	1.49	12	3.66	14	2.79
	50	58	1.75						
O ₂	0	83	1	45	1	39	1	36	1
	2.4	49	2.18	55	.76	39	1.00	22	1.80
	3.8	42	2.67	59	.69	33	1.26	14	2.88
	4.8	36	3.25	47	.94	30	1.39	15	2.76
	7.2	31	3.91	47	.94	28	1.48	9	4.85
	9.6	33	3.62	40	1.16	32	1.28	6	7.46
	10.8	24	5.35	38	1.26	23	1.85		

TABLE VI-III (cont'd)
Stern-Volmer Data for Excited B1

Quencher	Pressure (torr)	$\frac{3068\text{\AA}}{\Delta OD} \frac{I_0}{I}$	$\frac{3024\text{\AA}}{\Delta OD} \frac{I_0}{I}$	$\frac{2938\text{\AA}}{\Delta OD} \frac{I_0}{I}$	$\frac{2898\text{\AA}}{\Delta OD} \frac{I_0}{I}$
O ₂	12.0	23	37	23	23
	15.6	21	34	23	23
H ₂	0	93	51	45	42
	2.5	87	79	64	34
	3.0	76	76	65	22
	5.0	90	102	77	21
	7.5	81	97	70	21
	10	89	110	84	15
	15	90	118	85	12
	17	87	125	84	10
	20	86	137	99	13
	25	93	143	96	9
	1	1	1	1	1
CH ₄	0	80	41	36	36
	7	105	34	27	Completely quenched
					1.31
					1.40
					1.85
					1.85
					1.30
					2.20
					2.25
					3.4
					4.5
					5.3
					3.8
					5.9

TABLE VI-III (cont'd)
Stern-Volmer Data for Excited Bi

Quencher	Pressure (torr)	3068Å		3024Å		2938Å		2898Å		
		$\frac{\Delta OD}{I_0}$	$\frac{I}{I_0}$	$\frac{\Delta OD}{I_0}$	$\frac{I}{I_0}$	$\frac{\Delta OD}{I_0}$	$\frac{I}{I_0}$	$\frac{\Delta OD}{I_0}$	$\frac{I}{I_0}$	
CH ₄	10	115	.53	39	1.12	34	1.06			
	15	117	.51	34	1.31	31	1.18			
	21	116	.52	34	1.31	26	1.46			
	30	118	.50	34	1.31	24	1.65			
	32	118	.50	32	1.44	21	1.87			
	54	115	.53	24	1.99	18	2.22			
	60	114	.53	26	1.80	17	2.30			
	70	127	.43	21	2.32	17	2.30			
	80	121	.48	21	2.32	18	2.22			
	90	123	.46	24	1.99	21	1.87			
	C ₂ H ₆	0	80	1	40	1	35	1	32	1
		6.5	84	.96	41	.96	40	.86	Completely quenched	
10		87	.92	35	1.17	33	1.09			
20		87	.92	35	1.17	27	1.37			
30		92	.90	31	1.38	32	1.12			
45		112	.58	33	1.28	23	1.66			
60	112	.58	21	2.15	20	1.95				

TABLE VI-III (cont'd)
Stern-Volmer Data for Excited B1

Quencher	Pressure (torr)	3068Å		3024Å		2938Å		2898Å	
		$\frac{\Delta OD}{I_0/I}$	$\frac{\Delta OD}{I_0/I}$	$\frac{\Delta OD}{I_0/I}$	$\frac{\Delta OD}{I_0/I}$	$\frac{\Delta OD}{I_0/I}$	$\frac{\Delta OD}{I_0/I}$	$\frac{\Delta OD}{I_0/I}$	$\frac{\Delta OD}{I_0/I}$
C ₂ H ₆	75	125	.46	19	2.40	19	2.40	19	2.08
	90	120	.49	14	3.40	16	2.58	16	2.58
C ₂ H ₄	0	65	1	36	1	30	1	29	1
	0.7	45	1.7	35	1.02	28	1.09	23	1.29
	1.3	38	2.1	34	1.04	30	1.00	22	1.35
	2.0	30	2.8	30	1.20	32	.91	19	1.59
	2.4	29	2.9	32	1.11	32	.91	16	2.00
	4.0	23	3.9	33	1.09	27	1.13	17	1.82
	6.0	14	6.7	33	1.08	20	1.30	9	3.64
	7.4	10	10.3	26	1.47	25	1.19		
	8.0	11	8.7	33	1.09	18	2.23		
	10	9	10.8	29	1.28	24	1.30		

TABLE VI-III (cont'd)
Stern-Volmer Data for Excited Bi

Quencher	Pressure (torr)	$\frac{3068\text{\AA}}{\Delta OD} \frac{I_0}{I}$	$\frac{3024\text{\AA}}{\Delta OD} \frac{I_0}{I}$	$\frac{2938\text{\AA}}{\Delta OD} \frac{I_0}{I}$	$\frac{2898\text{\AA}}{\Delta OD} \frac{I_0}{I}$
CO ₂	0	83	47	39	38
	.54	46	41	38	33
	1.09	42	36	30	29
	1.63	34	32	31	28
	2.18	28	27	31	19
	2.72	22	27	29	20
	3.26	19	22	29	24

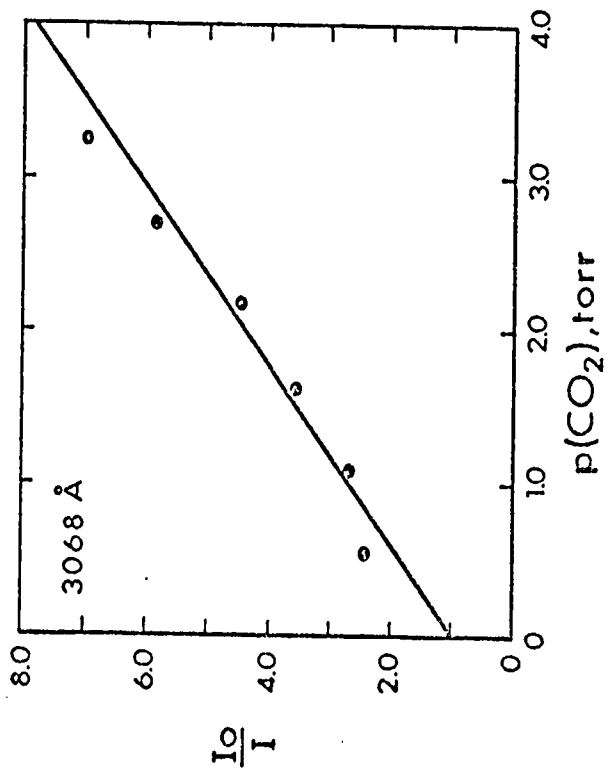


FIGURE 6-4: Stern-Volmer Plot for Excited Bi

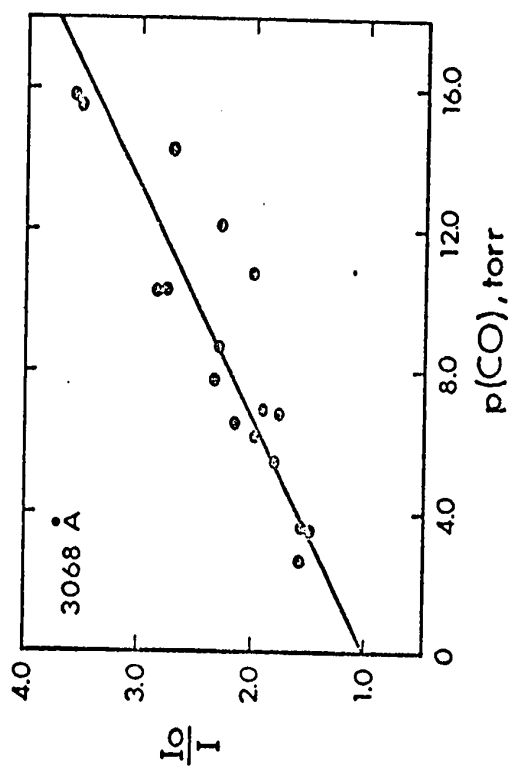


FIGURE 6-5: Stern-Volmer Plot for Excited B1

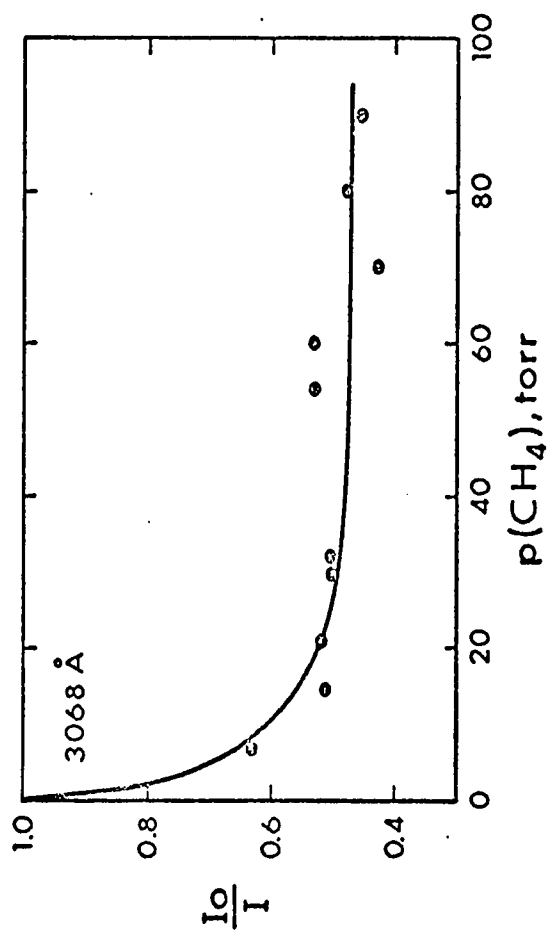


FIGURE 6-6: Stern-Volmer Plot for Excited B1

$\log I_1/I_{10}$ where I_{10} is the intensity with no filter. These plots were linear in the density range 0.2 - 1.4. The slope, γ , varied somewhat from plate to plate, with wavelength and with developing conditions. Averages were found for each wavelength used. The values were: $\gamma = 0.8$ for the bismuth lines; $\gamma = 0.6$ for the 3233 and 3268Å Sb lines; and $\gamma = 0.3$ for the 2529 and 2598Å Sb lines.

To ensure that the base of all emission lines fell in the linear region of plate sensitivity, all plates for quantitative emission work were pre-exposed to a shaded white light so as to produce a background plate density of about 0.2 OD units. Under these conditions the change in plate density, ΔD_n , produced by emission of intensity I_n from a species of concentration C_n is given by:

$$\Delta D_n = \gamma \log \left(\frac{I_n + I'}{I'} \right)$$

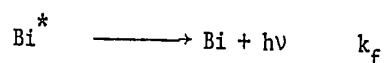
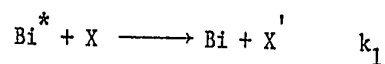
where I' is the intensity of the background fogging radiation. Rearrangement of the above formula, and manipulation to eliminate proportionality constants leads to:

$$\frac{I_n}{I_m} = \frac{10^{\Delta D_n/\gamma} - 1}{10^{\Delta D_m/\gamma} - 1} = \frac{C_n}{C_m}$$

Two assumptions are implicit in this derivation; firstly that the effects on the plate of exposure to diffuse white light and to sharp atomic emission are simply additive, and secondly that the peak heights are not distorted by spectroscopic slit effects. Experiments to

determine the validity of the second assumption are not possible since the fluorescent light reaching the photographic plate does not come with uniform distribution from all parts of the cell.

For the simple system where only quenching or fluorescence is possible, the kinetics are straightforward:



$$I_0/I = 1 + (k_1/k_f)[X]$$

If, however, the excited state is also populated by collisional processes such as quenching of higher states to the state being studied, then the relationship between I and $[X]$ is complex. Plots of I_0/I may be curved and, if population from higher states is more rapid than collisional deactivation of the state being studied, I may increase with pressure. The observed variation in line shapes with pressure implies that changes in transition probabilities are occurring, and these changes may also lead to curvature in the plots of I_0/I vs p . It is not possible to distinguish between this effect and that described in the preceding paragraph.

For the cases where the simple linear relationship holds, results are given in Table VI-IV in the form of $p_{1/2}$, the pressure of added quencher required to halve the emission intensity. Cases where curvature or enhancement are observed are also noted. These results are estimated to be accurate to $\pm 30\%$; the main sources of error are incomplete evacuation of the cell between flashes, variation of γ with

TABLE VI-IV

Quenching Half Pressures for Excited Bismuth (torr)

State	$^4P_{1/2}$	$^4P_{5/2}$	$^2P_{3/2}$	$^2P_{1/2}$
Wavelength (\AA)	3068	3024	2938	2898
Xe	>>100	>>100	35	E
CO	7	17	8	9
N ₂	>100	33	8	15
O ₂	3	E	17	2
H ₂	>600	E	E	4
CH ₄	E	70	50	>7
C ₂ H ₆	E	C	C	>7
C ₂ H ₄	1.0	~30	~30	3.0
CO ₂	0.65	2.6	6	3.2

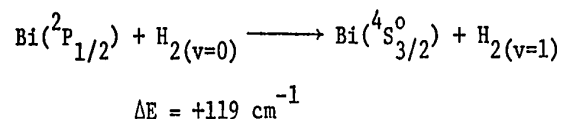
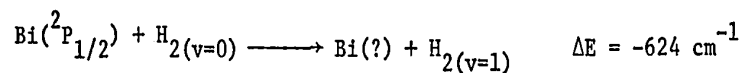
E Enhancement

C Curvature

developing conditions, and the assumption that emission peak heights are proportional to emission intensity.

The ${}^4P_{5/2}$, ${}^2P_{3/2}$, and ${}^2P_{1/2}$ states of Bi lie in an energy region where many other states of atomic bismuth are to be found.

Energy transfer processes involving the conversion of relatively small amounts of energy to vibrational and translational modes of the quenching molecule are therefore available. For example, the quenching of the ${}^2P_{1/2}$ state by H_2 can take place by processes such as:



Enhancement of the transitions from the ${}^4P_{5/2}$ and ${}^2P_{3/2}$ states by H_2 very likely occurs because of similar processes causing quenching to these levels from higher states. It is not possible to estimate the importance of quenching to low-lying states in the deactivation of these species.

A different situation pertains with regard to the ${}^4P_{1/2}$ state observed at 3068\AA . There is no other state within $10,000 \text{ cm}^{-1}$ below this level and only the ${}^2P_{3/2}$ state lies within 8000 cm^{-1} above. Complications brought about by quenching to the ${}^4P_{1/2}$ level from higher electronic states are therefore reduced since any observed quenching must involve the transfer of large amounts of energy.

The only observed transition from the ${}^4P_{1/2}$ state other than that to the ground state at 3068\AA was a weak line at 4622\AA

(${}^4P_{1/2} \rightarrow {}^2D_{3/2}^{\circ}$). Quenching of this emission was qualitatively similar to the quenching of the 3068Å line except in the case of added C_2H_6 where the 4622Å line decreased in intensity while the emission at 3068 Å was enhanced. This observation, indicating an alteration in the relative transition probabilities for collisionally induced as compared to spontaneous emission from a given atomic state, has important implications with respect to energy transfer studies. Additional examples of this phenomenon, which has not been noted before, will be given in the next section dealing with the quenching of excited antimony atoms.

With the exception of C_2H_6 the similarity of the intensity variations in the two lines from the ${}^4P_{1/2}$ state as a function of pressure of added gases noted in the above paragraph, and the absence of curvature in the plots for efficient quenchers as listed in Table VI-IV, imply that variations in transition probabilities are not important.

A value of 2.9 nsec has recently been obtained for the lifetime of the ${}^4P_{1/2}$ state of bismuth (120). Since it is estimated that 97% of the emission from this state is concentrated in the 3068Å line (120) the reciprocal of the measured lifetime has been used as k_f in the expression

$$\sigma^2 = \frac{k_f}{[X]_{1/2}} \left(\frac{8\pi RT}{\mu} \right)^{-1/2}$$

to calculate quenching cross sections for $Bi({}^4P_{1/2})$. $[X]_{1/2}$ is the concentration of quencher corresponding to $p_{1/2}$ and all other symbols have been defined previously. The results of these calculations are

given in Table VI-V, together with some quenching cross sections for other species which are included for comparison. Since no account has been taken of imprisonment of resonance radiation, the data for Bi in Table VI-V are an upper limit. The relative magnitudes of the quoted cross sections are correct.

TABLE VI-V
 Quenching Cross Sections (\AA^2)

Quencher	Hg(3P_1) ^a		Tl($^2S_{1/2}$) ^b		Pb($^3P_1^o$) ^c		Bi($^4P_{1/2}$)	
	Temp. ($^{\circ}\text{K}$)	300	1400	1400	1400	300		
H ₂		9.8	<0.03		0.4		<0.15	
O ₂		23	13.2		15		110	
N ₂		0.35	6.4		5.7		<3.5	
CO		7	13.6		13		46	
CO ₂		2.5	32.5		32.5		620	
Xe							<<6	
CH ₄		0.06					<0.5	
C ₂ H ₆		0.4					<0.6	
C ₂ H ₄		42					330	

a Reference (7)

b Reference (74)

c Reference (76)

2. The Quenching of Excited Antimony Atoms

The UV absorption spectrum of trimethylantimony (TMSb) consists of a continuum between 2100 and 2400Å with a maximum at 2250Å ($\epsilon = 1.0 \times 10^4 \text{ l mole}^{-1} \text{ cm}^{-1}$). The spectrum, recorded on a Cary Model 14 spectrometer, is shown in Figure 6-1. The species detected in absorption following the flash photolysis of TMSb in argon are listed in Table VI-VI. No additional spectra were recorded in the presence of H_2 , CH_4 , C_2H_6 , C_2H_4 , CO , or CO_2 . A dark reaction between TMSb and O_2 precluded the possibility of work with this gas. The states of atomic antimony which were detected in emission and absorption are shown on the energy level diagram (113) given in Figure 6-7.

Observations on the mechanism of photolysis and on other characteristics of the TMBi and TMSb systems were qualitatively similar.

Four atomic lines were observed in emission with sufficient intensity for quantitative work. The upper states involved were the $^2\text{P}_{3/2}$ state observed at 2529 and 3233Å, corresponding to the $^2\text{P}_{1/2} \rightarrow ^2\text{D}_{3/2}^{\circ}$ and $^2\text{P}_{1/2} \rightarrow ^2\text{P}_{1/2}^{\circ}$ transitions respectively. Quenching experiments were performed with 0.05 torr TMSb made up to 200-p torr argon and p torr substrate. Treatment of data was identical to that discussed for bismuth, and the errors involved were the same. Typical I_0/I vs p plots are shown in Figures 6-8, 9, 10. The data are compiled in Table VI-VII and summarized in Table VI-VIII in the form of quenching half-pressures where these could be measured.

The pressure-induced variation in relative emission intensities from the same state, first noted with bismuth, is demonstrated more clearly in the case of antimony. Figure 6-11 reproduces microdensitometer trances showing the effect of added H_2 on the two lines

TABLE VI-VI

Species Observed in Absorption in Flashed TMSb

Species	Transition	$\lambda(\text{Å})$	Comments
$\text{Sb}(^4\text{S}_{3/2}^{\circ})$	$^4\text{P}_{1/2} + ^4\text{S}_{3/2}^{\circ}$	2311	Also at 2175Å ^o
$\text{Sb}(^2\text{D}_{3/2}^{\circ})$	$^2\text{P}_{1/2} + ^2\text{D}_{3/2}^{\circ}$	2598	
$\text{Sb}(^2\text{D}_{5/2}^{\circ})$	$^2\text{P}_{3/2} + ^2\text{D}_{3/2}^{\circ}$	2528	
$\text{Sb}(^2\text{P}_{1/2}^{\circ})$	$^2\text{P}_{3/2} + ^2\text{P}_{1/2}^{\circ}$	3030	
$\text{Sb}(^2\text{P}_{3/2}^{\circ})$	$^2\text{P}_{3/2} + ^2\text{P}_{3/2}^{\circ}$	3233	
$\text{Sb}_2(\text{X}^1_{2g}^+)$? ← X	2100	Reference (121)
$\text{Sb}_2(\text{X}^1_{g}^+)$	F ← X	2240	
$\text{Sb}_2(\text{X}^1_{g}^+)$	D ← X	2900	
CH_3	B ← X	2160	

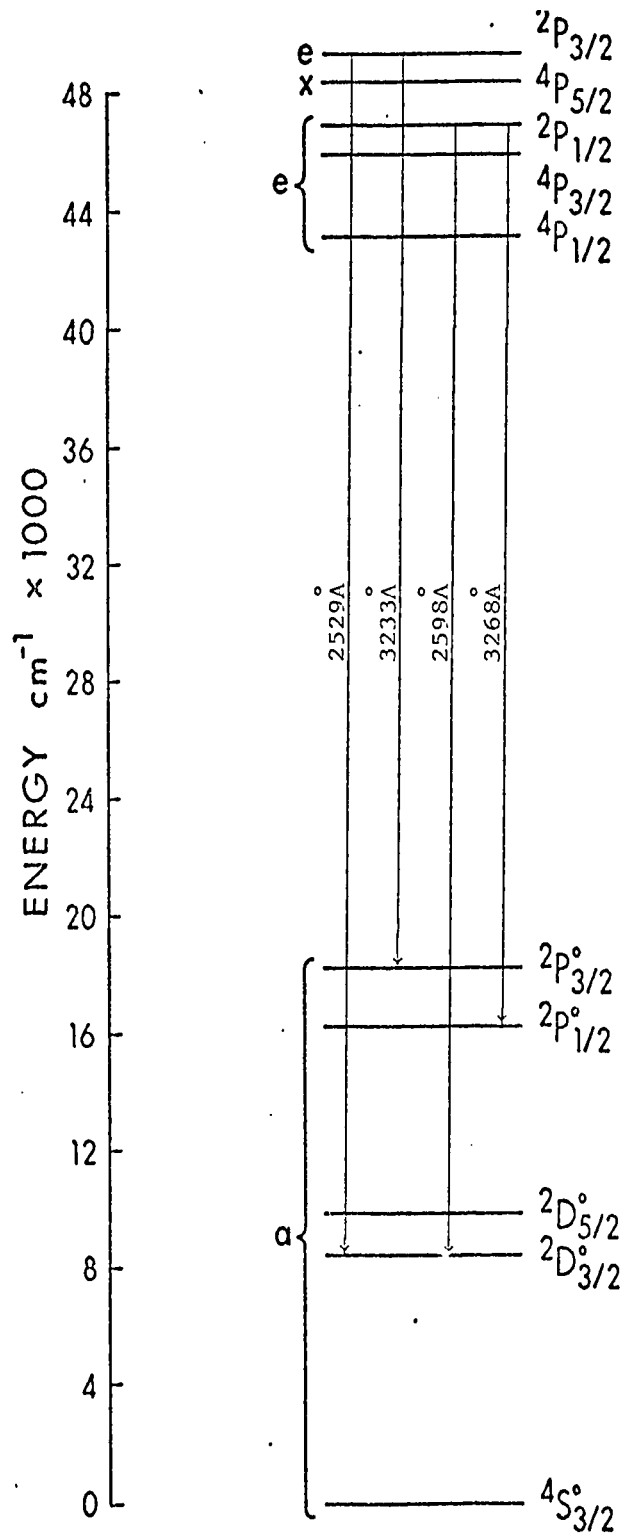


FIGURE 6-7: Energy Level Diagram for Sb; a, states detected in absorption; e, states detected in emission; x, states not detected.

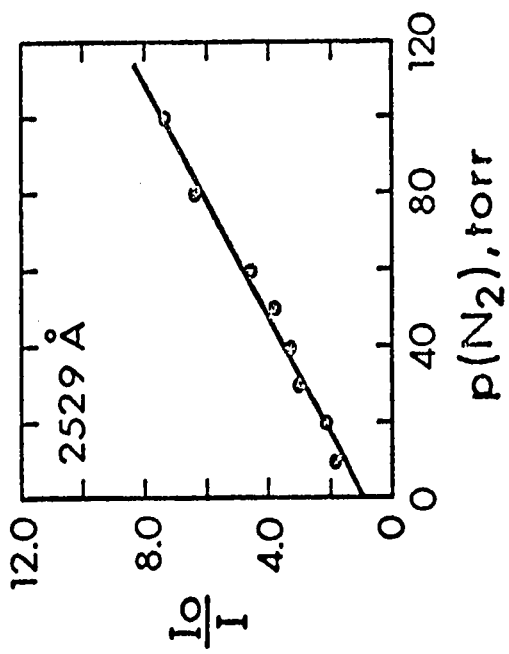
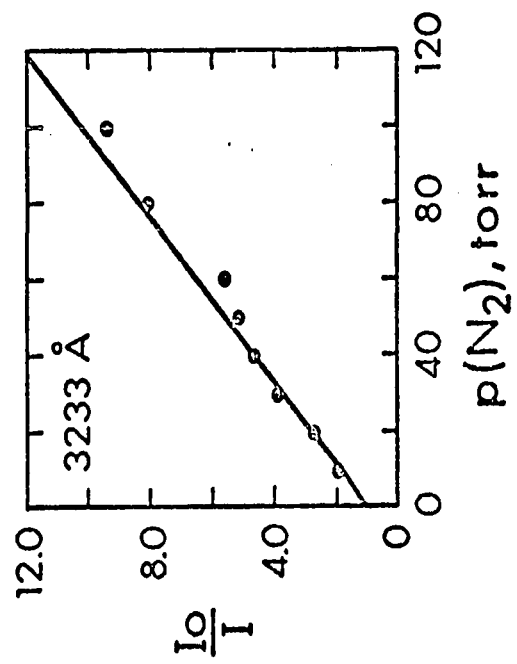


FIGURE 6-8: Stern-Volmer Plot for Excited Sb

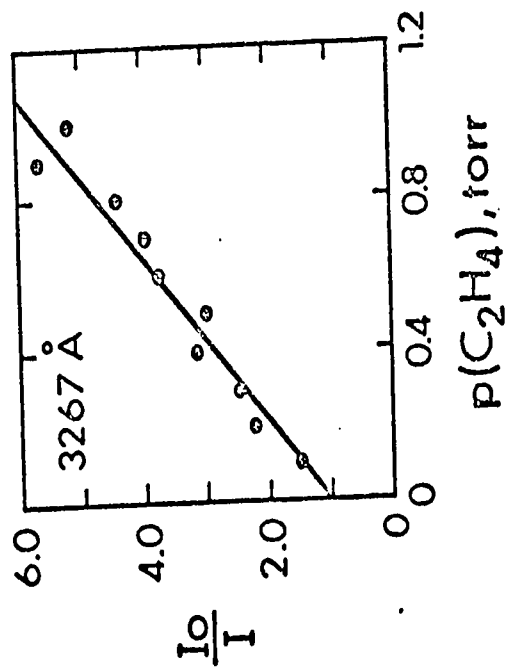
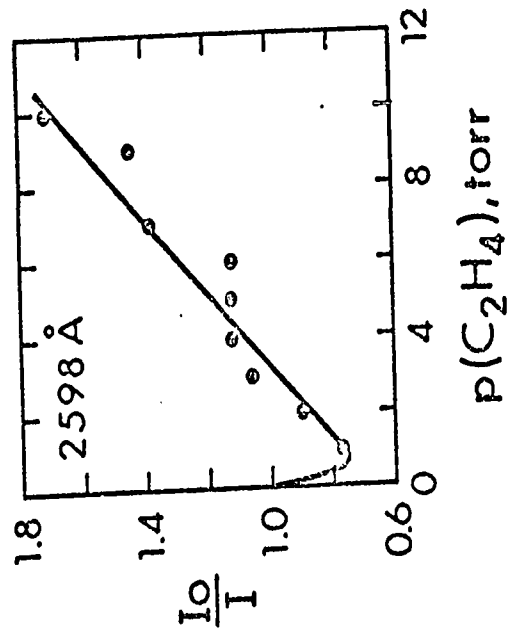


FIGURE 6-9: Stern-Volmer Plot for Excited Sb

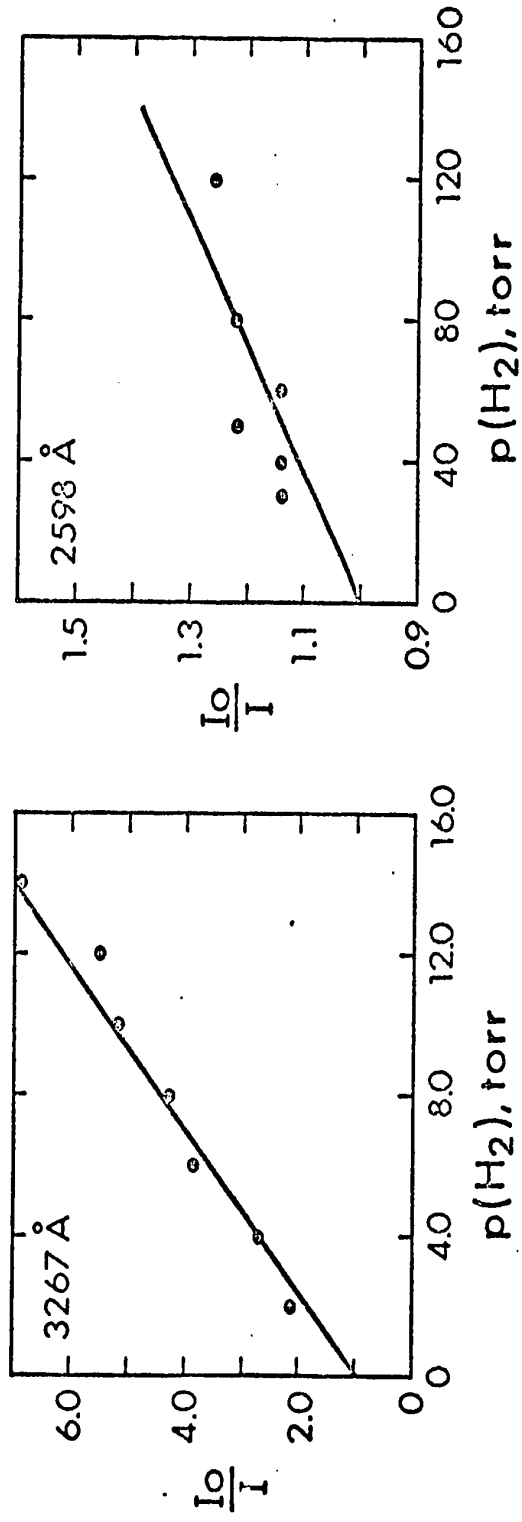


FIGURE 6-10: Stern-Volmer Plot for Excited Sb

TABLE VI-VII
Stern-Volmer Data for Excited Sb

Quencher	Pressure (torr)	$\frac{\Delta OD}{I_0} \frac{\circ}{I}$	$\frac{\Delta OD}{I_0} \frac{\circ}{I}$	$\frac{\Delta OD}{I_0} \frac{\circ}{I}$	$\frac{\Delta OD}{I_0} \frac{\circ}{I}$	$\frac{\Delta OD}{I_0} \frac{\circ}{I}$
Xe	0	29	1	34	1	38
	20	24	1.26	30	1.15	25
	40	22	1.40	23	1.55	25
	60	18	1.77	21	1.70	33
	80	15	2.18	20	1.80	40
	100	15	2.18	16	2.30	39
CO	0	27	1	35	1	32
	2.0	20	1.43	30	1.19	26
	4.0	13	2.33	29	1.23	25
	6.0	14	2.14	22	1.68	23
	8.0	10	3.12	17	2.20	23
	10.	9	3.49	18	2.08	22
	12.			17	2.20	21
	14.			16	2.37	21
	16.			13	2.94	21
						41

1
1
1.29
1.35
1.49
1.49
1.57
1.65
1.65

3268Å
I₀/I

2598Å
I₀/I

3233Å
I₀/I

2529Å
I₀/I

Completely
quenched

3.84

0.74

0.73

0.59

0.56

0.60

TABLE VI-VII (cont'd)
Stern-Volmer Data for Excited Sb

Quencher	Pressure (torr)	$\frac{2529\text{\AA}}{\Delta OD} \frac{I_0}{I}$	$\frac{3233\text{\AA}}{\Delta OD} \frac{I_0}{I}$	$\frac{2598\text{\AA}}{\Delta OD} \frac{I_0}{I}$	$\frac{3268\text{\AA}}{\Delta OD} \frac{I_0}{I}$	
CO	20			22	1.57	
	30			18	1.91	
	40			15	2.34	
	0	39	48	43	1	58
	10	24	28	31	1	39
	20	22	20	24	2.08	37
	30	16	14	22	2.31	36
	40	15	12	20	2.58	28
	50	13	11	19	2.73	27
	60	11	10	10	5.58	25
N ₂	80	8	7		22	
	100	7	6	16	3.32	19
	0	50	56	50	1	67
	2.0	35	37	44	1.22	36
	4.0	35	29	45	1.18	29
	6.0	34	26	43	1.26	21
	0	1	1	1	1	1
	2.0	1.64	1.64	1.64	1.22	2.11
	4.0	1.64	2.16	1.18	1.18	2.70
	6.0	1.70	2.44	1.26	1.26	3.85

TABLE VI-VII (cont'd)
Stern-Volmer Data for Excited Sb

Quencher	Pressure (torr)	2529Å		3233Å		2598Å		3268Å	
		ΔOD	$\frac{I_0}{I}$	ΔOD	$\frac{I_0}{I}$	ΔOD	$\frac{I_0}{I}$	ΔOD	$\frac{I_0}{I}$
H ₂	8.0	32	1.84	23	2.80	46	1.14	19	4.26
	10.	32	1.84	18	3.56	44	1.22	16	5.15
	12.	26	2.38	17	3.86	43	1.26	15	5.52
	14.	23	2.76			41	1.32	13	6.88
	16.	26	2.38			44	1.22	14	5.91
	20	22	2.70	15	4.15	45	1.18	12	7.03
	30	18	3.34	11	5.76	46	1.14	11	7.24
	40	16	3.88			46	1.14		
	50	13	5.11			44	1.22		
	60					46	1.14		
	80	9	6.47			44	1.22		
	100	7	8.82			43	1.26		
CH ₄	0	24	1	48	1	28	1	39	1
	.18			37	1.35				
	.36			28	1.84				
	.54			25	2.09				
	.72			26	2.00				

TABLE VI-VII (cont'd)
Stern-Volmer Data for Excited Sb

Quencher	Pressure (torr)	$\frac{2529\text{\AA}}{\Delta OD} \frac{I_0}{I}$	$\frac{3233\text{\AA}}{\Delta OD} \frac{I_0}{I}$	$\frac{2598\text{\AA}}{\Delta OD} \frac{I_0}{I}$	$\frac{3268\text{\AA}}{\Delta OD} \frac{I_0}{I}$
CH ₄	.91		23 2.30		
	1.0	28 .83		26 1.09	36 1.10
	1.13		23 2.30		
	1.36		20 2.71		
	1.59		19 2.88		
	1.81		20 2.71		
	2.0	27 .87		21 1.41	27 1.51
	3.0	27 .87		16 1.92	28 1.46
	4.0	28 .83		16 1.92	24 1.72
	5.0	23 1.05		13 2.42	21 2.00
	6.0	25 .96		12 2.35	19 2.23
	7.0	20 1.24		12 2.64	18 2.35
	8.0	22 1.11		11 2.90	14 3.07
	9.0	19 1.32		12 2.64	16 2.67
10	19 1.32		8 4.08	13 3.36	

TABLE VI-VII (cont'd)

Stern-Volmer Data for Excited Sb

Quencher	Pressure (torr)	$\frac{2529\text{\AA}}{\Delta OD} \frac{I_0}{I}$	$\frac{3233\text{\AA}}{\Delta OD} \frac{I_0}{I}$	$\frac{2598\text{\AA}}{\Delta OD} \frac{I_0}{I}$	$\frac{3268\text{\AA}}{\Delta OD} \frac{I_0}{I}$
C ₂ H ₆	0	39	40	36	57
	0.2		24	35	
	0.4		20	33	
	0.6		15	29	
	0.8		11	26	
	1.0	43		26	45
	1.2			23	
	1.4			28	
	1.6			25	
	2.0			24	38
	3.0			19	29
	4.0			16	24
	5.0			13	20
6.0			10	19	
8.0				15	
10				13	

TABLE VI-VII (cont'd)
Stern-Volmer Data for Excited Sb

Quencher	Pressure (torr)	2529Å		3233Å		2598Å		3268Å	
		ΔOD	$\frac{I_0}{I}$	ΔOD	$\frac{I_0}{I}$	ΔOD	$\frac{I_0}{I}$	ΔOD	$\frac{I_0}{I}$
CO ₂	0	27	1	33	1	28	1	38	1
	1.0	22	1.28	26	1.31	20	1.49	32	1.22
	2.0	17	1.73	21	1.66	15	2.06	26	1.53
	3.0	14	2.15	18	1.95	13	2.43	20	2.05
	4.0	14	2.15	15	2.36			19	2.16
	5.0	10	3.12	14	2.54			15	2.78
	6.0			12	3.00			13	3.24
C ₂ H ₄	0	24	1	46	1	27	1	57	1
	0.1			36	1.34			41	1.48
	0.2			32	1.53			29	2.20
	0.3			28	1.77			26	2.48
	0.4			25	2.00			21	3.14
	0.5			23	2.21			22	2.96
	0.6			23	2.21			18	3.74
	0.7			22	2.31			17	3.93
0.8			21	2.44			15	4.40	

TABLE VI-VII (cont'd)
Stern-Volmer Data for Excited Sb

Quencher	Pressure (torr)	$\frac{2529\text{\AA}}{\Delta OD} \frac{I_0}{I}$		$\frac{3233\text{\AA}}{\Delta OD} \frac{I_0}{I}$		$\frac{2598\text{\AA}}{\Delta OD} \frac{I_0}{I}$		$\frac{3268\text{\AA}}{\Delta OD} \frac{I_0}{I}$	
C ₂ H ₄	0.9			21	2.44			12	5.67
	1.0	21	1.17	19	2.71	26	1.05	13	5.19
	2.0	16	1.61			27	1.00		
	3.0	15	1.73			25	1.10		
	4.0	14	1.86			26	1.05		
	5.0	11	2.44			25	1.10		
	6.0	12	2.21			23	1.21		
	7.0	13	2.03			21	1.35		
	8.0	13	2.03			20	1.43		
	9.0	12	2.21			20	1.43		
10	10	2.70			18	1.61			

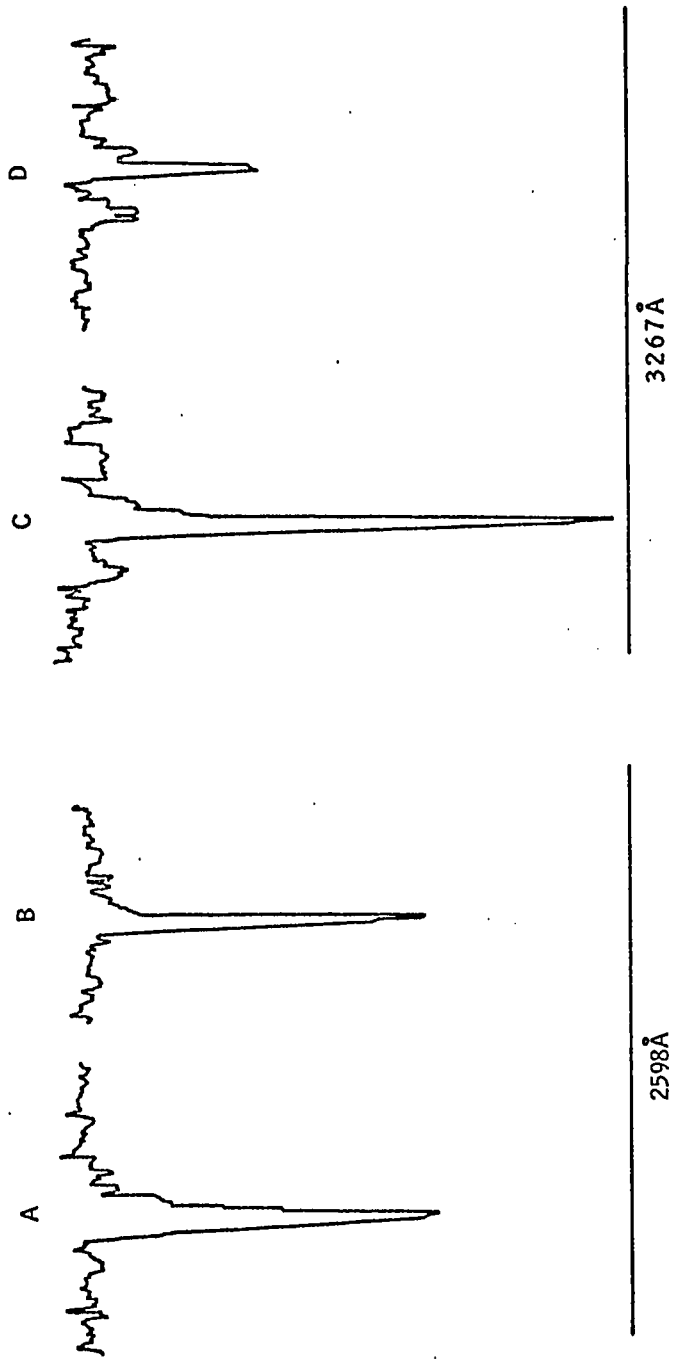
TABLE VI-VIII

Quenching Half Pressures for Excited Antimony (torr)

State	$^2P_{3/2}$	$^2P_{3/2}$	$^2P_{1/2}$	$^2P_{1/2}$
Wavelength (Å)	2529	3233	2598	3268
Xe	75	75	E	E
CO	4	9	35	~1
N ₂	12	12	35	35
H ₂	10	4	>>100	2.5
CH ₄	C	1	4	4
C ₂ H ₆	C	0.3	2.5	2.5
C ₂ H ₄	6	0.5	C	0.2
CO ₂	3	3	2	3

E Enhancement

C Curvature



A and C 0.43 torr TMSb + 200 torr Ar

B and D 0.43 torr TMSb + 200 torr Ar + 10 torr H₂

FIGURE 6-11: Effect of Added H₂ on Emission from Sb(²P_{1/2}) at 3268 and 2598 Å

from the $^2P_{1/2}$ state. The shape of the 2598Å line is changed by the H_2 and the intensity is only slightly reduced, whereas the 3268Å line is apparently quenched much more efficiently. Similar effects occur with CO and C_2H_4 . For the two transitions from the $^2P_{3/2}$ state, this effect is observed with H_2 , CO, CH_4 , C_2H_6 , and C_2H_4 .

Distinct satellite bands were not observed with any of the Sb atomic lines but as shown in Figure 6-11, the line shapes were affected by added gas pressure. The absence of satellite bands is probably due to the low intensities of the antimony transitions as compared to the Bi 3068Å resonance line; the satellite bands could therefore not be observed.

3. Discussion

When cross sections for the deactivation of excited atoms are determined by studying the quenching of atomic emission it is assumed that, after correction for imprisonment, the probability of the observed transition remains constant. The observation of collisionally induced emission from metastable states shows that this is not necessarily the case. The results of the present investigation demonstrate that collisional effects may cause variations even in the relative transition probabilities from the same state. Therefore, in quantitative quenching experiments where more than one terminating emission process is available, the possible role of this effect must not be overlooked.

The mechanisms of the quenching processes studied here are complex and cannot be derived since the reaction products were not analyzed. Some of the primary processes however can be inferred from the nature of the intermediates detected. For example, the observation of BiO in the TMBi-CO₂ system suggests that oxygen abstraction is a principal mode of quenching and in fact the reaction of Bi(²P_J) state atoms with CO₂(X¹Σ⁺) to produce BiO(X²Π) and CO(X¹Σ⁺) is symmetry and spin allowed. Similar reactions with Bi(⁴P_J) atoms are spin forbidden but heavy atom perturbations may facilitate the spin inversion. The failure to observe SbH or BiH in H₂ or hydrocarbons is surprising since the hydrogen abstraction reaction would be symmetry and spin allowed and energetically possible (the Bi-H bond strength being 53 kcal/mole (57)), and also since some states are quenched with relatively high efficiencies by these compounds.

In the cases of Xe, N₂, and CO, transient formation must be involved. In fact, the appearance of satellite bands is evidence for the existence of these complexes. Quenching can then occur if favourable potential surface crossings are available.

CHAPTER VII

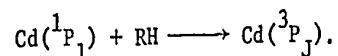
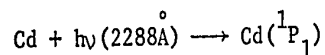
SUMMARY AND CONCLUSIONS

The flash photolysis of DMcd has been used to produce cadmium atoms in their ground and excited states at room temperature. This photolysis has been shown to lead directly to the formation of ground state cadmium atoms and methyl radicals. All the DMcd is destroyed in one flash, and the methyl radicals recombine rapidly to form ethane; this is a clean source of Cd.

The spectra of CdCH_3 and ZnCH_3 have been observed for the first time. The observed bands along with their vibrational assignments are given in Tables III-I, II, III, IV, V, VI, VII, VIII.

The reactions between Cd and Zn atoms, Zn being produced by the flash photolysis of DMZn, and Br and I atoms have been studied. Kinetic data could not be obtained from the experimental measurements; however, the $A^2\Pi - X^2\Sigma$ spectra of CdBr, CdI, ZnBr, and ZnI were recorded under the mild conditions of room temperature flash photolysis and these spectra afforded better vibrational analysis than could be achieved previously. The $A^2\Pi_{1/2} - X^2\Sigma$ components of the CdBr and ZnI spectra were observed and analyzed for the first time.

The flash photolysis of DMcd in a hydrocarbon has been shown to produce excited $\text{Cd}(^3P)$ atoms in sufficient quantities to allow quenching measurements. The mechanism of Cd^3 production is



The ground state cadmium produced in the flash photolysis of DMCD absorbs 2288Å light from the photo-lamp and is excited to the 1P_1 state; the $Cd(^1P_1)$ can then be collisionally deactivated by a hydrocarbon, or to a lesser degree by nitrogen, to one or more of the 3P states. It is also likely, therefore, that $Hg(^3P)$ plays a significant role in the $Hg(^1P_1)$ photosensitization of paraffins.

Absolute rate constants for the quenching of Cd^3 by a variety of substrates have been measured by monitoring the concentration of Cd^3 in the presence of quencher, using kinetic absorption spectroscopy. This method requires a minimum of assumptions and the possibility of errors of interpretation is therefore reduced. The results are listed in Table V-I. The rate constants for Cd^3 quenching by substituted ethylenes increase with the addition of methyl groups which are electron donating substituents and decrease with the progressive addition of fluorine atoms which are electron withdrawing agents. Thus the electrophilic nature of excited cadmium is demonstrated.

The rate parameters for the reaction



have been found to be

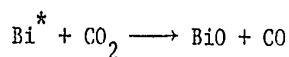
$$k = 4 \times 10^{10} \exp(-2300/RT).$$

Cadmium (3P_0) has been observed for the first time in Cd^* photosensitization and its role discussed. Equilibration of Cd^* and Cd^0 in several hundred torr of a hydrocarbon or nitrogen is rapid as compared to the rate of fluorescence. It is reasonable to assume that $Cd(^3P_2)$ is also in equilibrium with the other components of

the cadmium triplet although this could not be experimentally verified since the transition from $\text{Cd}(^3\text{P}_2)$ was very weak. Since the rate of quenching of Hg^0 by ethylene is only a factor of two less than that of Hg^* , and the $\text{Hg}^* - \text{Hg}^0$ splitting is 5 kcal/mole as compared to 1.6 kcal/mole for the $\text{Cd}^* - \text{Cd}^0$ splitting, it is likely that the rates of quenching of Cd^* and Cd^0 by ethylene are very similar.

Since Cd^* and Cd^0 equilibrate in hydrocarbons and nitrogen, and it is probable that this spin-orbit change will occur in other gases, and since Cd^* and Cd^0 are quenched at similar rates, results from previous attempts to measure Cd^* quenching cross sections are incorrect, although the relative values from these determinations should be correct. The previous studies ignored the formation of Cd^0 and thus used incorrect assumptions in the calculation of the cross section. The results of the present study (Table V-I) are shown to be consistent with the non-vertical nature of the transition involved in the reaction between Cd^3 and an olefin. Previous quenching cross section determinations obtained values very similar to those obtained with Hg^* , a result inconsistent with the small energy content of Cd^* as compared to Hg^* .

Flash photolysis of TMBi and TMSb resulted in the formation of excited bismuth and antimony atoms. In the course of the investigation of the reactions of Bi atoms the previously unobserved $\text{BiO}(X_2^2\pi_{3/2})$ state was detected by its $E + X_2$ spectrum. Also, the reaction



has been shown to occur; in this reaction Bi^* may be $\text{Bi}(^2\text{P}_j)$ since

the reaction would then be symmetry and spin allowed, and no other doublet states are present in significant amounts.

Apparent relative quenching rates of Bi^* and Sb^* by some substrates were obtained from measurements of the variation of emission intensity with quencher pressure. Quenching cross sections for $\text{Bi}(^4\text{P}_{1/2})$ were obtained and are listed in Table VI-IV. Possible complications in evaluating data from the other Bi^* states studied were shown to be due to the density of electronic states in the Bi manifold, and the resulting possibility of reactions involving the transfer of small amounts of energy. A previously unobserved manifestation of the phenomenon of collisionally-induced emission was discovered in the Bi^* and Sb^* quenching experiments. If an excited state displays two emissions to different terminating levels, the apparent quenching rate of that state can be different depending on the transition monitored. This is due to the fact that the transient van der Waals molecule formed has different transition probabilities than those of the free atom, and the relative transition probabilities of the two transitions from the same state also change.

The quenching of excited cadmium, bismuth, and antimony atoms has been studied at room temperature. The appearance of satellite bands in the interaction of Bi^* with various substrates such as Xe and CH_4 , the variation in relative transition probabilities observed with antimony and bismuth, and the great similarity between the reactions of excited cadmium and mercury observed in the present study, as well as the observation of emission from excited metal atom-substrate complexes observed in other studies, indicate that the formation of a

transitory van der Waals molecule is a general feature of the interaction of excited metal atoms with substrate.

BIBLIOGRAPHY

1. G. Cario and J. Franck, *Z. Physik*, 17, 202 (1923).
2. J. G. Calvert and J. N. Pitts, *Photochemistry*, John Wiley and Sons, 1966, Ch. II.
3. R. J. Cvetanović, *Prog. in Reaction Kin.*, 2, 39 (1964), Pergamon Press.
4. H. E. Gunning and O. P. Strausz, *Adv. in Photochem.*, 1, 209 (1963), Interscience Publishers.
5. A. B. Callear, *Photochemistry and Reaction Kinetics*, Cambridge University Press, 1967, Ch. 7.
6. A. C. G. Mitchell and M. W. Zemanski, *Resonance Radiation and Excited Atoms*, The MacMillan Company, 1934.
7. J. M. Campbell, Ph.D. Thesis, University of Alberta, 1972.
8. H. E. Gunning, S. Penzes, H. S. Sandhu and O. P. Strausz, *J. Amer. Chem. Soc.*, 91, 7684 (1969).
9. A. B. Callear and W. J. R. Tyerman, *Trans. Faraday Soc.*, 62, 2313 (1966).
10. A. B. Callear and R. J. Oldman, *Trans. Faraday Soc.*, 63, 2888 (1967).
11. A. B. Callear and R. J. Oldman, *Trans. Faraday Soc.*, 64, 840 (1968).
12. O. Stern and M. Volmer, *Physik. Z.*, 20, 183 (1919).
13. J. V. Michael and C. Yeh, *J. Chem. Phys.*, 53, 59 (1970).
14. Shigeru Tsunashima, Shin Satoh and Shin Sato, *Bull. Chem. Soc. Japan*, 42, 329 (1969).
15. M. G. Bellas, Y. Rousseau, O. P. Strausz and H. E. Gunning, *J. Chem. Phys.*, 41, 768 (1964).
16. A. Kato and R. J. Cvetanović, *Can. J. Chem.*, 45, 1845 (1967).
17. R. Payette, M. Bertrand, and Y. Rousseau, *J. Amer. Chem. Soc.*, 90, 5341 (1968).

18. R. B. Cundall and T. F. Palmer, *Trans. Faraday Soc.*, 56, 1211 (1960).
19. Shigeru Tsunashima and Shin Sato, *Bull. Chem. Soc. Japan*, 41, 284 (1968).
20. A. B. Callear and R. E. M. Hedges, *Trans. Faraday Soc.*, 66, 605 (1970).
21. A. B. Callear and R. E. M. Hedges, *Trans. Faraday Soc.*, 66, 615 (1970).
22. A. B. Callear and R. E. M. Hedges, *Nature*, 218, 163 (1968).
23. A. B. Callear and J. C. McGurk, *Chem. Phys. Letters*, 6, 417 (1970).
24. A. B. Callear and J. C. McGurk, *Chem. Phys. Letters*, 7, 491 (1970).
25. A. B. Callear and J. C. McGurk, *Nature*, 266, 844 (1970).
26. W. H. Breckenridge and A. B. Callear, *Chem. Phys. Letters*, 5, 17 (1970).
27. W. H. Breckenridge and A. B. Callear, *Trans. Faraday Soc.*, 67, 2009 (1971).
28. L. F. Bras, *J. Chem. Phys.*, 52, 1716 (1970).
29. J. A. Bellisio and P. Davidovits, *J. Chem. Phys.*, 53, 3474 (1970).
30. Y. Rousseau, O. P. Strausz and H. E. Gunning, *J. Chem. Phys.*, 39, 962 (1963).
31. A. B. Callear and R. E. M. Hedges, *Trans. Faraday Soc.*, 66, 615 (1970).
32. A. C. Vikis and D. J. LeRoy, *Can. J. Chem.*, 50, 595 (1972).
33. R. J. Cvetanovic, H. E. Gunning and E. W. R. Steacie, *J. Chem. Phys.*, 31, 573 (1959).

34. O. Oldenberg, *Z. Physik.*, 47, 184 (1927); 49, 609 (1928); 50, 580 (1928); 51, 41, 605 (1928); 55, 1 (1929).
35. W. M. Preston, *Phys. Rev.*, 51, 298 (1936).
36. H. Kuhn, *Proc. Roy. Soc. A*158, 212 (1937).
37. O. Jefimenko, *J. Chem. Phys.*, 39, 2457 (1963).
38. Y. Leycuras, *J. Quant. Spectrosc. Radiat. Transfer*, 6, 131 (1966).
39. J. Fiutak and M. Frackowiak, *Bull. Acad. Polon. Sci., Ser. Sci., Math., Astron., Phys.*, 11, 175 (1963).
40. A. Jablonski, *Z. Physik.*, 70, 732 (1932).
41. Keith J. Laidler, *J. Chem. Phys.*, 10, 34, 43 (1942).
42. J. Szudy, *Acta. Phys. Polon.*, 29, 605 (1966).
43. S. Ch'en and M. Takeo, *Rev. Mod. Phys.*, 29, 20 (1957).
44. A. Michels, H. Dekluyer and C. A. Ten Seldon, *Physica*, 25, 1321 (1959).
45. S. Penzes, O. P. Strausz and H. E. Gunning, *J. Chem. Phys.*, 45, 2322 (1966).
46. C. G. Freeman, M. J. McEvan, R. F. C. Claridge and L. F. Phillips, *Chem. Phys. Letters*, 9, 578 (1971).
47. C. G. Freeman, M. J. McEvan, R. F. C. Claridge and L. F. Phillips, *Trans. Faraday Soc.*, 67, 67 (1971).
48. P. D. Morten, C. G. Freeman, M. J. McEwan, R. F. C. Claridge and L. F. Phillips, *Chem. Phys. Letters*, 16, 148 (1972).
49. John R. Bates and Hugh S. Taylor, *J. Amer. Chem. Soc.* 50, 771 (1928).
50. John R. Bates, *Proc. Nat. Acad. Sci.*, 14, 849 (1928).
51. E. W. R. Steacie and Roger Potvin, *J. Chem. Phys.*, 7, 782 (1939).

52. E. W. R. Steacie and Roger Potvin, *Can. J. Research*, 16, 337 (1938).
53. E. W. R. Steacie and Roger Potvin, *Can. J. Research*, 18B, 47 (1940).
54. Paul Bender, *Phys. Rev.*, 36, 1535, 1543 (1930).
55. Leonard O. Olsen, *J. Chem. Phys.*, 6, 307 (1938).
56. E. W. R. Steacie and D. J. LeRoy, *J. Chem. Phys.*, 12, 34 (1944).
57. G. Herzberg, *Molecular Spectra and Molecular Structure, I. Spectra of Diatomic Molecules*, D. Van Nostrand Co., Princeton, N.J., 1950.
58. H. C. Lipson and C. G. Mitchell, *Phys. Rev.*, 48, 625 (1935).
59. E. W. R. Steacie and D. J. LeRoy, *J. Chem. Phys.*, 11, 164 (1943).
60. P. Agius and B. deB. Darwent, *J. Chem. Phys.*, 20, 1679 (1952).
61. S. Tsunashima and Shin Sato, *Bull. Chem. Soc. Japan*, 41, 2281 (1968).
62. Shin Sato, Chiharu Takahashi and S. Tsunashima, *Bull. Chem. Soc. Japan*, 43, 1319 (1970).
63. S. Tsunashima, Shun-ichi Hirokami and Shin Sato, *Can. J. Chem.*, 46, 995 (1968).
64. Shun-ichi Hirokami and Shin Sato, *Bull. Chem. Soc. Japan*, 43, 2389 (1970).
65. S. Tsunashima and Shin Sato, *Bull. Chem. Soc. Japan*, 40, 2987 (1967).
66. S. Tsunashima and Shin Sato, *Bull. Chem. Soc. Japan*, 41, 284 (1968).
67. S. Tsunashima, Shin Satoh and Shin Sato, *Bull. Chem. Soc. Japan*
68. R. J. Cvetanovic and A. B. Callear, *J. Chem. Phys.*, 23, 1182 (1955).
69. Heinrich E. Hunziker, *J. Chem. Phys.*, 50, 1288 (1969).
70. B. L. Kalra and A. R. Knight, *Can. J. Chem.*, 48, 1333 (1970).
71. B. L. Kalra and A. R. Knight, *Can. J. Chem.*, 50, (1972).
72. D. R. Jenkins, *Proc. Roy. Soc.*, A293, 493 (1966).
73. D. R. Jenkins, *Proc. Roy. Soc.* A303, 453 (1968).

74. D. R. Jenkins, *Proc. Roy. Soc.*, A303, 467 (1968).
75. D. R. Jenkins, *Proc. Roy. Soc.*, A306, 413 (1968).
76. D. R. Jenkins, *Proc. Roy. Soc.*, A313, 551 (1969).
77. D. R. Jenkins, *Trans. Faraday Soc.*, 64, 36 (1968).
78. E. M. Balewicz and T. M. Sugden, *Trans. Faraday Soc.*, 54, 830 (1958).
79. J. A. Bellisio, P. Davidovits and P. J. Kindlman, *J. Chem. Phys.*, 48, 2376 (1968).
80. D. A. McGillis and L. Krause, *Phys. Rev.*, 153, 44 (1967).
81. R. G. W. Norrish and G. Porter, *Nature*, 164, 658 (1949).
82. G. Porter, *Proc. Roy. Soc.*, A200, 284 (1950).
83. George Porter, *Technique of Organic Chemistry*, Vol. VIII, part II, p. 1058.
84. R. G. W. Norrish, *Chemistry in Britain*, 1, 289 (1965).
85. T. S. Godfrey and G. Porter, *Trans. Faraday Soc.*, 62, 7 (1966).
86. N. Basco and K. K. Yee, *Nature*, 216, 998 (1967).
87. N. Basco and K. K. Yee, *Spec. Letters*, 1, 13 (1968).
88. M. A. West, private communication.
89. A. Terenin and N. Prileshajewa, *Acta. Physicochemica U.R.S.S.*, 1, 759 (1935).
90. H. W. Thompson and J. W. Linnett, *J. Chem. Soc.*, 790 (1934).
91. H. W. Thompson and J. W. Linnett, *Proc. Roy. Soc.*, A150, 603 (1935); A156, 108 (1936).
92. E. W. R. Steacie, *Atomic and Free Radical Reactions*, Reinhold, New York, 1954.
93. J. A. Kerr, *Chem. Rev.*, 66, 465 (1966).
94. R. D. Anderson and H. A. Taylor, *J. Phys. Chem.*, 56, 498 (1952).

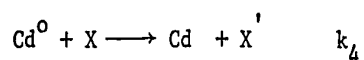
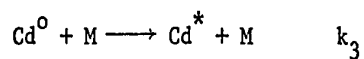
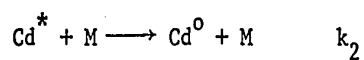
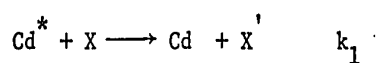
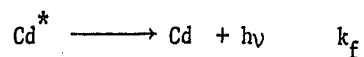
95. W. Finkelburg, *Kontinuierliche Spektren*, Springer, Berlin (1938).
96. C. H. Kohlmuier and B. S. Rabinovitch, *J. Chem. Phys.*, 38, 1692 (1963).
97. P. J. Young, R. K. Gosavi, J. Connor and O. P. Strausz, *Chem. Phys. Letters*, in press.
98. A. Shepp, *J. Chem. Phys.*, 24, 939 (1956).
99. P. Pringshiem, *Fluorescence and Phosphorescence*, Interscience Publishers, Inc., New York, 1949, p.102.
100. T. A. Grover and H. G. Bryant, *J. Phys. Chem.*, 70, 2070 (1966).
101. R. A. Holroyd and T. E. Pierce, *J. Phys. Chem.*, 68, 1392 (1964).
102. N. L. Raland and R. Pertel, *J. Amer. Chem. Soc.*, 87, 4312 (1965).
103. (a) D. J. Horne, R. K. Gosavi and O. P. Strausz, *J. Chem. Phys.*, 48, 5748 (1968).
(b) G. Greig, H. E. Gunning and O. P. Strausz, *J. Chem. Phys.*, 52, 3684 (1970).
(c) G. Greig, H. E. Gunning and O. P. Strausz, *J. Chem. Phys.*, 52, 4569 (1970).
104. K. Wieland, *Helv. Phys. Acta.*, 2, 46 (1929).
105. M. M. Patel, S. P. Patel and A. B. Darji, *Indian J. Pure Appl. Phys.*, 5, 526 (1967).
106. H. G. Howell, *Proc. Roy. Soc.*, A182, 95 (1943).
107. C. Ramasastry and K. R. Rao, *Indian J. Phys.*, 20, 100 (1946).
108. C. A. Heller and H. A. Taylor, *J. Chem. Phys.*, 57, 226 (1953).
109. F. W. Byron, Jr., M. N. McDermott and R. Novic, *Phys. Rev.*, 134, A615 (1964).
110. D. R. Jenkins, *Trans. Faraday Soc.*, 64, 36 (1968).

111. A. Kuppermann and L. M. Ruff, *J. Chem. Phys.*, 37, 2497 (1962).
112. J. M. Campbell, H. E. Gunning and O. P. Strausz, *Can. J. Chem.*, 47, 3759 (1969).
113. *Nat. Bur. Stand. (U.S.)*, Circ., 467 (III), (1958).
114. N. K. Bridge and H. G. Howell, *Proc. Phys. Soc.*, 67, 44 (1954).
115. R. F. Barrow, W. J. M. Gissane, and D. Richards, *Proc. Roy. Soc.*, A300, 496 (1967).
116. D. Guy, J. Grumberg, M-O. Faucheux, and L. Hermon, *C. R. Acad. Sci.*, B266, 1020 (1968).
117. O. Jefimenko and W. Curtis, *J. Chem. Phys.*, 27, 953 (1957).
118. F. Mies and A. L. Smith, *J. Chem. Phys.*, 45, 994 (1966).
119. R. F. Hampson, Jr., and H. Okabe, *J. Chem. Phys.*, 52, 1930 (1970).
120. P. T. Cunningham and J. K. Link, *J. Opt. Soc. Amer.*, 47, 1000 (1967).
121. G. Nakamura and T. Shidei, *Japan. J. Phys.*, 10, 11 (1935).

APPENDIX

Kinetic Treatment of Coupled J States for Cd(³P)

Given the reaction scheme



$$-\frac{d[\text{Cd}^*]}{dt} = k_f[\text{Cd}^*] + k_1[\text{Cd}^*][\text{X}] + k_2[\text{Cd}^*][\text{M}] - k_3[\text{Cd}^0][\text{M}]$$

$$-\frac{d[\text{Cd}^0]}{dt} = k_3[\text{Cd}^0][\text{M}] + k_4[\text{Cd}^0][\text{X}] - k_2[\text{Cd}^*][\text{M}].$$

For the Cd^{*} quenching experiments described in Chapter V, X corresponds to the quenching gas and M is CH₄. Rigorously the terms in M should be in (M + X) but as X is in the order of 10⁻³M this is negligible. Taking the derivative with respect to time of each of the above equations, after suitable substitution the following equation is derived:

$$\begin{aligned} -\frac{d[\text{Cd}^0]^2}{dt^2} &= (k_f + k_1[\text{X}] + k_2[\text{M}] + k_3[\text{M}] + k_4[\text{X}])\frac{d[\text{Cd}^0]}{dt} \\ &+ (k_f k_3[\text{M}] + k_f k_4[\text{X}] + k_1 k_3[\text{M}][\text{X}] + k_1 k_4[\text{X}]^2 \\ &+ k_2 k_4[\text{M}][\text{X}][\text{Cd}^0]). \end{aligned}$$

Assuming a solution of the form $[Cd^\circ] = e^{rt}$, substitution yields

$$(r^2 + br + c)e^{rt} = 0$$

where $b = k_f + k_1[X] + k_2[M] + k_3[M] + k_4[X]$

and $c = k_f k_3[M] + k_f k_4[X] + k_1 k_3[M][M] + k_1 k_4[X]^2 + k_2 k_4[X][M]$.

Dividing by the non-zero term e^{rt} , the roots of the resulting equation are

$$r = \frac{-b \pm \sqrt{b^2 - 4c}}{2}$$

Therefore

$$[Cd^\circ] = e^{rt}$$

where r is defined above.

$$\ln[Cd^\circ] = rt$$

$$\frac{d(\ln[Cd^\circ])}{dt} = \frac{1}{[Cd^\circ]} \frac{d[Cd^\circ]}{dt} = \frac{d(rt)}{dt} .$$

Therefore

$$\frac{-d[Cd^\circ]}{dt} = \frac{b \pm \sqrt{b^2 - 4c}}{2} [Cd^\circ] .$$

No further meaningful reduction of the above equation is possible. Using the experimental facts that $k_2[M]$ and $k_3[M]$ are much larger than k_f , $k_1[X]$, and $k_4[X]$ various numerical evaluations of the above equation were accomplished. If $k_1 = k_4$, decay of Cd° is equal to $k_f + k_1[X]$. If $k_4 = 0$, the data of Chapter V must be modified by a factor approaching $k_3/(k_2 + k_3)$.